2016

Thin Films of Semiconducting Polymers and Block Copolymers by Surface-initiated Polymerization

Sang Gil Youm
Louisiana State University and Agricultural and Mechanical College, syoum1@lsu.edu

THIN FILMS OF SEMICONDUCTING POLYMERS AND BLOCK COPOLYMERS BY SURFACE-INITIATED POLYMERIZATION

A Dissertation

Submitted to the Graduate Faculty of the
Louisiana State University and
Agricultural and Mechanical College
in partial fulfillment of the
requirements for the degree of
Doctor of Philosophy

in

The Department of Chemistry

by
Sang Gil Youm
B.S. Department of Chemistry, Hanyang University, Korea 2002
M.S. Department of Chemistry, Hanyang University, Korea 2004
August 2016

ACKNOWLEDGMENTS

Foremost and before starting my dissertation, I would like to say “family is all about”. Their unconditional love and support has been guiding me to finish my PhD course. Without them, my way at Louisiana State University would have been filled with doubt and regret.

I also would like to acknowledge Prof. Evgueni E. Nesterov for his mentorship and leadership to make me pursue PhD course. His deep knowledge always inspired me in many ways, so that I can become a better scientist.

I specially thank my committee members: Profs. Dave Spivak and Jayne Garno for their devotion to bring me fruitful knowledge, so that I could overcome what I couldn’t otherwise.

To group members: Drs. Euiyong Hwang, Jinwoo Choi, Brian Imsick, Carlos A. Chavez, and Sourav Chatterjee; Chien-Hung Chaing, Chun-han Wang, Peter Kei, Gerard Ducharme, Fetemeh Khamespanah. Thank you all for your support.

I want to convey my gratitude to Dr. Susan Verberne-Sutton for her support not only in science projects but also in many other aspects of my life in Baton Rouge. Dr. Lu Lu for her effort to make our research outcomes look beautiful with high-level AFM images. And I also would like to thank my neighbor Britney L. Hebert for making 4^{th} floor of CMB the most enjoyable work place.

Special thank should be delivered to Drs. Xin Li and John F. Ankner for their fruitful advise and help with studies neutron scattering; Dr. Yaroslav Losovyj for carrying out XPS analysis; Dr. Joseph Strzalka for all X-ray scattering experiments.

To my friends Yucheol Kim and Yumiko Kanke as well as all my friends who live in my home country.

TABLE OF CONTENTS

ABBREVIATIONS AND ACRONYMS

CP	Conjugated Polymer
BHJ	Bulk Heterojunction
oCVD	Oxidative Chemical Vapor Deposition
UV/vis	Ultraviolet/visible
AFM	Atomic Force Microscopy
XPS	X-ray Photoelectron Spectroscopy
IR	Infrared
SEM	Scanning Electron Microscopy
CV	Cyclic Voltammetry
NMR	Nuclear Magnetic Resonance
NR	Neutron Reflectometry
UPS	Ultraviolet Photoemission Spectroscopy
OLED	Organic Light-emitting Diode
OFET	Organic Field Effect Transistor
OPV	Organic Photovoltaic
acac	Acetylacetonate
dppe	1,2-bis(diphenylphosphino)ethane
dppp	1,3-bis(diphenylphosphino)propane
KCTP	Kumada Catalyst Transfer Polymerization
RAFT	Reversible Addition-Fragmentation Chain-Transfer
ATRP	Atomic-Transfer Radical Polymerization
HOMO	Highest Occupied Molecular Orbital
LUMO	Lowest Unoccupied Molecular Orbital
PT	Polythiophene
PPP	Poly(*p*-phenylene)
P3HT	Poly(3-hexylthiophene)
P3AT	Poly(3-alkylthiophene)
HT	Head-to-Tail
PCBM	Phenyl-C61-butyric acid methyl ester
PEDOT	Poly(3,4-ethylenedioxythiphene)
PPV	Poly(*p*-phenylene vinylene)
THF	Tetrahydrofuran
rr	Regioregular

ABSTRACT

The ability to control nanoscale morphology and molecular organization in organic semiconducting polymer thin films is an important prerequisite for enhancing the efficiency of organic thin-film devices, including organic light-emitting and photovoltaic devices. The current "top-down" paradigm for making such devices is based on utilizing solution-based processing (e.g. spin-casting) of soluble semiconducting polymers. This approach typically provides only modest control over nanoscale molecular organization and polymer chain alignment. A promising alternative to using solutions of pre-synthesized semiconducting polymers pursues instead a "bottom-up" approach to prepare surface-grafted semiconducting polymer thin films by surface-initiated polymerization of small-molecule monomers. This dissertation mainly focuses on development of an efficient method to prepare semiconducting polymer thin films utilizing surface-initiated Kumada catalyst transfer polymerization (SI-KCTP). In chapter 2, we describe SI-KCTP with a new Ni(II) external catalytic initiator to prepare polythiophene (PT) thin films. We provided evidence that the surface-initiated polymerization occurs by the highly robust controlled (quasi-"living") chain-growth mechanism. Extensive structural studies of the resulting thin films revealed detailed information on molecular organization and the bulk morphology of the films, and enabled further optimization of the polymerization protocol. Achieving such a complex mesoscale organization is virtually impossible with traditional methods relying on solution processing of pre-synthesized polymers. In addition to controlled bulk morphology, uniform molecular organization and stability, unique feature of SI-KCTP is that it can be used for the preparation of large-area uniformly nanopatterned polymer thin films. This was demonstrated using combination of particle lithography and surface-initiated polymerization.

We expanded scope of the surface-initiated polymerization towards all-conjugated diblock copolymer (polythiophene-*b*-poly(*para*-phenylene)) thin films, which is described in chapter 3. In addition to the preparation of such films, we carried out detailed structural studies and investigated optoelectronic characteristics of the films.

In chapter 4, we studied using SI-KCTP to prepare poly(3,4-ethylenedioxithophene) (PEDOT) thin films. PEDOT is a practically important highly conductive conjugated polymer. Our investigation of the properties of a surface-confined PEDOT film revealed that, after doping with iodine, the film became highly conductive, with conductivity comparable to that of inorganic semiconductors. Therefore, surface-confined PEDOT films may find applications in replacing traditional inorganic electrode for the fabrication of flexible organic electronics.

CHAPTER 1. A GENERAL OVERVIEW

1.1. Introduction to Conjugated Polymers (CPs)

Polymers – often called plastics – had long been considered typical insulating materials with no ability to conduct electricity. Their conductivity normally lies within the range from 10^{-16} S m^{-1} to 10^{-12} S m^{-1}. Indeed, polymers are used as an insulating coating material for electric wires to prevent them from short-circuits. The milestone discovery of conducting polymers (CPs) by Heeger, MacDiarmid, and Shirakawa in 1977,[1] however, has overturned this concept. Originally, polyacetylene, the first generation conducting polymer (Figure 1.1), prepared by Shirakawa by polymerizing acetylene over Ziegler-Natta catalyst, was an unstable non-conducting material. However, Shirakawa and MacDiarmid found that after exposing a neutral polyacetylene film to chlorine, bromine, or iodine vapor, it acquired 10^9 greater conductivity than the original unexposed film. The principle behind this phenomenon is that the oxidizer (halogen) vapor takes one electron away from the π-electron system of the polymer, creating a "hole" – that is p-doping – in the conjugated backbone. This "hole" causes the polymer to have positive charge and this charge can spread along the polymer backbone, the phenomenon which is called "delocalization" or "conjugation", thereby giving the term "conjugated polymer", and resulting in increasing conductivity. The conductivity increase can also be explained by using an approach derived from the band theory.

Although the doped polyacetylene used to be called "organic metal" for it featuring a significant conductivity, it found very little practical applications because of the unstable nature of the polymer under ambient conditions and low processability due to extremely low solubility in any organic solvent.

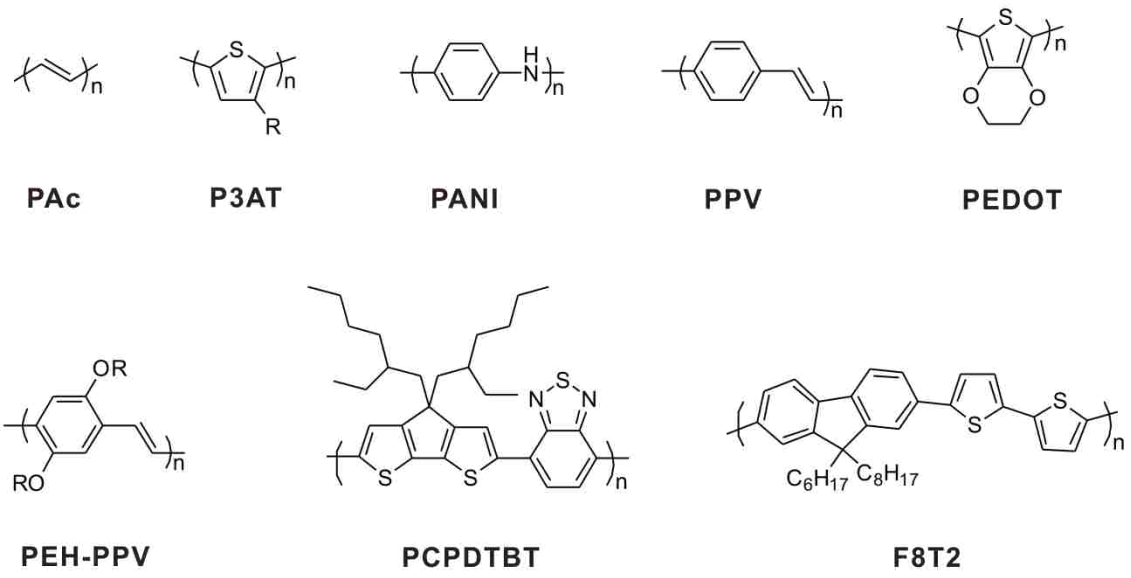

Figure 1.1. Molecular structures of representative conjugated polymers.

Further on, second generation conjugated polymers have been investigated extensively since 1980s to address the issues with polyacetylene by introducing a ring structure with more atoms having not only carbon but also sulfur or nitrogen in a repeating unit, and installing alkyl side chains as solubilizing groups. Typical representatives of this generation of conjugated polymers, such as poly(akylthiophene) (PAT),[2] polyaniline (PANI),[3,4] or poly(*p*-phenylene vinylene) (PPV)[5] derivatives are shown in Figure 1.1. Despite these polymers being not as highly conductive as doped polyacetylene (their conductivity lies within the range from 10^{-2} to 10^{4} S m^{-1} [1] for what they have been named "semiconducting polymers"), this is enough for the application of these polymers in organic devices. The third generation CPs, arguably the most important class nowadays, are very attractive to researchers and have more intricate structures (Figure 1.1). Donor-acceptor (DA) type copolymers have emerged in the recent years since Havinga and colleagues[6,7] first introduced them in 1992. The DA copolymers are defined by alternating units with electron-rich and electron deficient properties along a polymer backbone. Such architecture

lowers down the band gap through the so called "push and pull" effect, and results in shifting spectroscopic characteristics of the polymer towards the lower energy end of the spectrum. This particularly benefits photovoltaic applications as it allows to increase the number of absorbed solar light photons and thus to improve the efficiency of the device. Besides investigation into new conjugated polymers in terms of molecular structure, further attempts to increase crystallinity of the known CPs became a major area of interest in the organic polymer materials field.[8-10]

These days, applications of CPs are being extensively developed, ranging from compact-size capacitors,[11,12] electromagnetic shielding films, and antistatic coatings[13] to high-performance organic electronic elements such as light-emitting diodes (OLEDs),[14-16] organic field-effect transistors (OFETs),[17-19] chemo- and biosensors,[20-22] organic photovoltaic devices (OPVs)[23-27] holographic elements,[28-30] and logic gates.[31] Despite plethora of these remarkably promising applications, there are still numerous issues remaining to fully understand physical/chemical properties of CPs and to deliver large-scale commercialization of CP-based devices. For example, although development of OPVs has produced spectacular achievements in the past decade, total efficiency of organic polymer solar cells still remains around 10%, a relatively low value to allow effective commercialization. The minimum efficiency of a photovoltaic device to make it commercially successful should be approximately 15-20%. In addition to efficiency, mechanical and chemical stability of most organic electronic devices against external factors such as light, pressure, humidity, etc. is poor compared to inorganic devices, which mainly comes from the nature of the device fabrication processes or inherit properties stemming from the molecular structure of CPs. In the next sections of this chapter, the origin of those undesired issues will be

explained, and several suggested improvement solutions developed by the research community over the past years will be discussed.

1.2. Anisotropy of CP thin films and its effect on bulk morphology from nano- to macroscale

Before getting deeper into discussing those issues mentioned above, one must understand fundamental phenomena happening during opto-electronic processes in a device, and we will discuss them with a focus on OPVs. Below is the description of generally accepted processes happening in organic polymer solar cells (Figure 1.2).

1) Absorption of incident light (typically in the donor layer) and generation of excitons.

2) Diffusion of the excitons to the interface between donor and acceptor layers.

3) Dissociation of the excitons into positive and negative charge carriers.

4) Charge transport and charge collection toward electrodes.

In addition to these principal steps, there may be other possible mechanisms,[27,32] involving more complicated steps occurring during the exciton dissociation/charge transport events (e.g. formation of charge-separated state [CS state], ground-state charge transfer complex [CTC], etc.). We will not be discussing these mechanisms, as they are rather more complicated, and at the end lead to the same basic conclusions on the functioning of an organic solar cell. Therefore, it is reasonable to limit the discussion by the opto-electronic process with four elementary steps mentioned above. Particularly, exciton and charge transport property will be discussed here in terms of architecture of the CP active layer, called the donor-acceptor layer.

Theoretically, one isolated CP chain (for example, polyacetylene chain) is a one-dimensional material possessing a single electronic feature along backbone of the chain, π-conjugation. With multiple CP chains in a condensed system, however, interchain interactions

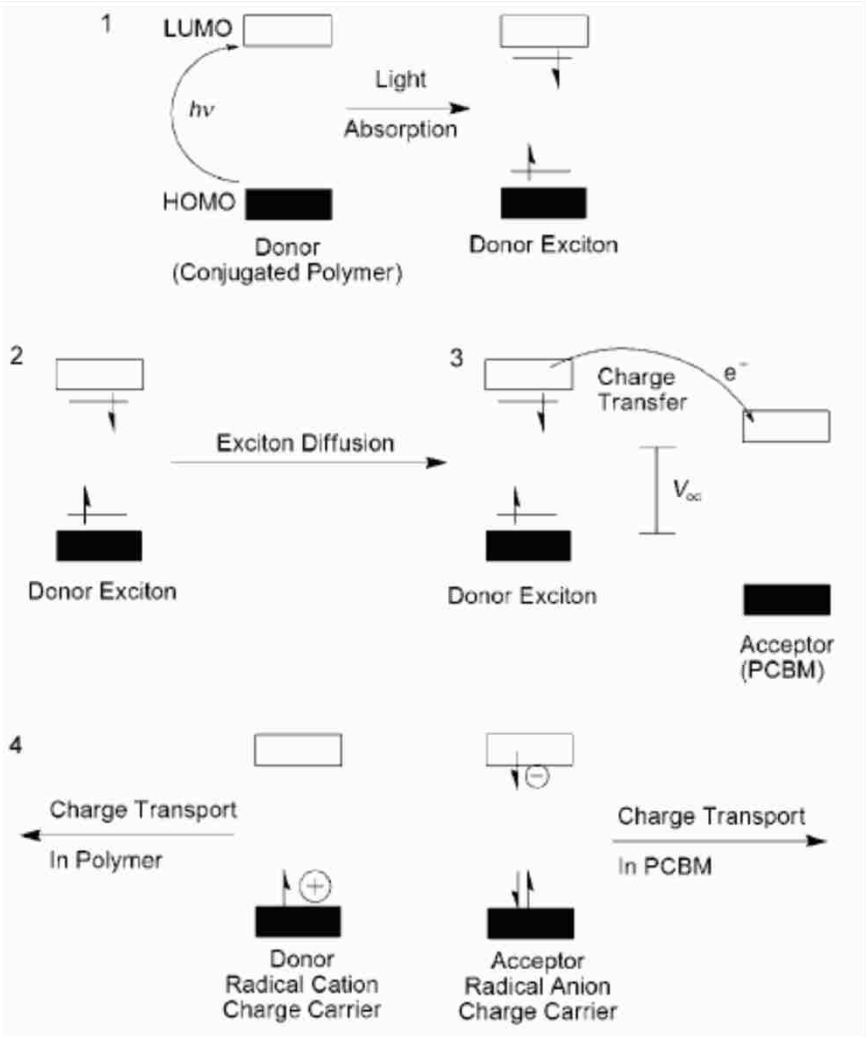

Figure 1.2. Simplified photoexcitation process in OPV. Reproduced with permission from Ref. 32 Copyright © 2008 WILEY-VCH Verlag GmbH & Co. KGaA, Weinheim.

such as formation of weak bonds through π-electron systems, van der Waals forces, and hydrogen bonding between the chains can occur. Since strength of intrachain π-electron interactions within CPs is substantially different from that of interchain electronic interactions, with at least an order of magnitude difference, CPs in a bulk system inherently possess an anisotropic nature, with anisotropy extending to their physical/chemical properties, and electrical/optical properties as well.[33,34] Due to such an anisotropy, intramolecular charge mobility along the polymer backbone, $\mu_{\parallel}$, is substantially greater than intermolecular charge

mobility occurring by hopping between chains, $\mu_{\perp}$, because associated intrachain bandwidth is comparably greater than interchain bandwidth.[35,36] Polyacetylene crystal is a simple and well-defined system to investigate anisotropy of the charge mobility in CPs, as polyacetylene is capable of forming a highly conjugated system with a nearly perfect single crystal structure. Bleier et al.[37] determined in their research that charge mobility along the backbone of *trans*-polyacetylene (intramolecular charge mobility) was 50 times higher than that of in a transverse direction (intermolecular charge mobility). Hoofman et al.[33] studied anisotropic nature of charge mobility for polydiacetylene-(bis-*p*-fluorobenzene sulfonate) (pFBS) using pulse-radiolysis time-resolved microwave conductivity (PR-TRMC) technique which revealed that mobility along the backbone was at least an order of magnitude higher than in the transverse direction. According to these anisotropy studies, it is well established that ideal molecular conformation and alignment of CP chains for a best-performing device are such that intramolecular pathways orient in the direction toward the electrodes for enhanced charge mobility (Figure 1.3C) rather than when intermolecular charge transfer pathways are respectively for bridging two electrodes (Figure 1.3A and 1.3.B). Fabricating active layers fitting this ideal model with other CPs, however, has

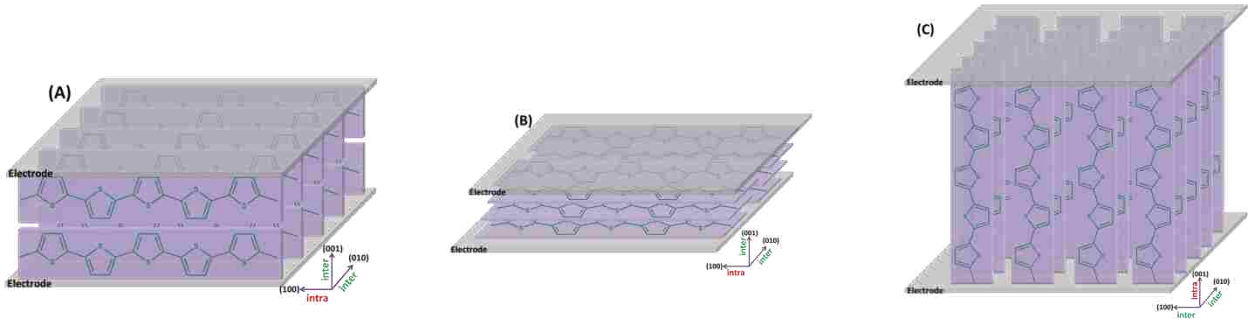

Figure 1.3. Schematic ideal architectures of a conjugated polymer in an OPV with different geometry (a) edge-on orientation, (b) face-on orientation, and (c) vertical orientation. Green color represents "intermolecular" direction. Red color shows "intramolecular" direction.

been highly challenging and remained subject of interest for over a few decades.

For practical purpose, flexible CPs (as alluded above, most likely the first generation CPs shown in Figure 1.1) are easily made into an "ideal" single crystal by simple solid state topological polymerization or other simple practical methods,[32,37] which can be a convenient experimental model for theoretical treatment of anisotropy measurements. More recently developed CPs have a more rigid and sophisticated molecular structures causing more complicated interactions between chains as well as along the backbone (for instance, poly(3-alkyl-thiophene) (P3AT) or its derivatives that comprise second and third generation CPs). No methods can achieve a nearly ideal single crystal system with these CPs to measure absolute anisotropy of charge mobility but a number of studies were carried out utilizing indirect controlled crystallization, (e.g., high-pressure crystallization,[38,39] mechanical blade/rubbing method,[40] post-deposition procedures [thermal or solvent annealing],[41] mechanical stretching,[42-44] formation of nanofibrils,[45] or lithography technique, etc.[46]). As a consequence of the inability of these indirect methods to achieve full control over crystalline organization, only partially ideal arrangement could be recorded; thus, the anisotropic nature of CPs including charge mobility can vary depending upon experimental conditions and measurement methods. In addition, due to the finite molecular weight of CPs and the intrinsic disorder disturbing linearity of the chain, charge transport through metal electrodes in a device is always limited by interchain transport process. Therefore, various factors, such as structure of repeating unit, molecular weight, chain conformation, and crystallinity, which are fundamental features to control nano/mesoscale (even up to macroscale) morphology, have been thoroughly investigated with the goal to achieve high charge mobility.

In general, three primary features have major influence on morphology and charge transport of CPs based on bottom-up construction of a polymer architecture. First is the nanoscale molecular assembly controlled by intermolecular interactions (Figure 1.4A).[47] Each repeating unit in different chains can electronically overlap through intermolecular interactions to display distinct spatial arrangements depending on the angle between the interaction direction and transition moment of the chain direction; this can result in appearance of J-aggregation or H-aggregation as can be assessed from absorption and emission spectra. These spatial arrangements are significantly affected by the shape of the repeating unit and a chain conformation which is caused by the side chain configuration (so called regioregularity); for instance, head-to-tail, head-to-head, or tail-to-tail poly(3-alkylthiophene) (HT-, HH-, or TT-P3AT). HH- and TT-P3ATs display substantial steric repulsion between the neighboring repeating units due to close proximity between side chains causing torsional twisting of the polymer chain backbone.

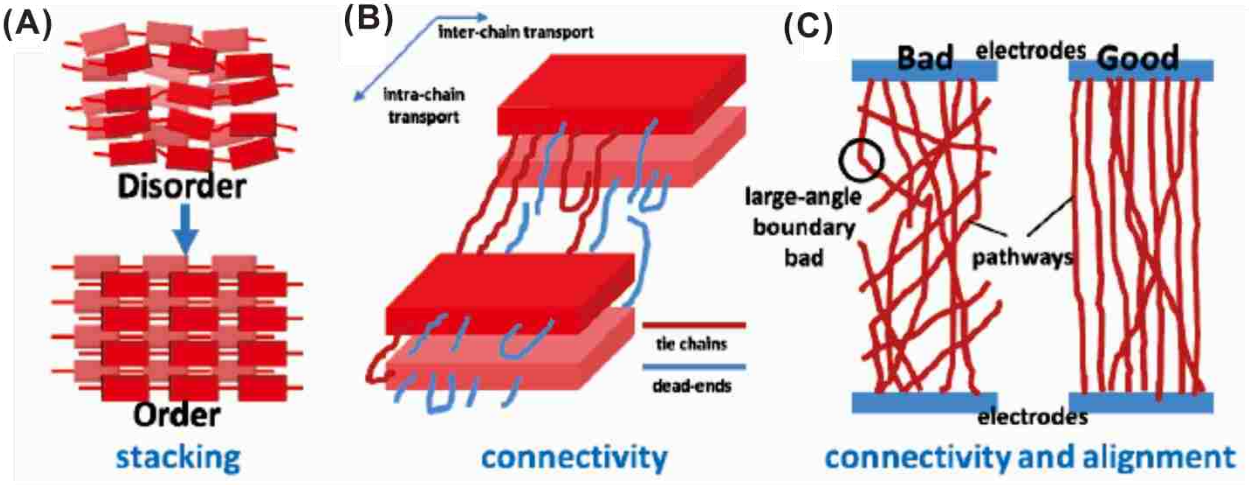

Figure 1.4. A general scheme of the three primary classes of the bottom-up construction of a conjugated polymer architecture. (A) nanoscale molecular assembly, (B) connectivity at meso-, microscale, and (C) macroscale alignment. Reproduced with permission from Ref. 47 Copyright © 2013 Elesvier

The twisted chain would disturb conjugation along the backbone introducing an energy barrier, and then eventually reducing intramolecular charge transport. It also causes intermolecular interaction to be less favorable and therefore decreases portion of crystalline region in a system.[47]

Connectivity between polymer crystalline regions at the meso- or microscale is the second feature that contributes to the efficiency of charge transport. Since commonly used CPs are prone to have a polycrystalline or semicrystalline nature (with each crystalline region introducing distinct energy states), one must take into account connectivity between neighboring grain boundaries of the crystalline regions (Figure 1.4B). Different ways to connect crystalline domains result in formation of energy barriers, with larger barriers interrupting charge transport pathways and causing charge carriers to be trapped at the grain boundaries. A grain boundary of the crystalline regions may consist of three types of chains: chain ends, chain folding (sometimes called loop), and tie chain that interconnects two different boundaries.[47] The chain end and folding induces the intermolecular charge transfer by hopping, which obviously decreases the transport efficiency. Meanwhile, in the case of the tie chain connection, charge can travel through the intramolecular pathway, thus resulting in the increased transport efficiency. In good agreement with this notion, the ratio between the chain end/folding and the tie chain was demonstrated to be associated with the average charge mobility.

The final feature responsible for the charge transport is the total fraction of crystalline region and its alignment from microscale to macroscale (Figure 1.4C). It is clear that the higher total fraction of the crystalline region in a film corresponds to fewer grain boundaries and therefore the existence of more efficient charge transfer pathways; resulting in the overall better charge transport characteristics. Thus, an ideal system would be the one in which CP is

composed of a single crystal over an entire device (or at least, large crystalline fraction in the thin-film device). Kim et al.[9] reported that a microdevice made of a high quality single crystal poly(3-hexylthiophene) (P3HT) wire prepared by a self-seeding method from a dilute polymer solution featured high-current sensing with a well-resolved gate modulation of the channel conductance and demonstrated higher field-effect mobility relative to a similar geometry device prepared using a crystalline 3-hexylthiophene oligomer. The difference was mainly due to enhanced intramolecular charge transport along the aligned polymer backbone spanning across the electrodes.

Li et al.[10] fabricated an organic single crystal donor-acceptor heterojunction device utilizing pinned droplet of a mix solution, which crystallized in a sequential fashion introducing extended single-crystalline heterojunctions with consistent donor-top and acceptor-bottom structure over the device.

In summary, CPs are intrinsically anisotropic, with the efficiency of charge transport along the conjugated backbone (intramolecular transport) being different than the efficiency of charge transport in between the neighboring chains (intermolecular transport). For an ideal case, intramolecular charge transport always overwhelms intermolecular charge transport, so that a best-performing ideal device must be composed of single crystalline CP chains aligned in a way that CP chains span the gap between two electrodes along with the electrode direction, so called "edge on", in order to connect electrodes via intramolecular pathway. Unfortunately, due to inherent limit on the polymer molecular weight and disordered nature of CPs, anisotropic characteristics of CPs, including charge transport, are always limited by contribution from intermolecular pathway. Therefore, the bulk polymer morphology, ranging from nanoscale to

microscale, plays an important role in electrical properties of CPs, and controlling the morphology has remained challenging over several decades.

1.3. Conventional fabrication methods toward the ideal CP thin film for organic electronics

The first generation of OPVs was reported in 1980s and early 1990s using polyacetylene[48] or poly(*p*-phenylene-vinylene) (PPV)[49] as a component of a single layer. Their total efficiency was too low, typically from 0.001 to 0.01%, to be commercialized.[50] From a physical standpoint, the lifetime of an exciton is less than 1 ns and therefore during the lifetime it can travel only a few nanometers (generally within 5 to 10 nm).[51] This is substantially shorter than a thickness of CP layer required to absorb reasonable amount of photons for a single layer device; this issue equally affects a bilayer device shown in Figure 1.5A. Thus, only a low number of initially generated excitons are able to reach to the phase interface resulting in a low efficiency. In 1992, Sariciftci et al.[52] discovered the ultrafast electron transfer (<100 fs) that occurred between poly(2-methoxy-5-(2-ethyl-hexyloxy)-1,4-phenylene vinylene) (MEH-PPV) as a donor component and buckminsterfullerene (C_{60}) as an acceptor on a time scale considerably faster than time decay of the exciton. Then, a few years later, bulk heterojunction (BHJ) solar cell with bicontinuous phase segregation was demonstrated. Yu et al.[53] first described a BHJ solar cell containing a mixed working layer with MEH-PPV and C_{60} derivative, PCBM, having a high energy conversion efficiency depending upon mixing ratio (maximum efficiency up to 2.9 % could be achieved). This value was at least two orders of magnitude higher than that of the previous single layer solar cell devices. A key factor in increased efficiency of this device was that the acceptor, MEH-PPV, and the donor, PCBM, formed continuous interpenetrating networks in an active layer derived by spontaneous phase separation. Consequently, it introduced relatively large interface area between the donor and the acceptor phases, which allowed charge

separation to occur, and gave a shorter distance for each charge to travel toward electrodes. This phase separation originates from reaching thermodynamic equilibrium as a result of interplay between interfacial energy, solubility, and crystallinity of each component. On the basis of morphology issues mentioned above and numerous theoretical/experimental studies of photoexcitation process, the ideal architecture of a BHJ solar cell device for the best performance has been suggested (Figure 1.5B).

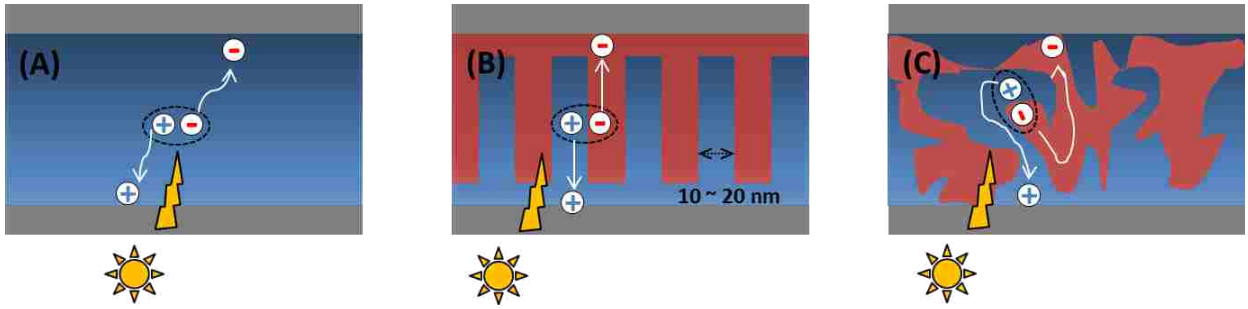

Figure 1.5. Schematic diagrams of solar cell devices and charge transport pathway in (A) single layer, (B) ideal bulk heterojunction layer, and (C) real bulk heterojunction layer.

1) Phase separation between the donor and acceptor domains should be formed at the 10 - 20 nm length scale to allow for excitons traveling without non- or radiative decay.

2) A columnar-like and continuous architecture through the working layer towards electrodes is needed for the fast and efficient charge transport; thus, highly ordered alternating donor-acceptor crystalline structures with continuous pathways, as close as possible to a perfect periodic structure, would be required.

Since the initial introduction of the BHJ solar cell concept, there has been a rapid progress towards achieving the ideal morphology for enhancing the device performance. Indeed, a wide variety of device fabricating methods have been explored, but most common ways for OPVs remain solution-based spin casting,[54] roll-to-roll casting,[55] or inkjet printing,[56] to target

control of weak intermolecular forces, leading to a large amount of disorder. Thereby, many parameters have been identified which can influence morphology of the working layer, such as choice of solvent,[57-59] polymer molecular weight,[23,60] various post-deposition treatment,[61] etc.

Solvents for each donor and acceptor component govern solubility of them, which affect domain size, miscibility, or crystallinity. For example, it is well known that using chlorinated aromatic solvents during device fabrication results in substantially better efficiency for a solar cell device prepared with PCBM as an acceptor than using non-polar solvents like toluene, hexane, or even THF.[62,63] TEM images for an active layer with toluene revealed PCBM-rich domains with around 600 nm size, which was one order of magnitude larger than the size suggested for the ideal case. On the other hand, despite the similar crystalline structure of PCBM-rich domain (as confirmed by selected area electron diffraction (SAED)), chlorobenzene as a solvent provided PCBM-rich domains with 80 nm size, thus resulting in higher photovoltaic efficiency.

The higher the molecular weight of CPs, the larger the fraction of the tie chains connecting the grain boundary, which increases charge mobility as was described in the previous section. However, since a long CP chain folds with more defects compared to a short CP chain, there is a certain limit on how much the optical and electronic properties of CPs can be changed by simple increasing the polymer chain length. In addition, π-electron conjugation length along a polymer chain, in which photoexcitation can proceed without significant energy loss, is restricted by intrinsic nature of long-chain molecules, such as rotation of bonds, formation of kinks, or folding. Therefore, increasing molecular weight of CPs beyond a certain point generally does not significantly influence optical/electronical properties of the CPs.

Annealing, the most widely used procedure for post-deposition treatment, is also a common method to control morphology. One can simply change a fraction of crystalline region or align direction of crystalline domains by heating the active layer up to the glass transition temperature of components, and allow kinetically slow phase separation to facilitate formation of crystalline architecture within the domains. Solvent annealing enables reorganization of crystal structure of the domains in the same way as the thermal annealing does. However, it is recognized that the efficiency of the annealing process in enhancing the device performance depends on the nature of constituents. For example, in poly[2-methoxy-5-(3′,7′dimethyloctyloxy) -1,4-phenylenevinylene]/PCBM (MDMO-PPV/PCBM) system, annealing always forces the

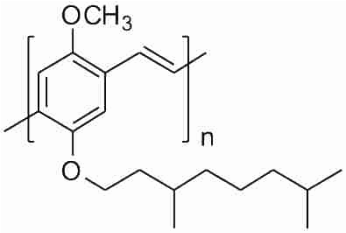

MDMO-PPV

polymer to form large domain aggregations therefore resulting in large PCBM single crystals, which causes low efficiency in a solar cell.[41] This was explained by the different diffusion rates and crystallization kinetics for each component: PCBM can easily diffuse into MDMP-PPV domains forming single crystals and increasing domain size. In contrast, annealing for P3HT/PCBM system always improves device performance. A series of publications[64,65] have revealed that the annealing process introduced and stabilized a nanoscale interpenetrating network with crystalline order of components by rearranging long and thin single crystal P3HT nanowires into PCBM domains therefore resulting in improving total crystallinity of the layer.

In addition to the several important factors mentioned above, other parameters have been also elucidated as having a major influence on morphology and device performance. Among these parameters are compound ratio,[66,67] polymer regioregularity,[68] and the presence of various impurities.[69] However, most procedures produce rather random crystal structures and greatly mixed morphologies of the active layer, which leads to disconnection of exciton or charge transport, appearance of energy barriers between domains, energy loss, and eventually low efficiency of a device, as depicted in the previous sections. No method to date can deliver a simple way to make the intramolecular pathway for charges and excitons through electrodes over an entire active layer, instead, the semi-crystal structure is dominated across the films, because of the lack of ability to precisely control CPs on the surface (Figure 1.5C). Therefore, in order to accomplish an optimized morphology, further study is required for direct control of the CPs structure and thin-film morphology.

Another drawback of the previously mentioned approaches is low thermal and photostability of an active layer composed of organic CPs. Various structural factors such as rigidity of molecular structure, high molecular weight, strong inter/intramolecular interactions of CPs, etc. render significant aggregations, therefore solubility of CPs can dramatically drop without the presence of solubilizing substituents. Thus, the presence of long solubilizing side chains for enhancing solubility of CPs is inherently necessary for classical solution-based fabrication methods (e.g. spin-coating, roll-to-roll, or inkjet printing). A fundamental problem with solubilizing substituents is that they are a potential site for photodegradation, either with or without presence of moisture and oxygen. It has been shown that, for PPV or MEH-PPV systems, photo-oxidation occurring not only on the phenylene part but also on the vinylene part and side chains contributes to the degradation process.[70] Despite P3AT being more stable than MEH-PPV

system against photodegradation (P3HT can last around 700 h before complete photobleaching[71]), it also undergoes photo-oxidation reaction that would occur on the α-hydrogen of an alkyl chain via superoxide oxygen anion formation turning the chain into an acid or aldehyde group (Figure 1.6A).[72] This process also induces chain scission to break the CPs backbone; this is reflected in the gradual decreasing intensity of the P3AT 600 nm band in UV/vis spectra. Thermo-cleavage of the alkyl side groups is another possible pathway for the degradation during thermal annealing. Frechet and coworkers[54] found that, in poly-(3-(2-methylhexyloxycarbonyl)dithiophene) (P3MHOCT)/PCBM system, carboxylic ester group of 2-methyl-2-hexanol side chains underwent cleavage into carboxyl groups upon heating at around 200℃. Further heating up to 300℃ resulted in complete degradation leaving unsubstituted polythiophene that formed an insoluble component. This dramatic degradation altered the morphology of the active layer and ultimately changed the optical properties of the device (Figure 1.6B).

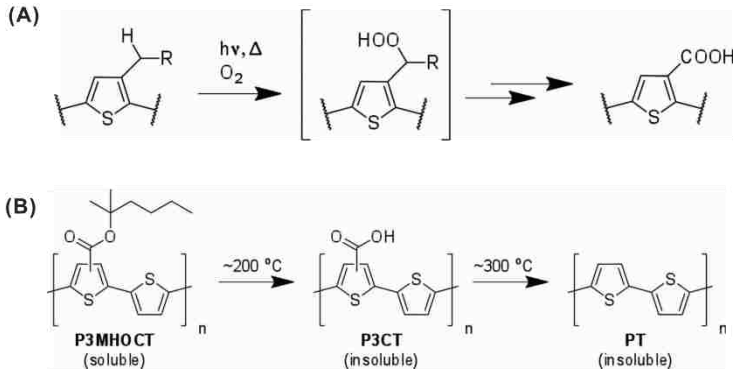

Figure 1.6. Examples of possible degradations (A) photodegradation pathway of P3AT. Reproduced with permission from Ref. 72 Copyright © 2010 Elsevier (B) thermal pathway with annealing on P3HMOCT layer. Reproduced with permission from Ref. 54 Copyright © 2007 American Chemical Society

In conclusion, through consideration of the morphology and the stability issues, it becomes clear that even though the classical device fabrication approaches based on solution processing of CPs ("top-down" paradigm) have been rapidly growing over the last few decades and remain the most accessible ways to prepare CP-based devices, there is still a substantially large gap between the perfectly controlled ideal system and the real world. Consequently, "bottom-up" paradigm (e.g., surface-initiated polymerization via an electrochemical or chemical reaction) has been an attractive emergent field offering an alternative approach for device fabrication[54] which can enable precise and simple control over the CP's structure depending upon the polymerization reaction conditions. In the following section, I will briefly cover a general concept of the "bottom-up" approach and go into details of surface-initiated polymerizations.

1.4. Development of bottom-up strategy for CP thin films

1.4.1. Overview

The "bottom-up" approach (Figure 1.7.B) is a counter strategy to the "top-down" method (Figure 1.7.A), and it aims to directly grow polymer brushes on the surface via electrochemical or chemical reactions of monomer molecules. For surface-initiated polymerization, the process begins from a catalytic initiator molecule attached on the target inorganic solid substrate (it could be a flat surface or nano- to microparticle of any shape) through physisorption or chemical bonding with an anchoring group (it can be a polymerization monomer itself or a particular external initiator depending on the reaction system), and therein the entire polymer chain connects to the surface by a physical or chemical link. Due to this feature, the surface-initiated polymerization has several advantages over the top-down methods.[73]

The most impressive aspect is the improved physical/chemical properties of the polymer thin-film system. Since the polymerization starts from the sterically crowded surface, this forces the growing polymer chains to end up as conformationally stretched molecules uniformly oriented at a certain angle with respect to the surface normal. This uniform organization would be very hard to accomplish using any of the top-down procedures. Although some adjustments and modifications to this general model (as was proved in our study of thin films described in a later chapter) may be required, it is clear that at least transition moment of CP chains (which is a preferred intramolecular transport pathway) shows an upward overall orientation. This unique

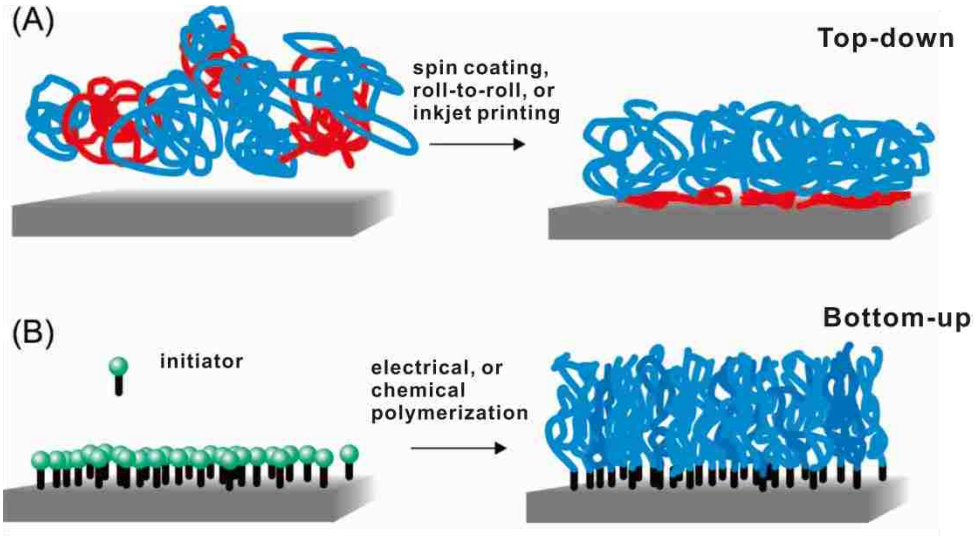

Figure 1.7. Schematic of "top-down" and "bottom-up" approaches for fabricating CP films. (A) Top-down approach. (B) Bottom-up approach. Black rods and green balls are anchoring groups and initiators, respectively. Reproduced with permission from Ref. 75 Copyright © 2009 American Chemical Society

chain architecture would particularly benefit applications requiring charge transport across the film, such as OPV applications.[74] In addition, if one can grow polymer chains long enough to form relatively thick films (i.e. beyond 100 nm thickness) in order to absorb large amount of

photons, it could enable charges or excitons to travel along the chains to the electrodes without disconnection, yielding significantly improved charge transport characteristics.

Another important characteristic of a thin film prepared using bottom-up procedure is substantially increased stability relative to the films obtained using solution-based traditional fabrication procedures. As mentioned above, the solution-based methods inherently require conjugated polymers to possess long alkyl substituents to increase solubility of CPs, which would increase the possibility of photo- and thermal degradation under the device operating conditions. On the other hand, surface-initiated polymerization which occurs at the interface between the substrate and monomer solution, i.e. in heterogeneous conditions, does not require having solubilizing substituents unless a reactive monomer used in the polymerization itself has low solubility. Hence, one would expect that thin films prepared by surface-initiated polymerization would be substantially more stable against environmental factors such as light and oxygen, but also will resist mechanical actions such as sonication; these important characteristics will be considered in the later chapters. Moreover, from a geometrical standpoint, the bulky solubilizing substituents can cause steric repulsion between the chains resulting in low surface coverage with CPs on the surface as well as slowing down the polymerization rate. Thus, when surface-initiated polymerization is carried out with substituent-free monomers, one can expect higher density of surface coverage by CPs.

Currently, most common surface-initiated polymerizations include either electrochemical polymerizations, or various controlled radical polymerizations. Monomers of CPs, indeed, can be potentially polymerized by electrochemical methods because they easily produce stable radical cations/anions via simple application of proper oxidation/reduction potential on the monomer, and can stabilize these species by conjugation with their π-electrons. Controlled radical

polymerization has little application towards CP preparation, unless CPs are components of a side chain. Instead, a number of transition metal-catalyzed coupling reactions has been widely employed towards surface-initiated polymerization. Until Surface-Initiated Kumada Catalyst Transfer Polymerization (SI-KCTP) had been developed,[75,76] preparation of surface-confined CP thin films by chemical (rather than electrochemical) surface-initiated polymerization remained a challenge in the materials field. In the following sections, we will briefly discuss the electrochemical polymerization and review recent developments along SI-KCTP.

1.4.2. Electrochemical polymerization for the preparation of CP thin films

The first electrochemical synthesis of CPs was carried out in 1862 by Letheby[77] who reported insoluble blue-black shiny powder of polyaniline. At that time, scientists did not understand the nature and structure of this material (or only partially understood it) due to its insolubility and lack of general knowledge of polymer field, as well as unavailability of suitable analytical tools for structural characterization. Before Heeger, MacDiarmid, and Shirakawa discovered doped polyacetylene in 1977[1] and a few attempts for CP films at the electrode surface, the electrochemical polymerization had not been considered as a general synthetic way. Nowadays, various CP films resulting from the electrochemical polymerization of pyrrole,[78] aniline,[79] thiophene,[80] and fluorene,[81] among other monomers, have been prepared and thoroughly investigated.

While a number of applications of electrochemically prepared CP films, such as stimuli-responsive surfaces,[82] charge transport layers,[83] and sensors,[84] have been accomplished recently, several aspects including better understanding of mechanistic details must been considered for further utilizing electrochemical polymerization in preparation of thin films for organic electronics as they decisively affect the quality of the fabricated thin-film materials. Unlike

controlled radical polymerization, the mechanism of electrochemical polymerization does not follow a simple chain propagation, but it more likely goes in a step-growth fashion[85] involving initial formation of σ-oligomers, radical-radical (RR) coupling between the oligomers, proton elimination, followed by nucleation and growth. Additionally, the debates about involvement and role of σ-mers, radical-radical (RR) coupling, or Coulombic repulsion still remain open. Despite the σ-mers intermediate has been generally accepted, some evidence obtained by UV/vis, NMR spectroscopies, ESR, and cyclic voltammetry (CV) confirm that π-mers can also exist during electropolymerization and decay very quickly, and therefore would not be able to participate in the subsequent polymerization step.[86-88] Radical-radical (RR) coupling is another factor to be considered due to the presence of Coulombic repulsion. Although theoretical analysis including Debye-Smoluchovski theory[89] and kinetic experiments[90] state that even small charged molecules could be coupled to make dimer, it is clear that Coulombic repulsion is a retarding factor for the polymerization. Indeed, kinetic rate is increased during electrochemical polymerization carried out at low temperature due to the reduced Coulombic repulsion.

Besides several ambiguous mechanistic issues, many reaction conditions crucially impact properties of the fabricated materials. Based on a way to apply electric potential to the reaction, one can distinguish three polymerization methods: potentiodynamic, potentiostatic, and galvanostatic polymerization. Potentiodynamic polymerization utilizes sweep of potential ranging between oxidation and reduction potentails so that a final product would be neutral. Meanwhile, potentiostatic and galavnostatic polymerizations are carried out at a constant potential so that the material ends up doped at the end of the polymerization. In case of potentiodynamic method, due to successive sweeping within the range of redox states, solvent molecules can be entrapped into a polymer matrix or incorporated with the oligomers. Then,

volume of the polymer matrix would be expanded or impure polymer chains can be produced.[85] From a mechanism standpoint, the electrochemical coupling reaction can lead to rather disordered polymers instead of polymers with a perfect chain structure as different positions in a monomer molecule, particularly for monomers with no substituents, can be available for the coupling reaction (see Figure 1.8, where three possible sites, i.e., para- and two meta- positions, are available for the coupling at the beginning of polymerization[91]), or isomeric radicals can be formed. Another important feature is the difference in electrochemical potentials between monomer, oligomer, and polymer molecule, meaning that each monomer addition step has its own

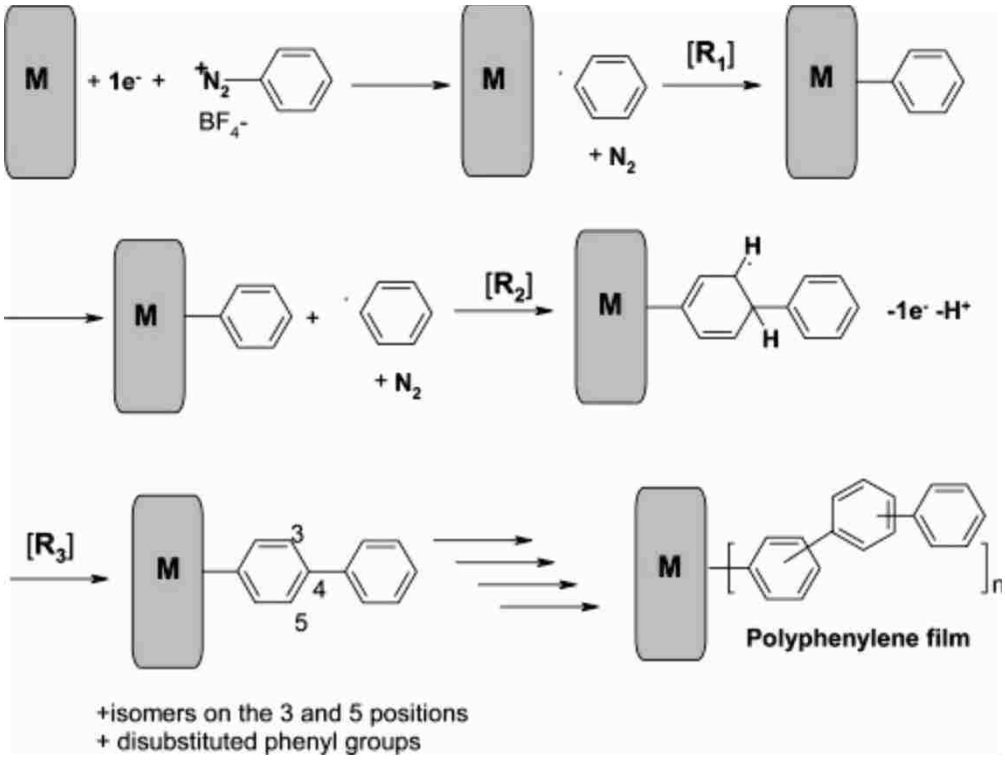

Figure 1.8. Possible reaction pathway for electrochemical polymerization to afford disordered polyphenylene films on the metal electrode. In this polymerization, three possible C-C couplings can occur: one through para- and two through meta-positions. Coupling at the ortho-position is less favorable due to steric hindrance. But as polymer chains grow, coupling at the ortho-position also becomes possible. Reproduced with permission from Ref. 90 Copyright © 2006 American Chemical Society

potential barrier as polymerization propagates.[85] Therefore, the kinetic rate is continuously altered through the polymerization. This kinetic rate change results in different length and structure of polymer chains at the end of the polymerization, thus hindering precise control of the reaction. The last factor to be considered is temperature. The monomer coupling reaction rates and proton elimination rates, which are chemical processes, are changed with temperature, and therefore affect the reaction in an opposite way of Coulombic repulsion.[85] Generally, the Coulombic repulsion increases as raising temperature, hence, at higher temperature, σ-intermediates are either decayed quickly or cannot form at all. This feature would hamper the coupling reaction. On the other hand, increasing temperature generally renders high kinetic rates, which affords long polymer chains. As a result of interplay between all these factors, electrochemical polymerization is mechanistically very complicated, and strongly dependent on even small experimental condition changes, which generally results in low reproducibility.

1.4.3. Metal-catalyzed surface-initiated polymerization for the preparation of CP thin films

As stated in the overview section, surface-initiated polymerization is to grow polymers from polymerization initiators pre-anchored on the surface using a certain appropriate polymerization protocol such as ATRP,[92] or RAFT.[93] Since, in this approach, one can implement the same polymerization techniques as in solution, accurate control over a polymerization process would be conveyed by various factors (e.g. reaction time, temperature, monomer to initiator feed ratio, etc.) so that not only nanoscale organization but also macroscale ordering would be implemented precisely. However, it is worth noting that, in the "bottom-up" paradigm, not all polymerization methods mentioned above can be applied to prepare CP films, because most of the available polymerization techniques for CPs (based on Suzuki, Heck, or Stille coupling, etc.) follow a "step-growth" mechanism. Polymerization processes following step-

growth mechanism generally cannot be used for surface-initiated polymerization as most of monomer quickly proceeds to react in the solution rather than on the surface. Thus, it remained a challenge for some time, until McCullough and Yokozawa recently developed Kumada catalyst-transfer polymerization (KCTP) that follows "living" (or controlled) chain-growth mechanism, and Kiriy first introduced surface-initiated KCTP (SI-KCTP) concept.[94,95]

The first attempt for SI-KCTP was carried out by Kiriy's group[75] using photo-crosslinked poly(4-bromostyrene) films on solid substrates which were treated with a solution of $Ni(PPh_3)_4$ to form surface tethered external Ni(II) catalytic initiators. Due to low reactivity of the external initiator, and interplay with undesirable side reactions such as chain termination, reinitiation, and extensive homocoupling during the oxidative addition of $Ni(PPh_3)_4$ to surface-immobilized bromobenzene precursor, only relatively short P3HT brushes, up to 10 nm long, could be grown on the surface, and the polymerization was accompanied with large amount of precipitation indicating abundance of chain-transfer steps and therefore less robust chain-growth mechanism. Also, the P3HT brushes ended up grafted not only at the film-solution interface but also deeply inside of the interpenetrating poly(4-bromostyrene) network.

Locklin's group[96] has developed a further modified SI-KCTP method to fabricate polythiophene and poly(*p*-phenylene) thin films using Ar-Ni(COD)$(PPh_3)_2$ external catalytic initiator covalently immobilized on a gold surface (Figure 1.9). This Ni(II) initiator is more effective and robust than the Ar-Ni$(PPh_3)_2$Br initiator, resulting in a somewhat higher thickness of the polymer films (14 nm for polythiophene and 42 nm for poly(*p*-phenylene)) and less precipitation in the monomer solution. This indicates that the polymerization takes place on the surface rather than in solution. In order to improve the external initiator's efficiency and increase thickness of the polymer films, Kiriy's group[97] has employed the ligand exchange step with

bidentate ligands to convert Ar-Ni(Bipy)-Br functional group on the Ni center into Ar-Ni(dppp)-Br or Ar-Ni(dppe)-Br, where dppp is 1,2-bis(diphenylphosphino)propane and dppe is 1,3-bis(diphenylphosphino)ethane, which has been proven to be more efficient as external catalytic initiator than Ar-Ni(PPh_3)$_2$-Br or Ar-Ni(Bipy)-Br functional groups (Figure 1.10). In order to do

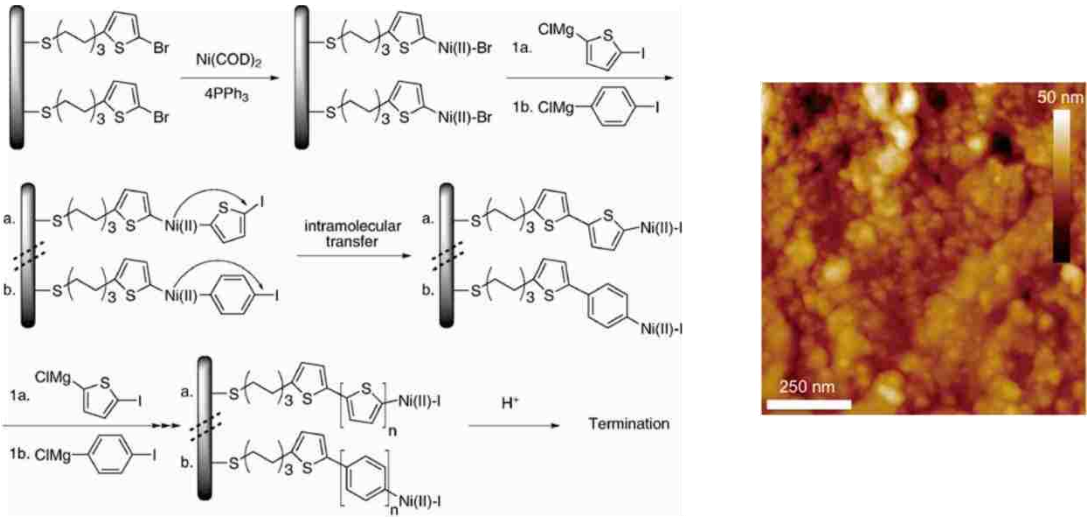

Figure 1.9. Preparation of surface-confined PT and PPP films using surface-initiated polymerization and AFM image of the PPP film prepared by Locklin group. Reproduced with permission from Ref. 96 Copyright © 2009 Royal Society of Chemistry

this, they anchored bromobenzene on silica microparticles using silane chemistry and then reacted it with a Et_2Ni(Bipy) solution to activate end groups followed by a dppp or dppe ligand exchange step to produce Ar-Ni(dppp or dppe)-Br external catalytic initiators covalently immobilized on the surface of the particles. This was followed by polymerization using 5-bromo-3-hexyl-2-thienylmagnesium chloride. Based on SEM, TGA, and GPC studies, they demonstrated thickness of CPs shell to be about 20 nm and determined (after dissolving the silica particles with HF) that the polymer molecular weight was around 40,000 g/mol, with high regioregularity of the P3HT chain. These results revealed significantly improved performance in

surface-initiated polymerization compared to previous methods. However, in terms of overall process, ligand exchange step was a relatively complicated procedure, especially considering that $Et_2Ni(Bipy)$ is unstable, air-sensitive, and not an easily available compound. The limited degree of freedom on the surface can possibly cause steric hindrance between dppp or dppe during the ligand exchange step leaving defects on the surface and low density of the polymer thin films.

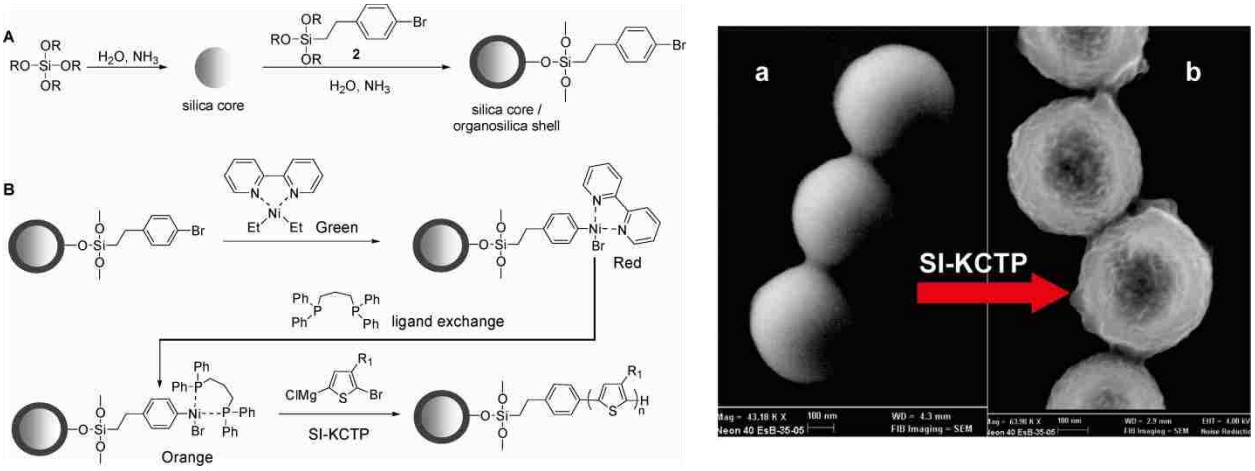

Figure 1.10. Procedure for surface-initiated polymerization utilizing a ligand exchange step as developed by Kiriy group. Reproduced with permission from Ref. 97 Copyright © 2009 American Chemical Society

Moreover, "step-growth" polymerization initiated by $Et_2Ni(Bipy)$ itself was observed to hinder polymerization on the surface and instead prompted polymerization in the monomer solution.

Later, Luscombe group[98] developed another way to prepare an external catalytic initiator for SI-KCTP. They surface-immobilized an aryl halide precursor using a phosphonic acid anchoring group on ITO, then converted it to Ni(II) catalytic species, $Ar\text{-}Ni(PPh_3)_2\text{-}X$, by the reaction with bis(1,5-cyclooctadiene)nickel(0)/$4PPh_3$ ($Ni(COD)_2/4PPh_3$). The ligand exchange step was conducted by immersing the surface-modified ITO slide into a solution of 1,3-bis(diphenylphosphino)propane (dppp) to afford Ar-Ni(dppp)-X as an external initiator (Figure

1.11). As a result, the kinetic of polymerization followed, to a certain level, controlled chain-growth polymerization mechanism, as was confirmed by a reproducible profilometry measurements, and allowed to prepare poly(3-methylthiophene) (P3MT) films with up to 200 nm thickness. The polymer thin film was stable under doping conditions, indicating that it could be used as a potential organic electronic device. Nevertheless, the surface-initiated polymerization rate was slow compared to the similar reaction in solution, and it took more than 1 day to obtain P3MT film with 80 nm thickness. This procedure also required a complicated ligand exchange step, which likely left defects on the surface due to the steric hindrance between bulky ligands.

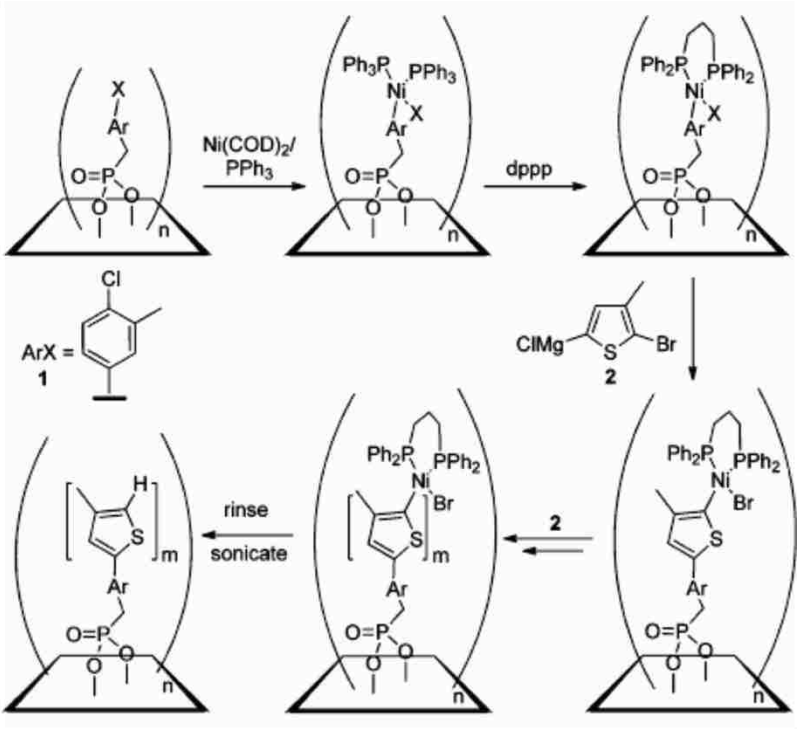

Figure 1.11. Surface-initiated polymerization for poly(3-methylthiophene) film developed by the Luscombe group. Reproduced with permission from Ref. 98 Copyright © 2012 American Chemical Society

1.5. Research focus

Controlling bulk morphology and chain organization of CPs, and preparing thin films with continuous and highly ordered architecture is the key factor for the availability of better performing, robust and reliable organic electronic, optoelectronic, and sensing devices. Numerous and broad research efforts have been carried out to achieve this goal with different approaches ranging from the top-down paradigm (e.g., traditional solution-based spin coating, inkjet printing, or nanolithography) to the bottom-up methods, such as electrochemical polymerization, click reaction, or surface-initiated metal-catalyzed polymerization. Unfortunately, to date, very few processes have been able to achieve the desired structure and morphology with accurate controllability and wide accessibility to fabricate organic devices. There is still a large room to be filled with further research. One of the most attractive approaches, as mentioned in the preceding section, is SI-KCTP. Recent development of SI-KCTP showed potentially great promise to fabricate well-controlled and ordered CP thin-film structures. In principle, this method allows one to grow polymer chains in the general direction along the surface normal, and to precisely control molecular structure and bulk morphology of the resulting thin films. This dissertation research was focused on the development of SI-KCTP with the purpose both to improve this method, and to better understand structural and mechanistic aspects of the surface-initiated polymerization, and of the resulting thin films.

In chapter 2, I discuss a new approach for SI-KCPT using an external catalyst system developed in our laboratory. In particular, we recently developed a simple and efficient way to obtain a highly reactive external initiator, Ar-Ni(dppp)-X, via direct oxidative addition of $Ni(dppp)_2$ to an aryl halide precursor. In the solution polymerization catalyzed by this initiator, we demonstrated that this catalytic initiator can efficiently polymerize thienylmagnesium

monomers in a well-controlled chain-growth fashion to afford polythiophenes with high molecular weight and low polydispersity index (PDI). In this project, I exploited this system for surface-initiated polymerization to afford surface-confined CP thin films. With this method, a thick (up to 100 nm) and uniform polythiophene (PT) film could be obtained within an hour, which is substantially faster than with any other previous methods. Detailed structural studies of the surface-confined PT films using neutron reflectometry (NR), grazing incidence small/wide angle X-ray scattering (GISAXS/GIWAXS), ultraviolet photoelectron spectroscopy (UPS), and other methods revealed a complex and unique structure and morphology of the films. In addition, nanopatterned columnar PT films were prepared by combining surface-initiated polymerization with particle lithography.

One of the major advantages of controlled chain-growth polymerization is that it can be used to prepare structurally well-defined block copolymer thin films. Although many examples of the preparation of block copolymers using KCTP have been demonstrated in solution, no previous attempts have been made using surface-initiated polymerization. Chapter 3 describes our new successful approach for all-conjugated diblock copolymer thin films: polythiophene-*b*-poly(*p*-phenylene) and poly(*p*-phenylene)-*b*-polythiophene films. Using state-of-the-art characterization methods, I confirmed that both the polymerization rate and the photophysical properties of the resulting thin films strongly depends upon the sequence in the block copolymers. I demonstrated that surface-initiated polymerization is a superior method toward CP thin films with complex and well defined molecular architectures for future applications.

In Chapter 4, I applied surface-initiated polymerization to directly prepare a poly(3,4-ethylenedioxythiophene) (PEDOT) film as a hole transporting layer on the surface, without the need to use poly(styrene sulfonate) (PSS) as an additive (which is normally required to enhance

solubility and processability of PEDOT). I used various techniques (such as IR spectroscopy, CV, and AFM studies) to confirm structure and bulk mesoscale organization of the PEDOT films on the surface. Using 4-point probe measurement I demonstrated that oxidative doping of the surface-confined PEDOT film with iodine vapor made conductivity 100 times higher than that of the neutral undoped films.

1.6. References

(1) Shirakawa, H.; Louis, E. J.; Macdiarmid, A. G.; Chiang, C. K.; Heeger, A. J. Synthesis of Electrically Conducting Organic Polymers - Halogen Derivatives of Polyacetylene, (CH)x. *J. Chem. Soc.,Chem. Commun.* **1977**, 578-580.

(2) Roncali, J. Conjugated Poly(Thiophenes) - Synthesis, Functionalization, and Applications. *Chem. Rev.* **1992**, *92*, 711-738.

(3) Chiang, J. C.; Macdiarmid, A. G. Polyaniline - Protonic Acid Doping of the Emeraldine Form to the Metallic Regime. *Synth. Met.* **1986**, *13*, 193-205.

(4) Macdiarmid, A. G.; Chiang, J. C.; Richter, A. F.; Epstein, A. J. Polyaniline - a New Concept in Conducting Polymers. *Synth. Met.* **1987**, *18*, 285-290.

(5) Sakamoto, J.; Rehahn, M.; Wegner, G.; Schlueter, A. D. Suzuki Polycondensation: Polyarylenes a La Carte. *Macromol. Rapid Commun.* **2009**, *30*, 653-687.

(6) Havinga, E. E.; Tenhoeve, W.; Wynberg, H. A New Class of Small Band-Gap Organic Polymer Conductors. *Polym. Bull.* **1992**, *29*, 119-126.

(7) Havinga, E. E.; Tenhoeve, W.; Wynberg, H. Alternate Donor-Acceptor Small-Band-Gap Semiconducting Polymers - Polysquaraines and Polycroconaines. *Synth. Met.* **1993**, *55*, 299-306.

(8) Wang, Y.; Torres, J. A.; Stieg, A. Z.; Jiang, S.; Yeung, M. T.; Rubin, Y.; Chaudhuri, S.; Duan, X.; Kaner, R. B. Graphene-Assisted Solution Growth of Vertically Oriented Organic Semiconducting Single Crystals. *ACS Nano* **2015**, *9*, 9486-9496.

(9) Kim, D. H.; Han, J. T.; Park, Y. D.; Jang, Y.; Cho, J. H.; Hwang, M.; Cho, K. Single-Crystal Polythiophene Microwires Grown by Self-Assembly. *Adv. Mater.* **2006**, *18*, 719-723.

(10) Li, H.; Fan, C.; Fu, W.; Xin, H. L.; Chen, H. Solution-Grown Organic Single-Crystalline Donor-Acceptor Heterojunctions for Photovoltaics. *Angew. Chem. Int. Ed.* **2015**, *54*, 956-960.

(11) Kou, Y.; Xu, Y. H.; Guo, Z. Q.; Jiang, D. L. Supercapacitive Energy Storage and Electric Power Supply Using an Aza-Fused Pi-Conjugated Microporous Framework. *Angew. Chem. Int. Ed.* **2011**, *50*, 8753-8757.

(12) Carlberg, J. C.; Inganas, O. Poly(3,4-Ethylenedioxythiophene) as Electrode Material in Electrochemical Capacitors. *J. Electrochem. Soc.* **1997**, *144*, L61-L64.

(13) Soto-Oviedo, M. A.; Araujo, O. A.; Faez, R.; Rezende, M. C.; De Paoli, M. A. Antistatic Coating and Electromagnetic Shielding Properties of a Hybrid Material Based on Polyaniline/Organoclay Nanocomposite and Epdm Rubber. *Synth. Met.* **2006**, *156*, 1249-1255.

(14) Chen, X. W.; Liao, J. L.; Liang, Y. M.; Ahmed, M. O.; Tseng, H. E.; Chen, S. A. High-Efficiency Red-Light Emission from Polyfluorenes Grafted with Cyclometalated Iridium Complexes and Charge Transport Moiety. *J. Am. Chem. Soc.* **2003**, *125*, 636-637.

(15) Gross, M.; Muller, D. C.; Nothofer, H. G.; Scherf, U.; Neher, D.; Brauchle, C.; Meerholz, K. Improving the Performance of Doped Pi-Conjugated Polymers for Use in Organic Light-Emitting Diodes. *Nature* **2000**, *405*, 661-665.

(16) Kulkarni, A. P.; Tonzola, C. J.; Babel, A.; Jenekhe, S. A. Electron Transport Materials for Organic Light-Emitting Diodes. *Chem. Mater.* **2004**, *16*, 4556-4573.

(17) Facchetti, A. Semiconductors for Organic Transistors. *Mater. Today* **2007**, *10*, 28-37.

(18) Usta, H.; Facchetti, A.; Marks, T. J. N-Channel Semiconductor Materials Design for Organic Complementary Circuits. *Acc. Chem. Res.*. **2011**, *44*, 501-510.

(19) Veres, J.; Ogier, S.; Lloyd, G.; de Leeuw, D. Gate Insulators in Organic Field-Effect Transistors. *Chem. Mater*. **2004**, *16*, 4543-4555.

(20) Chen, L. H.; McBranch, D. W.; Wang, H. L.; Helgeson, R.; Wudl, F.; Whitten, D. G. Highly Sensitive Biological and Chemical Sensors Based on Reversible Fluorescence Quenching in a Conjugated Polymer. *Proc. Natl. Acad. Sci. U. S. A.* **1999**, *96*, 12287-12292.

(21) Thomas, S. W.; Joly, G. D.; Swager, T. M. Chemical Sensors Based on Amplifying Fluorescent Conjugated Polymers. *Chem. Rev.* **2007**, *107*, 1339-1386.

(22) McQuade, D. T.; Pullen, A. E.; Swager, T. M. Conjugated Polymer-Based Chemical Sensors. *Chem. Rev.* **2000**, *100*, 2537-2574.

(23) Kim, J. S.; Lee, J. H.; Park, J. H.; Shim, C.; Sim, M.; Cho, K. High-Efficiency Organic Solar Cells Based on Preformed Poly(3-Hexylthiophene) Nanowires. *Adv. Funct. Mater.* **2011**, *21*, 480-486.

(24) Polman, A.; Atwater, H. A. Photonic Design Principles for Ultrahigh-Efficiency Photovoltaics. *Nat. Mater.* **2012**, *11*, 174-177.

(25) Norris, D. J.; Aydil, E. S. Materials Science. Getting Moore from Solar Cells. *Science* **2012**, *338*, 625-626.

(26) Stals, P. J.; Li, Y.; Burdynska, J.; Nicolay, R.; Nese, A.; Palmans, A. R.; Meijer, E. W.; Matyjaszewski, K.; Sheiko, S. S. How Far Can We Push Polymer Architectures? *Journal of the American Chemical Society* **2013**, *135*, 11421-11424.

(27) Thompson, B. C.; Frechet, J. M. Polymer-Fullerene Composite Solar Cells. *Angew. Chem. Int. Ed.* **2008**, *47*, 58-77.

(28) Hirabayashi, K.; Kanbara, H.; Mori, Y.; Kurihara, T.; Shimizu, M.; Hiyama, T. Multilayer Holographic Recording Using a Two-Color-Absorption Photopolymer. *Appl. Opt.* **2007**, *46*, 8402-8410.

(29) Birnkrant, M. J.; Li, C. Y.; Natarajan, L. V.; Tondiglia, V. P.; Sutherland, R. L.; Lloyd, P. F.; Bunning, T. J. Layer-in-Layer Hierarchical Nanostructures Fabricated by Combining Holographic Polymerization and Block Copolymer Self-Assembly. *Nano Letters* **2007**, *7*, 3128-3133.

(30) Blanche, P. A.; Bablumian, A.; Voorakaranam, R.; Christenson, C.; Lin, W.; Gu, T.; Flores, D.; Wang, P.; Hsieh, W. Y.; Kathaperumal, M.; Rachwal, B.; Siddiqui, O.; Thomas, J.; Norwood, R. A.; Yamamoto, M.; Peyghambarian, N. Holographic Three-Dimensional Telepresence Using Large-Area Photorefractive Polymer. *Nature* **2010**, *468*, 80-83.

(31) Fabiano, S.; Usta, H.; Forchheimer, R.; Crispin, X.; Facchetti, A.; Berggren, M. Selective Remanent Ambipolar Charge Transport in Polymeric Field-Effect Transistors for High-Performance Logic Circuits Fabricated in Ambient. *Adv. Mater.***2014**, *26*, 7438-7443.

(32) Kumar, J. S. D.; Das, S. Photoinduced Electron Transfer Reactions of Amines: Synthetic Applications and Mechanistic Studies. *Res. Chem. Intermed.* **1997**, *23*, 755-800.

(33) Hoofman, R. J. O. M.; Siebbeles, L. D. A.; de Haas, M. P.; Hummel, A.; Bloor, D. Anisotropy of the Charge-Carrier Mobility in Polydiacetylene Crystals. *J. Chem. Phys.* **1998**, *109*, 1885.

(34) Heeger, A. J.; Kivelson, S.; Schrieffer, J. R.; Su, W. P. Solitons in Conducting Polymers. *Rev. Mod. Phys.* **1988**, *60*, 781-850.

(35) Heeger, A. J. Semiconducting Polymers: The Third Generation. *Chem. Soc. Rev.* **2010**, *39*, 2354-2371.

(36) Coropceanu, V.; Cornil, J.; da Silva Filho, D. A.; Olivier, Y.; Silbey, R.; Brédas, J.-L. Charge Transport in Organic Semiconductors. *Chem. Rev.* **2007**, *107*, 926-952.

(37) Bleier, H.; Roth, S.; Shen, Y. Q.; Schäfer-Siebert, D.; Leising, G. Photoconductivity Intrans-Polyacetylene: Transport and Recombination of Photogenerated Charged Excitations. *Phys. Rev. B: Condens. Matter* **1988**, *38*, 6031-6040.

(38) Boudouris, B. W. H., V.; Jimison, L.H.; Toney, M.F.; Salleo, A. Segalman, R.A. Real-Time Observation of Poly (3-Alkylthiophene) Crystallization and Correlation with Transient Optoelectronic Properties. *Macromolecules* **2011**, *44*, 6653-6658.

(39) Jimison, L. H. T., M.F.; McCulloch, I.; Heeney, M.; Salleo, A. Charge-Transport Anisotropy Due to Grain Boundaries in Directionally Crystallized Thin Films of Regioregular Poly (3-Hexylthiophene). *Adv. Mater.* **2009**, *21*, 1568-1572

(40) Patel, S. N.; Su, G. M.; Luo, C.; Wang, M.; Perez, L. A.; Fischer, D. A.; Prendergast, D.; Bazan, G. C.; Heeger, A. J.; Chabinyc, M. L.; Kramer, E. J. Nexafs Spectroscopy Reveals the Molecular Orientation in Blade-Coated Pyridal 2,1,3 Thiadiazole-Containing Conjugated Polymer Thin Films. *Macromolecules* **2015**, *48*, 6606-6616.

(41) Yang, X.; van Duren, J. K. J.; Janssen, R. A. J.; Michels, M. A. J.; Loos, J. Morphology and Thermal Stability of the Active Layer in Poly(P-Phenylenevinylene)/Methanofullerene Plastic Photovoltaic Devices. *Macromolecules* **2004**, *37*, 2151-2158.

(42) Biniek, L.; Leclerc, N.; Heiser, T.; Bechara, R.; Brinkmann, M. Large Scale Alignment and Charge Transport Anisotropy of Pbttt Films Oriented by High Temperature Rubbing. *Macromolecules* **2013**, *46*, 4014-4023.

(43) Schuettfort, T.; Watts, B.; Thomsen, L.; Lee, M.; Sirringhaus, H.; McNeill, C. R. Microstructure of Polycrystalline Pbttt Films: Domain Mapping and Structure Formation. *ACS Nano* **2012**, *6*, 1849-1864.

(44) DeLongchamp, D. M.; Kline, R. J.; Jung, Y.; Germack, D. S.; Lin, E. K.; Moad, A. J.; Richter, L. J.; Toney, M. F.; Heeney, M.; McCulloch, I. Controlling the Orientation of Terraced Nanoscale "Ribbons" of a Poly(Thiophene) Semiconductor. *ACS Nano* **2009**, *3*, 780-787.

(45) Liu, J.; Sun, Y.; Gao, X.; Xing, R.; Zheng, L.; Wu, S.; Geng, Y.; Han, Y. Oriented Poly(3-Hexylthiophene) Nanofibril with the Pi-Pi Stacking Growth Direction by Solvent Directional Evaporation. *Langmuir* **2011**, *27*, 4212-4219.

(46) Aryal, M.; Trivedi, K.; Hu, W. Nano-Confinement Induced Chain Alignment in Ordered P3ht Nanostructures Defined by Nanoimprint Lithography. *ACS Nano* **2009**, *3*, 3085-3090.

(47) Wang, H.; Xu, Y.; Yu, X.; Xing, R.; Liu, J.; Han, Y. Structure and Morphology Control in Thin Films of Conjugated Polymers for an Improved Charge Transport. *Polymers* **2013**, *5*, 1272-1324.

(48) Tang, C. W. Two-Layer Organic Photovoltaic Cell. *Appl. Phys. Lett.* **1986**, *48*, 183-185.

(49) Karg, S.; Riess, W.; Dyakonov, V.; Schwoerer, M. Electrical and Optical Characterization of Poly(Phenylene-Vinylene) Light Emitting Diodes. *Synth. Met.* **1993**, *54*, 427-433.

(50) Glenis, S.; Horowitz, G.; Tourillon, G.; Garnier, F. Electrochemically Grown Polythiophene and Poly(3-Methylthiophene) Organic Photovoltaic Cells. *Thin Solid Films* **1984**, *111*, 93-103.

(51) Stubinger, T.; Brutting, W. Exciton Diffusion and Optical Interference in Organic Donor-Acceptor Photovoltaic Cells. *J. Appl. Phys.* **2001**, *90*, 3632-3641.

(52) Sariciftci, N. S.; Smilowitz, L.; Heeger, A. J.; Wudl, F. Photoinduced Electron Transfer from a Conducting Polymer to Buckminsterfullerene. *Science* **1992**, *258*, 1474-1476.

(53) Yu, G.; Gao, J.; Hummelen, J. C.; Wudl, F.; Heeger, A. J. Polymer Photovoltaic Cells: Enhanced Efficiencies Via a Network of Internal Donor-Acceptor Heterojunctions. *Science* **1995**, *270*, 1789-1791.

(54) Bjerring, M.; Nielsen, J. S.; Nielsen, N. C.; Krebs, F. C. Polythiophene by Solution Processing. *Macromolecules* **2007**, *40*, 6012-6013.

(55) Krebs, F. C.; Fyenbo, J.; Jorgensen, M. Product Integration of Compact Roll-to-Roll Processed Polymer Solar Cell Modules: Methods and Manufacture Using Flexographic Printing, Slot-Die Coating and Rotary Screen Printing. *J. Mater. Chem.* **2010**, *20*, 8994-9001.

(56) Polino, G.; Shanmugam, S.; Bex, G. J. P.; Abbel, R.; Brunetti, F.; Di Carlo, A.; Andriessen, R.; Galagan, Y. Photonic Flash Sintering of Ink-Jet-Printed Back Electrodes for Organic Photovoltaic Applications. *ACS Appl. Mater. Interfaces* **2016**, *8*, 2325-2335.

(57) Zhao, K.; Xue, L.; Liu, J.; Gao, X.; Wu, S.; Han, Y.; Geng, Y. A New Method to Improve Poly(3-Hexyl Thiophene) (P3ht) Crystalline Behavior: Decreasing Chains Entanglement to Promote Order-Disorder Transformation in Solution. *Langmuir* **2010**, *26*, 471-477.

(58) Zhao, K.; Khan, H. U.; Li, R.; Su, Y.; Amassian, A. Entanglement of Conjugated Polymer Chains Influences Molecular Self-Assembly and Carrier Transport. *Adv. Funct Mater.* **2013**, *23*, 6024-6035.

(59) Xu, Y.; Liu, J.; Wang, H.; Zheng, L.; Han, Y. Formation of Parallel Aligned Nano-Fibrils of Poly(3,3 '"-Didodecylquaterthiophene) Induced by the Unimer Coils in Solution. *Rsc Adv.* **2013**, *3*, 12069-12074.

(60) Brinkmann, M.; Rannou, P. Molecular Weight Dependence of Chain Packing and Semicrystalline Structure in Oriented Films of Regioregular Poly(3-Hexylthiophene) Revealed by High-Resolution Transmission Electron Microscopy. *Macromolecules* **2009**, *42*, 1125-1130.

(61) Kim, B. G.; Jeong, E. J.; Chung, J. W.; Seo, S.; Koo, B.; Kim, J. A Molecular Design Principle of Lyotropic Liquid-Crystalline Conjugated Polymers with Directed Alignment Capability for Plastic Electronics. *Nat. Mater.* **2013**, *12*, 659-664.

(62) Hoppe, H.; Sariciftci, N. S. Morphology of Polymer/Fullerene Bulk Heterojunction Solar Cells. *J. Mater. Chem.* **2006**, *16*, 45-61.

(63) Hoppe, H.; Niggemann, M.; Winder, C.; Kraut, J.; Hiesgen, R.; Hinsch, A.; Meissner, D.; Sariciftci, N. S. Nanoscale Morphology of Conjugated Polymer/Fullerene-Based Bulk-Heterojunction Solar Cells. *Adv. Funct Mater.* **2004**, *14*, 1005-1011.

(64) Yang, X.; Loos, J.; Veenstra, S. C.; Verhees, W. J. H.; Wienk, M. M.; Kroon, J. M.; Michels, M. A. J.; Janssen, R. A. J. Nanoscale Morphology of High-Performance Polymer Solar Cells. *Nano Letters* **2005**, *5*, 579-583.

(65) Kim, Y.; Choulis, S. A.; Nelson, J.; Bradley, D. D. C.; Cook, S.; Durrant, J. R. Device Annealing Effect in Organic Solar Cells with Blends of Regioregular Poly(3-Hexylthiophene) and Soluble Fullerene. *Appl. Phys. Lett.* **2005**, *86*, 063502.

(66) Li, G.; Shrotriya, V.; Huang, J.; Yao, Y.; Moriarty, T.; Emery, K.; Yang, Y. High-Efficiency Solution Processable Polymer Photovoltaic Cells by Self-Organization of Polymer Blends. *Nat. Mater.* **2005**, *4*, 864-868.

(67) Reyes-Reyes, M.; Kim, K.; Carroll, D. L. High-Efficiency Photovoltaic Devices Based on Annealed Poly(3-Hexylthiophene) and 1-(3-Methoxycarbonyl)-Propyl-1- Phenyl-(6,6)C61 Blends. *Appl. Phys. Lett.* **2005**, *87*, 083506.

(68) Kim, Y.; Cook, S.; Tuladhar, S. M.; Choulis, S. A.; Nelson, J.; Durrant, J. R.; Bradley, D. D. C.; Giles, M.; McCulloch, I.; Ha, C.-S.; Ree, M. A Strong Regioregularity Effect in Self-Organizing Conjugated Polymer Films and High-Efficiency Polythiophene:Fullerene Solar Cells. *Nat. Mater.* **2006**, *5*, 197-203.

(69) Cowan, S. R.; Leong, W. L.; Banerji, N.; Dennler, G.; Heeger, A. J. Identifying a Threshold Impurity Level for Organic Solar Cells: Enhanced First-Order Recombination Via Well-Defined Pc84bm Traps in Organic Bulk Heterojunction Solar Cells. *Adv. Funct Mater.* **2011**, *21*, 3083-3092.

(70) Chambon, S.; Rivaton, A.; Gardette, J.-L.; Firon, M.; Lutsen, L. Aging of a Donor Conjugated Polymer: Photochemical Studies of the Degradation of Poly 2-Methoxy-5-(3 ',7 '-Dimethyloctyloxy)-1,4-Phenylenevinylene. *J. Polym. Sci., Part A: Polym. Chem.* **2007**, *45*, 317-331.

(71) Brabec, C. J.; Zerza, G.; Cerullo, G.; De Silvestri, S.; Luzzati, S.; Hummelen, J. C.; Sariciftci, S. Tracing Photoinduced Electron Transfer Process in Conjugated Polymer/Fullerene Bulk Heterojunctions in Real Time. *Chem. Phys. Lett.* **2001**, *340*, 232-236.

(72) Manceau, M.; Chambon, S.; Rivaton, A.; Gardette, J.-L.; Guillerez, S.; Lemaître, N. Effects of Long-Term Uv–Visible Light Irradiation in the Absence of Oxygen on P3ht and P3ht:Pcbm Blend. *Sol. Energy Mater. Sol. Cells* **2010**, *94*, 1572-1577.

(73) Barbey, R.; Lavanant, L.; Paripovic, D.; Schüwer, N.; Sugnaux, C.; Tugulu, S.; Klok, H.-A. Polymer Brushes Via Surface-Initiated Controlled Radical Polymerization: Synthesis, Characterization, Properties, and Applications. *Chem. Rev.* **2009**, *109*, 5437-5527.

(74) Marshall, N.; Sontag, S. K.; Locklin, J. Surface-Initiated Polymerization of Conjugated Polymers. *Chem. Comm.* **2011**, *47*, 5681-5689.

(75) Senkovskyy, V.; Khanduyeva, N.; Komber, H.; Oertel, U.; Stamm, M.; Kuckling, D.; Kiriy, A. Conductive Polymer Brushes of Regioregular Head-to-Tail Poly(3-Alkylthiophenes) Via Catalyst-Transfer Surface-Initiated Polycondensation. *J. Am. Chem. Soc* **2007**, *129*, 6626-6632.

(76) Khanduyeva, N.; Senkovskyy, V.; Beryozkina, T.; Bocharova, V.; Simon, F.; Nitschke, M.; Stamm, M.; Grötzschel, R.; Kiriy, A. Grafting of Poly(3-Hexylthiophene) from Poly(4-Bromostyrene) Films by Kumada Catalyst-Transfer Polycondensation: Revealing of the Composite Films Structure. *Macromolecules* **2008**, *41*, 7383-7389.

(77) Letheby, H. Xxix.-on the Production of a Blue Substance by the Electrolysis of Sulphate of Aniline. *J. Chem. Soc.* **1862**, *15*, 161-163.

(78) Diaz, A. F.; Kanazawa, K. K.; Gardini, G. P. Electrochemical Polymerization of Pyrrole. *J. Chem. Soc.,Chem. Commun.* **1979**, 635-636.

(79) Waltman, R. J.; Bargon, J. Electrically Conducting Polymers - a Review of the Electropolymerization Reaction, of the Effects of Chemical-Structure on Polymer Film Properties, and of Applications Towards Technology. *Can. J. Chem.* **1986**, *64*, 76-95.

(80) Guay, J.; Diaz, A.; Wu, R.; Tour, J. M.; Dao, L. H. Electrooxidation of Soluble .Alpha.,.Alpha.-Coupled Thiophene Oligomers. *Chem. Mater.* **1992**, *4*, 254-255.

(81) Rault-Berthelot, J.; Simonet, J. The Anodic Oxidation of Fluorene and Some of Its Derivatives. *J. electroanal. chem. interfacial electrochem.* **1985**, *182*, 187-192.

(82) Zhang, Q. Q.; Liu, Z. Y.; Wang, K. F.; Zhai, J. Organic/Inorganic Hybrid Nanochannels Based on Polypyrrole-Embedded Alumina Nanopore Arrays: Ph- and Light-Modulated Ion Transport. *Adv. Funct Mater.* **2015**, *25*, 2091-2098.

(83) Lyutov, V.; Gruia, V.; Efimov, I.; Bund, A.; Tsakova, V. An Acoustic Impedance Study of Pedot Layers Obtained in Aqueous Solution. *Electrochem. Acta* **2016**, *190*, 285-293.

(84) Jiang, Z. M.; Li, G. Y.; Zhang, M. X. Electrochemical Sensor Based on Electro-Polymerization of Beta-Cyclodextrin and Reduced-Graphene Oxide on Glassy Carbon Electrode for Determination of Gatifloxacin. *Sens. Actuator B-Chem.* **2016**, *228*, 59-65.

(85) Heinze, J.; Frontana-Uribe, B. A.; Ludwigs, S. Electrochemistry of Conducting Polymers—Persistent Models and New Concepts. *Chem. Rev.* **2010**, *110*, 4724-4771.

(86) Hill, M. G.; Mann, K. R.; Miller, L. L.; Penneau, J. F. Oligothiophene Cation Radical Dimers. An Alternative to Bipolarons in Oxidized Polythiophene. *J. Am. Chem. Soc.* **1992**, *114*, 2728-2730.

(87) van Haare, J.; Havinga, E. E.; van Dongen, J. L. J.; Janssen, R. A. J.; Cornil, J.; Bredas, J. L. Redox States of Long Oligothiophenes: Two Polarons on a Single Chain. *Chem. Eur. J.* **1998**, *4*, 1509-1522.

(88) Hill, M. G.; Penneau, J. F.; Zinger, B.; Mann, K. R.; Miller, L. L. Oligothiophene Cation Radicals. .Pi.-Dimers as Alternatives to Bipolarons in Oxidized Polythiophenes. *Chem. Mater.* **1992**, *4*, 1106-1113.

(89) Debye, P. Reaction Rates in Ionic Solutions. *Trans. Elect. Soc.* **1942**, *82*, 265-272.

(90) Audebert, P.; Catel, J. M.; Le Coustumer, G.; Duchenet, V.; Hapiot, P. Electrochemistry and Polymerization Mechanisms of Thiophene−Pyrrole−Thiophene Oligomers and Terthiophenes. Experimental and Theoretical Modeling Studies. *J. Phys. Chem. B* **1998**, *102*, 8661-8669.

(91) Adenier, A.; Combellas, C.; Kanoufi, F.; Pinson, J.; Podvorica, F. I. Formation of Polyphenylene Films on Metal Electrodes by Electrochemical Reduction of Benzenediazonium Salts. *Chem.Mater.* **2006**, *18*, 2021-2029.

(92) Parvin, S.; Sato, E.; Matsui, J.; Miyashita, T. Surface Initiated Atom Transfer Radical Polymerization of N-Hydroxysuccinimide Methacrylate from Magnetite Surface as Precursor for Functional Polymer Shell. *Polym. J.* **2006**, *38*, 1283-1287.

(93) Rowe-Konopacki, M. D.; Boyes, S. G. Synthesis of Surface Initiated Diblock Copolymer Brushes from Flat Silicon Substrates Utilizing the Raft Polymerization Technique. *Macromolecules* **2007**, *40*, 879-888.

(94) Yokoyama, A.; Miyakoshi, R.; Yokozawa, T. Chain-Growth Polymerization for Poly(3-Hexylthiophene) with a Defined Molecular Weight and a Low Polydispersity. *Macromolecules* **2004**, *37*, 1169-1171.

(95) Sheina, E. E.; Liu, J.; Iovu, M. C.; Laird, D. W.; McCullough, R. D. Chain Growth Mechanism for Regioregular Nickel-Initiated Cross-Coupling Polymerizations. *Macromolecules* **2004**, *37*, 3526-3528.

(96) Sontag, S. K.; Marshall, N.; Locklin, J. Formation of Conjugated Polymer Brushes by Surface-Initiated Catalyst-Transfer Polycondensation. *Chem. Commun.* **2009**, 3354-3356.

(97) Senkovskyy, V.; Tkachov, R.; Beryozkina, T.; Komber, H.; Oertel, U.; Horecha, M.; Bocharova, V.; Stamm, M.; Gevorgyan, S. A.; Krebs, F. C.; Kiriy, A. "Hairy" Poly(3-Hexylthiophene) Particles Prepared Via Surface-Initiated Kumada Catalyst-Transfer Polycondensation. *J. Am. Chem. Soc.* **2009**, *131*, 16445-16453.

(98) Doubina, N.; Jenkins, J. L.; Paniagua, S. A.; Mazzio, K. A.; MacDonald, G. A.; Jen, A. K.; Armstrong, N. R.; Marder, S. R.; Luscombe, C. K. Surface-Initiated Synthesis of Poly(3-Methylthiophene) from Indium Tin Oxide and Its Electrochemical Properties. *Langmuir* **2012**, *28*, 1900-1908.

CHAPTER 2. POLYTHIOPHENE THIN FILMS BY SURFACE-CONFINED POLYMERIZATION: MECHANISTIC AND STRUCTURAL STUDIES*

2.1. Introduction

One of the persistent challenges in designing reliable electronic and optoelectronic devices based on thin films of semiconducting polymers remains the ability to effectively control mesoscale organization and molecular structure of the polymers in the bulk of the films. This control is important for improving device performance, for example, in enhancing the efficiency of organic polymer solar cells where low carrier mobility due to less than optimal convoluted charge transfer pathways in thin films represents one of the essential bottlenecks to achieving high light to current conversion efficiencies.[1-6] Similarly, controlling molecular organization in thin films of fluorescent and electroluminescent semiconducting polymers can improve the performance of polymer-based light-emitting and chemosensing devices.[7-11] Currently, almost all successful approaches to prepare thin-film semiconducting polymer devices utilize solution-based processing of soluble polymers, e.g. spin casting. In such processing schemes, some control over molecular organization and phase separation can be achieved indirectly, through the variation of experimental fabrication conditions, post-deposition thermal annealing, using low molecular weight additives, etc. These traditional approaches, however, offer limited options to precisely control over nanoscale molecular organization and alignment of semiconducting polymers in thin layers. Some improvement in controlling the organization and alignment in thin films can be achieved by utilizing the tools of supramolecular chemistry, but this approach is

---

* "Reproduced in part with permission from Youm, S. G.; Hwang, E.; Chavez, C.A.; Li, X.; Chatterjee, S.; Lusker, K. L; Lu, L.; Strzalka, J.; Ankner, J. F.; Losovyj, Y.; Garno, J. C.; Nesterov, E. E. *Chem. Mater.*, DOI: 10.1021/acs.chemmater.6b01957, Copyright 2016 American Chemiscal Society"

also limited. A viable alternative to using solutions of pre-synthesized semiconducting polymers employs a "grafting from" approach to prepare surface-attached polymer thin films using surface-confined (also often called surface-initiated) polymerization of monomers.[12] This approach allows *in situ* preparation of continuous as well as nanopatterned semiconducting polymer thin films and devices based on them directly from small-molecule monomers. In such a case, the monomers are not required to be functionalized with bulky solubilizing substituents, and this approach affords greater control over mesoscale organization in the films. In addition to better controlled mesoscale organization and molecular composition, the polymer films produced by surface-initiated polymerization benefit from greater mechanical, thermal, and chemical stability, relative to traditional spin-cast thin films. With all of these potential advantages, and despite some recent increase in interest in this area,[13-22] surface-confined *in situ* preparation of semiconducting polymer films remains largely unexplored, still lacking both efficient practical methods and fundamental knowledge of essential details of the polymerization process as well as detailed information on the structure of the resulting thin films. In this study, we attempted to fill this gap by carrying out an extensive development and optimization of the surface-initiated polymerization process, gaining better understanding of the polymerization mechanism, as well as detailed investigation of the structure and morphology of the produced surface-attached thin films.

Among various classes of semiconducting polymers, polythiophene (PT) and its various derivatives are among the most important organic electronic materials.[23, 24] These polymers show substantial charge transport efficiency, as well as good thermal stability and photostability. In addition, PT properties can be readily modified through chemical functionalization, and there are numerous synthetic approaches to preparation of polythiophenes and their analogs. One of

the most commonly used PT representatives is regioregular poly(3-hexylthiophene) (P3HT).[25, 26] This solution-processable polymer forms thin films which display good charge mobility and are relatively stable to thermal and photodegradation. Not surprisingly, extensive research efforts have been directed towards improving the molecular organization of P3HT in thin films with the goal of enhancing charge mobility and increasing the efficiency of the resulting devices.[27-33] While the majority of these efforts have targeted controlling morphology and organization in thin films of the pre-synthesized polymer, fewer attempts have been made to achieve such control by *in situ* surface-initiated polymerization of a suitable monomer.[20-22] Such polymerization has a number of advantages, including the possibility to prepare densely packed films of unsubstituted PTs. Functionalizing the PT backbone with bulky solubilizing substituents is required for solution processing as an unsubstituted polymer would be completely insoluble. Whereas it has been shown that interdigitation of solubilizing side groups can improve molecular ordering in thin films, such bulky side groups also disrupt close interchain packing and reduce the molecular organization and co-planarity of the polymer chains in the film, especially if the synthetic chemistry used to prepare the polymer does not afford 100% regioregularity (as the percentage of "head to tail" coupling of thienyl repeating units).[34-36] The solubilizing side groups may also reduce charge-transport in polymer thin film materials by effectively "diluting" the π-conjugated backbone. In addition, the α-carbon of the alkyl side chains has been shown to act as a reactive site for initiation of photo- and thermal degradation of semiconducting polymers.[37-38] Lacking these drawbacks, *in situ* prepared thin films of unsubstituted PT are expected to exhibit improved molecular organization as well as to show better stability than spin-cast films of alkyl-substituted pre-synthesized PTs. In addition to preparation of stable surface-confined polymer films, such

polymerization can serve as a convenient method for surface modification with organic semiconducting polymers for optoelectronic, sensing, and biomedical devices.[39-41]

Many earlier attempts at *in situ* preparation of PT thin films involved electrochemical polymerization.[42] However, electrochemical method is limited by the availability of the monomers (as not every monomer can be efficiently electropolymerized), and the strong dependence of the properties of the final polymers on subtle variations of experimental conditions (and the related poor reproducibility of the results). In contrast to electrochemical polymerization, using transition metal-catalyzed chemical polymerization to form various derivatives of regioregular PTs is highly versatile. With the availability of various methodologies (of which the most prominent are McCullough's Grignard metathesis polymerization[43, 44] and Rieke's organozinc derivatives coupling[45]) and highly efficient catalytic systems, and with proper choice of protecting groups, chemical polymerization can be carried out with a wide variety of suitably functionalized monomers, and delivers highly reproducible results. With all of these advantages, chemical polymerization appears to be a method of choice for the "grafting from" preparation of surface-confined thin-layer PT films. Surprisingly, until a few years ago this was almost an unexplored area. The groundbreaking discovery simultaneously by McCullough[46, 47] and Yokozawa[48, 49] that Ni-catalyzed regiocontrolled Kumada polymerization of 5-bromo-2-thienylmagnesium monomers follows a quasi-"living" chain-growth mechanism, opened up the possibility of surface-confined chemical polymerization. Up to now, a few independent research groups, most notably that of Kiriy, have carried out surface-initiated *in situ* preparation of regioregular poly(3-alkylthiophene) brushes through Kumada polymerization using surface-immobilized Ni(II) catalytic initiators.[50-52] This approach has produced mechanically stable surface-grafted PT thin films, however with an

apparently low surface density, and a limited degree of polymerization, possibly due to instability and lower activity of the metal catalytic site and the dominance of side reactions.[53, 54] Using Kiriy's methodology and a modified Ni catalyst to improve the "living" nature of the polymerization process, Locklin has demonstrated preparation of relatively thick (up to 42 nm) surface-attached poly(3-methylthiophene) films.[55] Nevertheless, all of the reported systems suffer from low activity and relative instability of the surface-immobilized Ni(II) catalyst, as well as from the complexity of the catalyst preparation; therefore, practical implementation of surface-initiated polymerization still remains a challenge.[13-15] Even more importantly, very little is known about the molecular organization and bulk morphology of surface-confined PT thin films and the ways that can be used to control these parameters.

Recently, we have found that the reaction of aryl bromides or aryl iodides with Ni(0) complex $Ni(dppp)_2$ (where dppp is 1,3-bis(diphenylphosphino)propane) at moderate temperatures produces a stable Ni (II) complex **1** that can be used as a highly efficient catalytic initiator of Kumada catalyst transfer polymerization (KCTP)[53, 56] of 5-bromo-2-thienylmagnesium monomers (Scheme 2.1).[57] The polymerization efficiently yields highly regi-

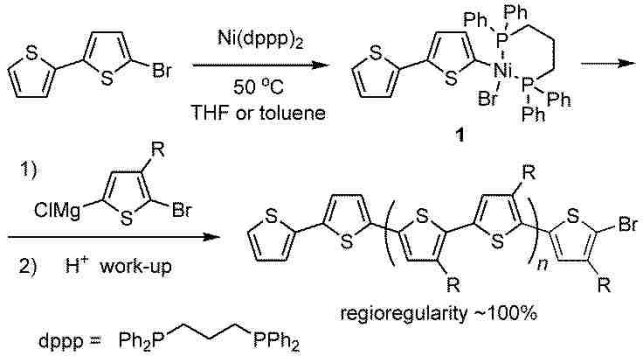

Scheme 2.1. Preparation of Ni(II) external catalytic initiator **1** and its use in preparing regioregular poly(3-alkylthiophene)s by controlled chain-growth Kumada catalyst transfer polymerization.

oregular (regioregularity, as a fraction of head-to-tail (HT) coupled 3-alkylthienyl units, is close to 100%) P3HT with the number average molecular weight (M_n) being linearly dependent on the monomer/catalyst **1** ratio. These and other experimental findings have pointed out on the controlled chain-growth mechanism of the polymerization initiated/catalyzed by **1**. In good agreement with this mechanism, each polymer chain was found to be terminated with the aryl group from catalyst **1** at one end, and (somewhat unexpectedly) predominantly with Br at the other end (Scheme 1). The experimental simplicity of preparation of the catalytic initiator **1** and the efficiency of the **1**-catalyzed KCTP prompted us to systematically investigate using this complex for the preparation of surface-attached PT thin films via surface-confined *in situ* polymerization. This chapter describes our studies of preparation of the surface-immobilized catalyst, mechanistic details of the polymerization process, and structural characteristics and properties of the resulting surface-confined PT thin films, as well as the use of this method for the preparation of nanopatterned PT films through particle lithography.

2.2 Results and Discussion

2.2.1. Preparation and characterization of the surface-immobilized catalytic initiator.

For the current study, we selected 2-(triethoxysilyl)-5-iodothiophene **2** as a precursor for the KCTP catalytic initiator (Figure 2.1). Reacting the triethoxysilyl group with activated inorganic oxide surfaces is a convenient method for the covalent surface immobilization of organic molecules.[58, 59] Direct, without a flexible aliphatic spacer, attachment of the anchoring silyl group to the thiophene unit was chosen in order to provide a tighter connection between the surface-attached semiconducting polymer brush and the supporting substrate to facilitate charge transfer in the eventual thin-film devices. Furthermore, we expected the short surface linker to help reduce the possibility of a homocoupling (disproportionation) reaction between adjacent

surface-immobilized Ni(II) initiator molecules – a catalyst-degradation process which had been previously demonstrated to efficiently occur with flexible long alkyl chain surface-attachment linkers.[54, 60] First, we studied the solution reaction between the iodothienyl precursor **2** and $Ni(dppp)_2$. The reaction of **2** with 2 equivalents of $Ni(dppp)_2$ to form catalytic initiator **3** was carried out in toluene at 45 °C, and monitored by ^{31}P NMR. We chose to use a two-fold excess of $Ni(dppp)_2$ in order to accelerate conversion of **2** to the active catalytic initiator **3**. Indeed, from a practical standpoint, the presence of unreacted $Ni(dppp)_2$ when it was taken in excess could not affect the surface immobilization of the catalytic initiator **3**, whereas the presence of unreacted iodothienyl precursor **2** (in case of its incomplete conversion to the catalytic initiator **3**) could undesirably result in incorporating unreactive **2** in the monolayer and therefore diminishing the surface density of catalytic initiator **3**. The main feature in tracking the reaction progress by ^{31}P NMR was a gradual intensity decrease of the singlet at 12.8 ppm corresponding to $Ni(dppp)_2$. After 24 h reaction time, this signal intensity decreased to 50% of the initial intensity, whereas no new signals could be observed in the ^{31}P NMR spectrum of the reaction mixture, indicating complete conversion of the iodo precursor **2** to the Ni(II) catalytic initiator **3** (Figure 2.1, *Direct method*). The lack of observable ^{31}P NMR signals from the Ni(II) square-planar complex **3** in toluene was in agreement with our previous findings.[57] When toluene was removed *in vacuo*, and the residual product was redissolved in THF, formation of the square-planar Ni(II) catalytic initiator **3** was then clearly evidenced by the presence of a pair of broad doublets (at approximately 18.9 and –1.3 ppm) in the ^{31}P NMR spectrum (Figure Appendix B.1). The as prepared solutions of catalytic initiator **3** were found to be relatively stable with respect to thermal degradation (e.g. they could be stored at –30 °C for up to three months without losing catalytic activity). Therefore, a toluene solution of **3** can be prepared in advance, and used for

surface immobilization when needed.

To prepare a surface-attached monolayer of the catalytic initiator, one can use either of two alternative procedures. In a more conventional approach (previously established by Kiriy,[50-52] Locklin,[55] et al.), a substrate with a surface-immobilized monolayer of an aryl halide precursor is converted to an active Ni(II) catalytic initiator via a suitable chemical reaction on the surface. In our case, this required reacting a substrate-immobilized monolayer of the iodothienyl precursor **2** with $Ni(dppp)_2$ (Figure 2.1, *Indirect method*). Alternatively, considering the preparation simplicity and relative stability in solution of the catalytic initiator **3**, it would be conceivable to prepare a monolayer of catalytic initiator by direct immobilization of **3** to a solid substrate (Figure 2.1, *Direct method*). Although both procedures are supposed to deliver the same surface-immobilized monolayer of catalytic initiator **3**, it could be possible that the lower efficiency and slow rate of the heterogeneous reaction between surface-bound iodothienyl precursor **2** and $Ni(dppp)_2$ could hinder the conversion of surface-immobilized iodothienyl precursor **2** to the active initiator **3**, and therefore might result in only partial conversion to **3** in the *Indirect method*. In this sense, *Direct method*, involving solution synthesis of **3**, looked more advantageous as it would offer complete surface coverage with catalytic initiator **3**. Since the latter approach has not been previously investigated, we decided to study both procedures in more detail, and compare their outcomes.

For this study, the immobilized monolayers of the iodo-precursor **2** and Ni(II) catalytic initiator **3** were prepared on quartz substrates by immersing the freshly activated substrates in solutions of **2** and **3**, respectively, in toluene at 55 °C for 60 h. After monolayer deposition, the substrates were thoroughly rinsed with toluene, and the composition of the monolayers was analyzed using high-resolution X-ray photoelectron spectroscopy (XPS). We found it

convenient to look at the iodine signal as it is characterized by two well-resolved peaks in the XPS spectrum, and the peak position is highly sensitive to the chemical state of iodine.[61, 62] The monolayer of iodothienyl precursor **2** showed two signals at approximately 633 and 622 eV which can be attributed to the I 3d5/2 and I 3d3/2 peaks (Figure 2.2A). The monolayer of Ni(II)

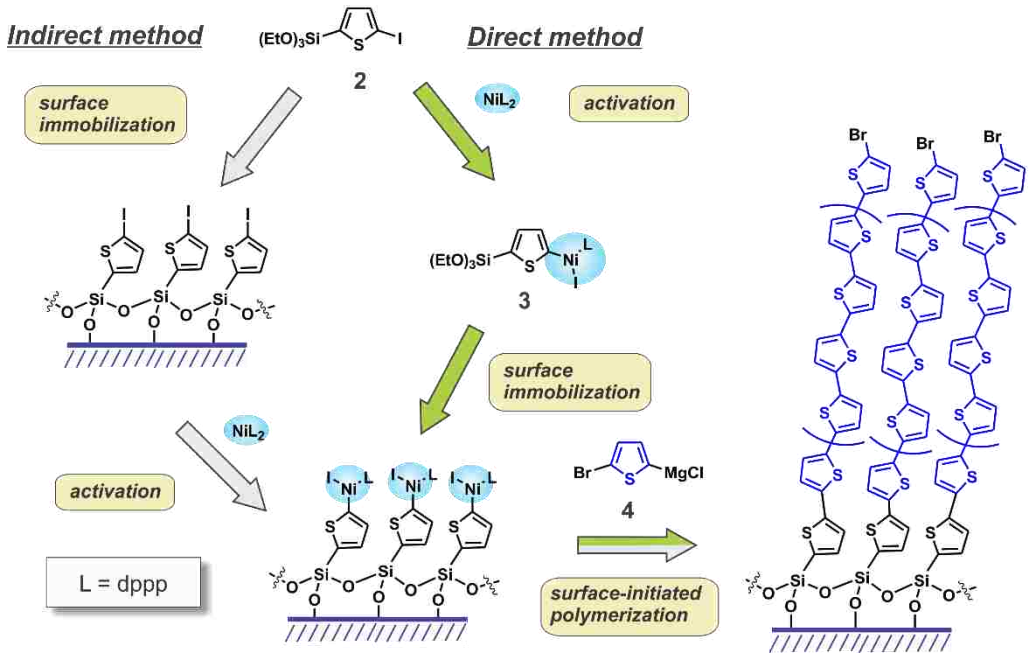

Figure 2.1. Two alternative methods for the preparation of surface-confined Ni(II) catalytic initiator of controlled chain-growth polymerization, and subsequent surface-initiated Kumada catalyst-transfer polymerization to yield surface-attached polythiophene thin films. In the *Indirect method* (on the left) the surface-immobilized Ni(II) catalytic initiator is prepared by a heterogeneous reaction between the monolayer of iodo-precursor **2** and $Ni(dppp)_2$. In contrast, the *Direct method* (on the right) relies on direct surface immobilization of the solution-prepared Ni(II) catalytic initiator **3**. The polymer chain alignment normal to the substrate surface is shown only for illustrative purpose, and does not reflect the actual morphology and mesoscale structure of the film.

catalytic initiator **3** (prepared via *Direct method*) displayed similar iodine signals but shifted toward lower binding energies (at approximately 629 and 618 eV). Indeed, one would expect a lower binding energy for the I^- anion attached to the Ni(II) center in **3** relative to the iodine covalently connected to an aromatic carbon atom in **2** (similar lower binding energies were found

for the ionic salts CsI and NaI[63]). Within the XPS sensitivity, no signals for the iodothienyl precursor **2** were observed in this monolayer, therefore indicating completeness of the solution conversion of **2** to **3** (as was already evidenced by ^{31}P NMR spectroscopy). For the *Indirect method*, chemical conversion of the monolayer of iodothienyl precursor **2** to the catalytic initiator **3** was monitored by XPS and showed that even prolonged (60 h) exposure of a monolayer of **2** to $Ni(dppp)_2$ solution at 55 °C resulted only in partial conversion to **3**, and approximately 70% of the surface-immobilized iodothienyl precursor **2** remained unreacted, as could be determined from integration of the deconvoluted XPS peaks characteristic of **2** and **3** (Figure 2.2A). The observed incomplete conversion was in line with the previous observations by Locklin,[54] and was likely related to steric effects in the densely packed monolayer. Therefore, the monolayer of catalytic initiator prepared by the *Indirect method* would be expected to have a lower surface density of Ni(II) catalytic molecules thus resulting in lower-density polymer films compared to the *Direct method*.

To better understand the chemical nature of the surface-immobilized catalytic initiator **3**, we also analyzed Ni 2*p* XPS peaks (Figure 2.2B). Although the structure of the signals in this region was relatively complex, they could be unambiguously attributed to Ni(II). Indeed, in the substrate prepared following the *Indirect method*, the center of gravity of the nickel main ($2p_{3/2}$) peak was found at a binding energy of 856.1 eV, with the second satellite peak positioned at 874.2 eV, which was consistent with values reported for divalent nickel in NiO and $Ni(OH)_2$.[64-66] The first satellite peak at 861.4 eV and the $2p_{1/2}$ peak at 873.9 eV also appeared close to values previously reported for divalent nickel. Overall, the intensity of the XPS signals was significantly higher for the substrates prepared following the *Direct method* compared to those prepared via *Indirect method*, which was consistent with substantially lower Ni(II) surface

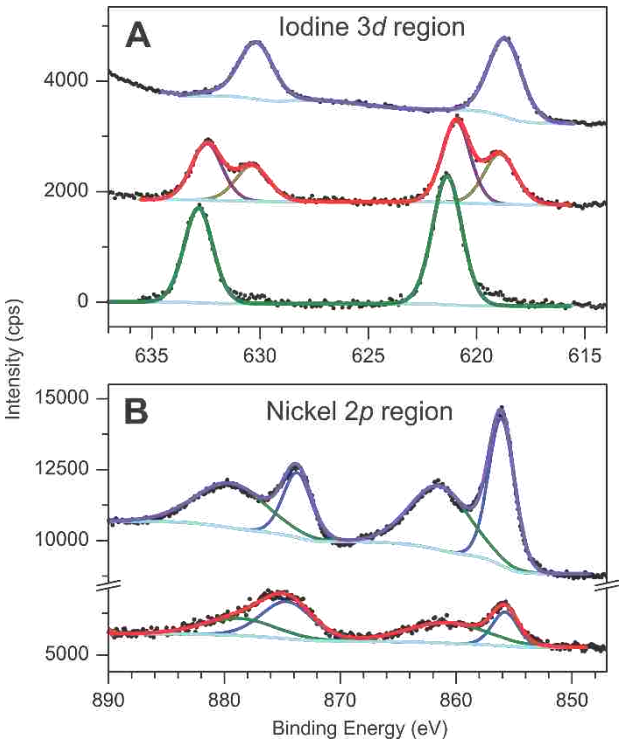

Figure 2.2 (A) High-resolution I 3*d* XPS spectra of monolayers of the surface-immobilized Ni(II) catalyst prepared by the *Direct method* (top violet trace) and by the *Indirect method* (middle red trace, deconvolution into two I 3*d* components is also shown), as well as of a monolayer of iodothiophene precursor **2** (bottom green trace). (B) High resolution Ni 2*p* XPS spectra for the surface-immobilized Ni(II) catalyst prepared by the *Direct method* (top violet trace) and by the *Indirect method* (bottom red trace). Shirley background (cyan traces) was applied to all spectra. Fitting parameters and deconvolution details are listed in Table 5.1 in the Experimental section.

coverage in the latter case.

Since XPS experiments could only provide qualitative information on the surface composition, we attempted to quantify the initiator surface coverage, in order to compare with previous results as well as to establish the superiority of the *Direct method* in the preparation of the surface-immobilized polymerization catalyst. Surface coverage by catalytic initiator **3** was quantitatively estimated in electrochemical studies using the approach described by Locklin.[54] For this purpose, the monolayers of catalytic initiator **3** were prepared following either *Direct method* or *Indirect method* using semiconducting indium tin oxide (ITO) substrates. The

substrates were than treated with an excess of the ferrocene-functionalized Grignard reagent **5** to convert active Ni(II) sites into electrochemically active ferrocene sites (Figure 2.3A). With an assumption that such a transformation happened quantitatively (which is justified considering the large excess of Grignard reagent **5** relative to the surface-immobilized Ni(II) centers), one could determine ferrocene surface coverage from cyclic voltammetry (CV) studies of the ferrocene-functionalized substrates using the well-defined ferrocene redox wave (Figure 2.3B). From the CV experiments, we estimated active catalytic initiator **3** surface coverage in the substrates prepared via *Indirect method* as 0.57×10^{13} molecules cm^{-2}, whereas the coverage in the substrates prepared via *Direct method* was 2.42×10^{13} molecules cm^{-2}. These results showing

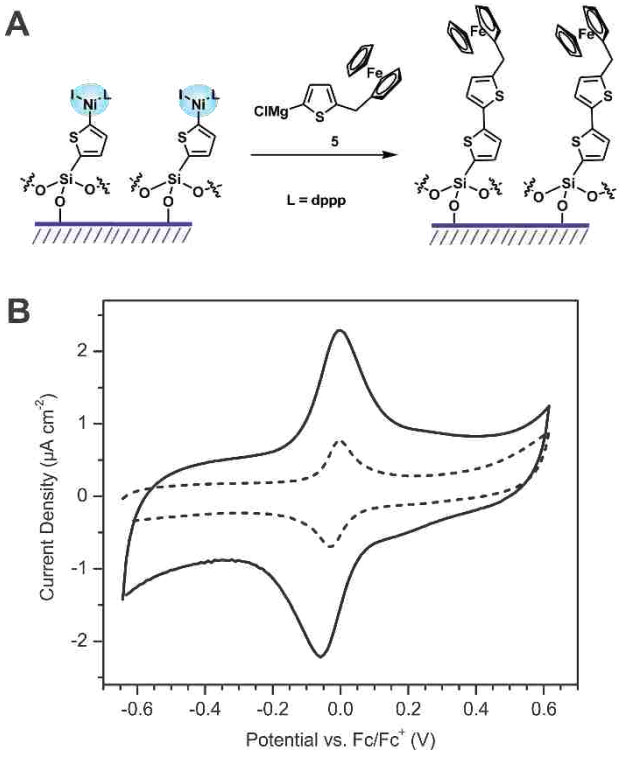

Figure 2.3. (A) Ferrocene functionalization of ITO surface immobilized Ni(II) catalytic initiator, and (B) cyclic voltammograms of the prepared ferrocene-coated substrates acquired in 0.1 M Bu_4NPF_6 in CH_2Cl_2, with sweep rate 0.1 V s^{-1}. Dashed trace shows CV data for a substrate prepared following the *Indirect method*, and solid trace – CV data for a substrate prepared by the *Direct method*.

approximately 4 times lower surface coverage in the substrates prepared via *Indirect method* were consistent with the results from XPS studies and showed that direct surface immobilization of the solution-prepared catalytic initiator **3** (*Direct method*) was a superior method to achieve high-density surface coverage by the catalytic initiator. The absolute value of the initiator **3** surface coverage on the ITO substrate was somewhat lower than the number previously reported by Locklin,[54] which might reflect differences in the measurement conditions or variations in ITO substrates, however we found our value of surface coverage to be quite reproducible and not to vary from sample to sample. Therefore, for the rest of this study we chose the *Direct method* as the procedure to prepare surface-immobilized catalytic initiator for surface-confined polymerization.

2.2.2. Development of surface-initiated polymerization protocol and properties of the resulting PT thin films.

Although the surface-immobilized polythiophene thin films are generally intended for use in electronic devices (and therefore should be deposited on conducting surfaces such as indium tin oxide (ITO)), we performed most of our studies on quartz substrates, as this enabled simple monitoring of reaction progress by UV/vis absorption spectroscopy, and the lower surface roughness of quartz substrates would enable measurements of the structural features of polymer films without accounting for the large surface roughness of commercial ITO substrates. After rinsing with a copious amount of toluene, the quartz slides with surface-immobilized Ni(II) catalytic initiator were immersed in a solution of 5-bromothiophen-2-yl magnesium chloride monomer **4** at room temperature to start controlled chain-growth polymerization yielding surface-attached polythiophene thin films (Figure 2.1). Monitoring of polymer film growth was performed using UV/vis absorption spectroscopy, and the uniformity of the film surface morphology was confirmed in AFM studies.

Carrying out polymerization for 6 h afforded a uniform PT film of approximately 20 nm thickness (determined by stylus profilometry). The UV/vis absorption spectrum of the PT film showed a vibronically structured broad band with a maximum at around 500 nm (Figure 2.4).

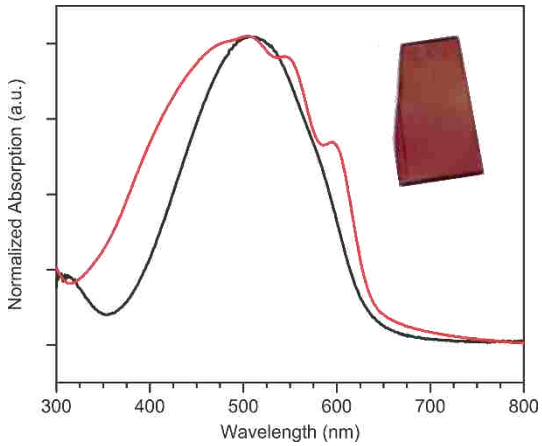

Figure 2.4. UV/vis absorption spectra of a PT thin film prepared by surface-initiated polymerization (red trace) and of a PT thin film prepared by electrochemical polymerization of bithiophene (black trace). Insert shows a photograph of the PT sample prepared by surface-initiated polymerization.

The presence of pronounced vibronic features in the absorption spectra of conjugated polymer films typically indicates better molecular organization and the presence of a certain level of molecular uniformity in the polymer chains alignment.[67-69] To highlight the advantage of our protocol, we also prepared a PT thin film using electrochemical polymerization of bithiophene on an ITO substrate. This approach is known to produce amorphous PT films with a low degree of molecular organization.[70, 71] Indeed, the UV/vis absorption spectrum of the electropolymerized PT thin film exhibited an absorption band with no vibronic features (Figure 2.4). Another striking difference between the chemically polymerized surface-confined and electropolymerized PT films was the remarkable stability of the former in the presence of organic solvents. Indeed, ultrasonicating slides modified with surface-confined PT films placed

in various organic solvents (such as chloroform, toluene, etc.) for extended periods (up to 6 h) resulted in no noticeable film degradation or delamination. This behavior becomes even more striking when one compares chemically polymerized surface-confined PT films with their spin-cast analogues (e.g. spin-cast P3HT films) as the latter can be completely washed off by organic solvents (even without ultrasonication). This particularly high solvent stability of the surface-confined thin films would be highly advantageous for the preparation of complex multilayer architectures as the next polymer layer can be solution-deposited over the surface-confined film without any solvent-related damage to the underlying layer; this property also would make surface-confined polymerization particularly suitable for surface modification of inorganic electrodes with organic semiconducting polymers.

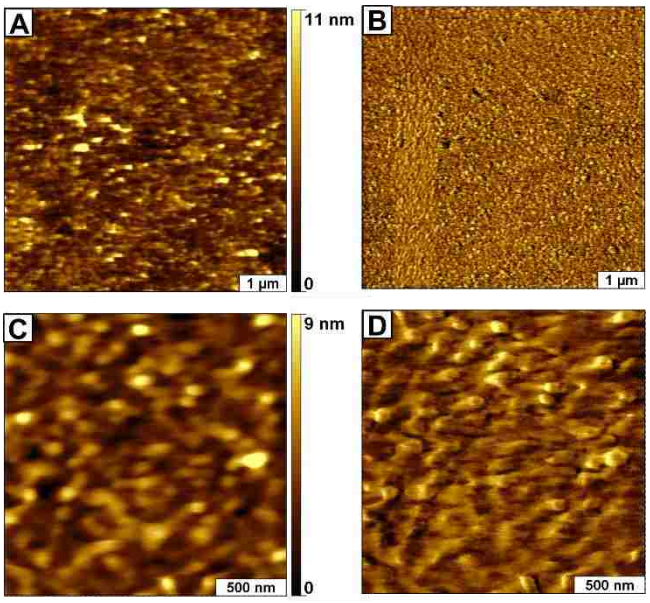

Figure 2.5. Morphology of a PT film prepared by surface-initiated polymerization on a quartz substrate viewed with contact mode AFM images. (A) Wide view topography (6 × 6 μm^2); (B) a simultaneously acquired lateral force image; (C) close-up topography view (2 × 2 μm^2); (D) corresponding lateral force image.

An AFM study revealed uniform coverage of the polythiophene thin films with low surface roughness (RMS roughness 1.4 nm). Representative AFM images are shown in Figure 2.5. The uniformity of the film surface was highly reproducible throughout the various samples prepared in this study. The film surface consisted of a few large circular domains of approximately 65 nm in diameter surrounded by smaller (about 40 nm) circular-shaped domains. We observed formation of a similar surface domain morphology throughout all surface-confined PT samples, and therefore infer that circular domain formation is related to the structure and mesoscale organization of the surface-confined polymer in the bulk thin films. More detailed studies of the structure and morphology of the polymer films are discussed below.

Cyclic voltammetry (CV) data on the PT film prepared by surface-initiated polymerization on an ITO substrate is shown in Figure 2.6A. The surface-confined PT film was found to be electrochemically stable and did not experience noticeable changes upon successive CV scanning. As expected for a covalently attached electroactive film, the peak current exhibited a linear dependence on the scan rate. The film showed a quasi-reversible anodic oxidation wave at Epa ~0.6 V (vs. Fc/Fc+ reference electrode), and a corresponding main cathodic wave at Epc ~–0.15 V. These two waves were centered at E1/2 ~0.38 V – a value similar to that reported for electropolymerized PT films (~0.35 V vs. Fc/Fc^+ reference electrode[72]), however, two features in the CV data were quite unusual. First, unlike electropolymerized PT films which typically show broad redox peaks, surface-confined PT film displayed rather narrow and sharp peaks. This could be explained by a much more uniform distribution of conjugation lengths in the surface-confined film. Second, the electrochemical data displayed large hysteresis – a separation between forward anodic and backward cathodic peaks. Hysteresis is normally observed in crystalline electroactive films and reflects strong

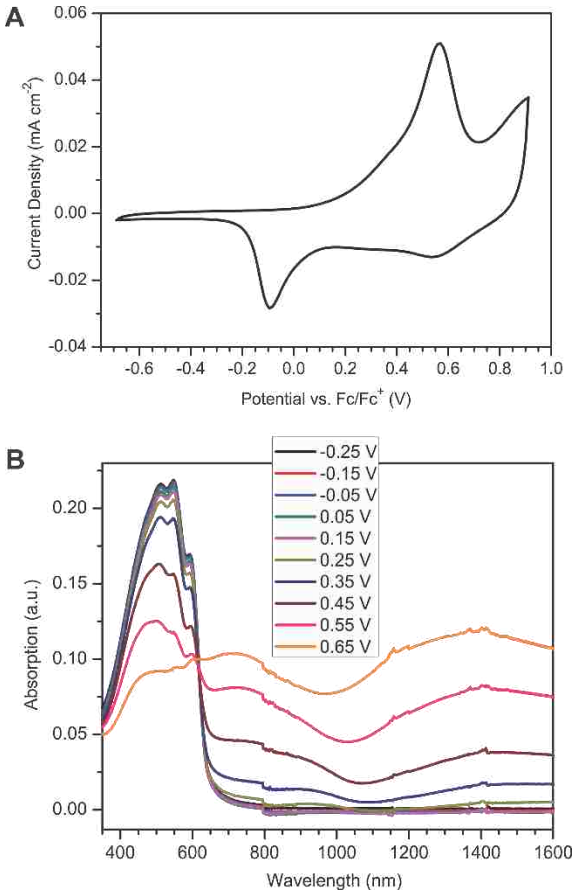

Figure 2.6. (A) Cyclic voltammogram of the PT film prepared by surface-initiated polymerization for 6 h. Data were acquired in 0.1 M Bu_4NPF_6 in CH_2Cl_2, with sweep rate 0.1 V s^{-1}. (B) Spectroelectrochemical studies of the PT film in A. The potentials were referenced to Fc/Fc^+ reference electrode.

attractive interactions between the crystal-packed molecules which oppose counterion ingress into the bulk structure.[73]

For electropolymerized PT films, hysteresis is normally not observed, in agreement with their amorphous nature. Further analysis of the CV curve in Figure 2.6A revealed that it looked quite similar to the CV data previously reported for thin films of thiophene oligomers (in particular, octamer and decamer) which also displayed significant hysteresis between sharp narrow anodic and cathodic waves.[74] As a preliminary conclusion, the electrochemical data of the surface-confined PT film were consistent with substantial crystallinity, with crystalline

domains formed by packing polymer chain segments with 8 to 10 thienyl repeating units. Further structural evidence in favor of this hypothesis is provided later in this chapter.

In spectroelectrochemical studies, absorption spectra of the surface-confined PT film were first obtained in the fully reduced (undoped) state of the polymer, and then were recorded as the potential was gradually stepped up toward oxidized (polaron and bipolaron) states (Figure 2.6B). In the electrochemically undoped, insulating state, the polymer film showed a vibronically structured π-π* transition in the range of 350–650 nm, with the optical bandgap determined from the onset of absorption estimated at 2.0 eV. As the potential was stepped up, the π–π* transition band of the neutral state was observed to gradually decrease, and was replaced with a broad band centered around 750 nm corresponding to a polaronic transition, as well as with an intense bipolaronic band positioned in the near-IR region (maximum at around 1400 nm). Although the bandgap value and spectroelectrochemical behavior of the surface-confined PT film were consistent with those of typical conventionally prepared PT thin films,[72] the surface-confined film did not show complete transition between neutral (undoped) and oxidized (polaronic/bipolaronic) states. Even at high positive potential, there was still a significant presence of the short-wavelength electronic band corresponding to the neutral state. This resistance of the surface-confined PT film to complete oxidation might again reflect its high crystallinity, and was consistent with the unusual features observed in the CV experiments (*vide supra*).

2.2.3. Experimental evidence of the controlled chain-growth mechanism of surface-initiated polymerization.

Although AFM studies revealed the relatively uniform surface morphology of the PT thin films, the advantages of surface-initiated polymerization could be fully implemented only if it indeed followed the controlled chain-growth mechanism. Although we previously showed

strong evidence for such a mechanism when **1**-initiated KCTP was carried out in homogeneous solution (Scheme 2.1), it was important to demonstrate that the robust controlled chain-growth mechanism remains operational in the case of heterogeneous surface-confined polymerization. This confirmation required monitoring both the rate of polymerization and the polymer structure and molecular weight distribution (polydispersity) in the surface-confined thin film. Due to complete insolubility of unsubstituted PT, we could not analyze structure, molecular weight, and polydispersity of the polymer upon its detachment from solid substrate, and thus could only rely upon studies of pristine films. A number of methods could be used for studies of organic thin films, however we specifically chose neutron scattering. Neutron scattering is an attractive tool for the structural characterization of soft organic materials due to the high neutron scattering cross section for light elements and the ability to tune contrast through isotopic labeling. Hydrogen and deuterium have differing scattering cross sections for neutrons so that site-selective deuteration can make some parts of the materials more visible than others without greatly altering other physical properties. Neutron reflectometry (NR) is a particularly suitable tool to study organic thin films.[75-79] The unique sensitivity of NR to the distribution of the deuterated material across the film could be used both to assess the kinetics of polymerization and the controlled (i.e. quasi-"living") character of the polymerization mechanism.

To evaluate both features, we prepared a PT thin-film sample consisting of stratified sublayers of deuterated PT (polydeuterothiophene, PDT) and "regular", non-deuterated PT. To prepare such a sample, we first immersed a quartz substrate with a surface-immobilized monolayer of catalytic initiator **3** in a solution of fully deuterated Grignard monomer **4** (i.e. **4**-D_2) and carried out surface-confined polymerization for 1 h. Then, in oxygen- and moisture-free conditions, we transferred the active substrate with an initially formed PDT film to a solution of

non-deuterated Grignard monomer **4** and kept it there for 6 h to allow for the PT outer layer to form (Figure 2.7A). The film was then treated with methanol to quench the active Ni(II) catalytic sites, and dried in nitrogen.

The NR studies of the resulting partially deuterated thin film produced a reflectivity pattern which was modeled using a two-layer slab model fitting approach to achieve the best fit

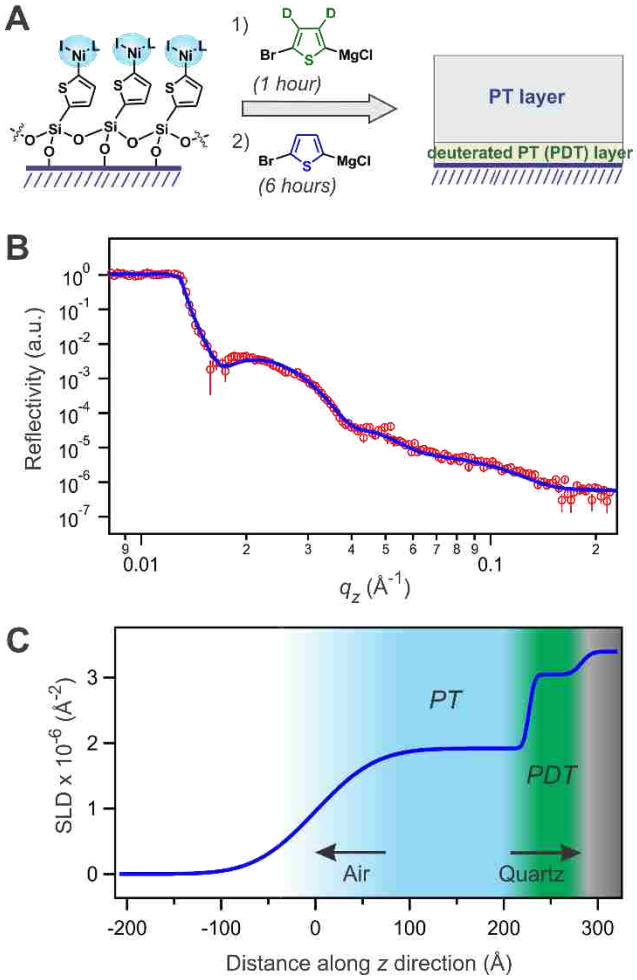

Figure 2.7. (A) Preparation of a stratified deuterated PT thin film on a quartz substrate by carrying out polymerization in a solution of fully deuterated monomer **4**-D_2 followed by polymerization in a non-deuterated monomer **4**. (B) Neutron reflectivity data for the resulting film (red circles) and the best fit to the data (blue solid line). (C) Scattering length density (SLD) profile based on the best-fit data presented in B shows the sharp interface between deuterated (PDT) and non-deuterated (PT) laterally stratified sublayers in the film.

of the experimental data (Figure 2.7B). Fitting the reflectivity vs. wavevector transfer data to a model calculated from the scattering length density (SLD) profile delivered an accurate distribution of the deuterated monomer/polymer as a function of film depth (Figure 2.7C). In agreement with the controlled chain-growth (quasi-"living") mechanism of surface-confined polymerization, the thin-film sample showed highly stratified distribution of the deuterated PDT and non-deuterated PT parts of the film. The PDT sublayer was clearly visible in the SLD profile due to the higher neutron scattering cross section of deuterium. The thickness of the PDT sublayer was about 6 nm (which corresponded to a growth rate of 6 nm h^{-1}), and it sharply transitioned to a non-deuterated PT sublayer of approximately 24 nm thickness. The almost constant SLD values within each constituent sublayer indicated uniform mass density of the polymer across the film thus revealing the persistence and high catalytic activity of reactive Ni(II) centers during polymerization. Even more important was the observation of a sharp interface between the deuterated PDT and non-deuterated PT sublayers. This indicated the robustness of controlled chain-growth polymerization in the surface-confined film as transferring the substrate from fully deuterated Grignard monomer **4**-D_2 to non-deuterated monomer **4** kept the initially formed active polymer chains alive and able to continue further polymerization – an important characteristic feature of truly quasi-"living" polymerization. It also indicated that polymerization front generally propagated in the direction normal to the quartz substrate. Although limited sensitivity of NR experiments could not guarantee that 100% of surface-confined polymer chains followed quasi-"living" polymerization, it is obvious, that any severe deviation from the sharp interface between the deuterated and non-deuterated sublayers would have indicated that different individual surface-attached polymer chains had grown at different kinetic rates throughout the film, and that further growth of some chains had terminated

prematurely by the time of substrate transfer (either due to degradation of the Ni(II) active sites or due to chain transfer to the monomer solution) – thus indicating a less robust, or even not quasi-"living" polymerization mechanism. Similarly diffuse interface would have resulted from random orientation (lack of uniform alignment) of growing polymer chains during surface-initiated polymerization. Therefore, within the sensitivity of NR experiments, our finding both of a sharp interface between sublayers, and a constant, non-changing SLD (and therefore constant polymer mass density) across each sublayer emphasized the controlled (quasi-"living") chain-growth character of the surface-initiated polymerization, as well as uniform orientation of the polymer chains in the film.

2.2.4. Development of surface-initiated polymerization – catalyst regeneration strategy for the preparation of PT films with larger thickness.

The controlled chain-growth mechanism of surface-initiated polymerization allows one to manipulate the thickness of the resulting PT films simply by varying polymerization time. We found that immersing a slide with surface-immobilized Ni(II) initiator in a 50 mM solution of 5-bromothiophen-2-yl magnesium chloride monomer **4** at room temperature for 6 h produced films with an approximately 20 nm thickness. Carrying out polymerization for 12 h afforded PT films with approximately 50 nm thickness. The roughly linear dependence of PT film thickness on the polymerization time reflected the quasi-"living" chain-growth character of the surface-confined polymerization. However, extending polymerization time for a period of longer than 12 h did not result in a further substantial increase in the film thickness, possibly due to eventual degradation of the active surface-bound Ni(II) catalytic sites. This degradation may involve Ni(II) center transfer to Grignard monomer **4** in solution (depicted as chain transfer degradation in Figure 2.8). Such an active center transfer would terminate further growth of a surface-immobilized polymer chain, and result in starting a new polymer chain in solution. An

alternative degradation pathway could involve disproportionation between two adjacent PT chains as also shown in Figure 8. The disproportionation pathway requires significant torsional bending of the surface-attached chains, and was shown by Locklin to be essential in the case of initiation with Ni(II) active catalyst attached to the surface via flexible alkyl linkages where such bending can be better accommodated.[54] The disproportionation releases the Ni(dppp)Br_2 catalytic species into solution, where it can initiate solution polymerization of a new PT chain. Although using rigid linkers in our case should diminish this pathway at early stages of surface-confined polymerization, it cannot be completely ruled out. Degradation of surface-bound Ni(II) catalytic initiator was supported by our observation of the formation of a noticeable amount of insoluble PT precipitate in solution upon extended polymerization times, although it would not be possible to determine which way (Ni(II) transfer to Grignard monomer, disproportionation, or both) this degradation has occurred.

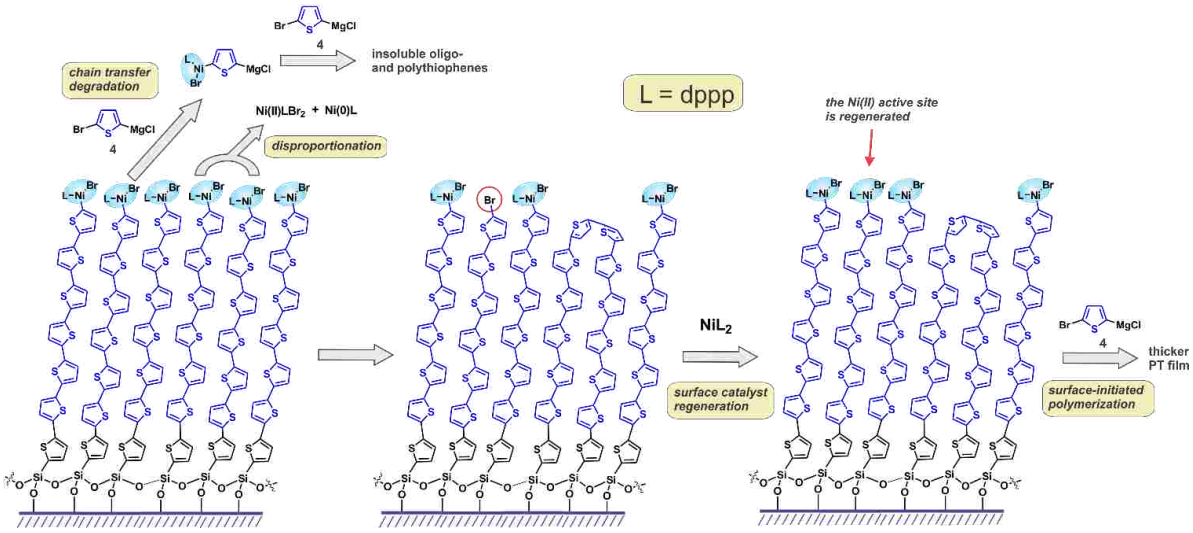

Figure 2.8. Schematic illustration of active surface catalyst degradation through chain transfer and disproportionation, as well as regeneration of the active Ni(II) catalytic initiator for the preparation of thicker polythiophene (PT) films by surface-initiated polymerization. The PT chain alignment normal to the substrate is shown only for illustrative purpose and does not describe the actual complex morphology in the film.

In order to further improve the versatility of surface-confined *in situ* polymerization for preparation of PT films of greater than 50 nm thickness, we have developed a protocol involving intermediate regeneration of the Ni(II) active catalytic center during surface-initiated polymerization. Indeed, if we assume that premature termination of surface-initiated polymerization predominantly occurs by Ni(II) transfer to monomer **4** in solution (chain transfer degradation, as discussed above), this process should terminate the affected surface-attached PT chains with a Br end group from the monomer (Figure 2.8). In such a case, the Ni(II) active catalytic site could be regenerated by reaction of the surface-confined film with a fresh solution of $Ni(dppp)_2$ as used in the *Indirect method* (Figure 2.8). Obviously, such "reactivation" cannot happen at sites that underwent degradation through a disproportionation mechanism. This "reactivated" polymer thin film can be subsequently exposed to Grignard monomer **4** to continue the surface-initiated polymerization. Since such polymerization should mainly happen at the sites on the film surface formed due to the premature termination of polymerization, the overall process is expected to result in a more uniform surface (and bulk) morphology of the resulting PT film.[80] Based on results from the optimization experiments, we developed a general protocol to achieve the best quality (and high thickness) of PT films produced by surface-initiated *in situ* polymerization. The protocol includes initial surface immobilization of Ni(II) catalytic initiator **3** followed by controlled chain-growth polymerization combined with periodic regeneration of the Ni(II) active catalytic center (by immersing the intermediate polymer film in a solution of $Ni(dppp)_2$ at 40 °C for 20 h). This protocol allowed us to prepare uniform PT thin films with up to 100 nm thickness (Figure 2.9). A very important finding was that an increase in the film thickness (tracked by an increase of optical absorbance in the UV/vis spectra) was not accompanied by a hypsochromic shift of the absorption band or a loss of vibronic fine structure

of the band, which indicated that initial molecular order and uniform chain orientation remained preserved even in the thicker films.

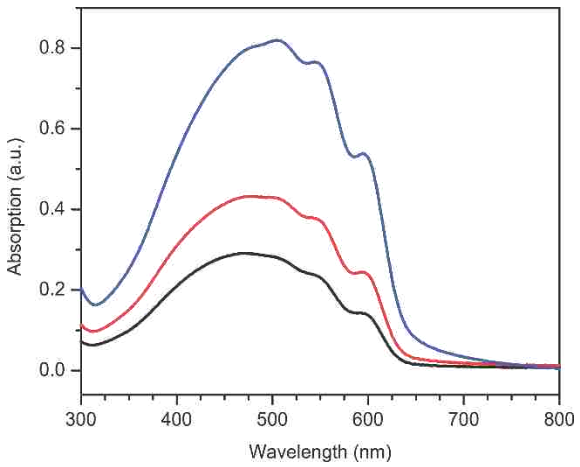

Figure 2.9. UV/vis absorption spectra of PT thin films prepared by surface-initiated polymerization on quartz substrates using intermediate regeneration of active surface catalytic initiator. Black trace corresponds to a PT film prepared by polymerization for 12 h without intermediate regeneration (film thickness ~30 nm), red trace corresponds to a PT film prepared by polymerization for 6 h followed by catalytic initiator regeneration (for 20 h), and with subsequent polymerization for another 6 h (film thickness ~50 nm). Blue trace corresponds to a PT film prepared with three intermediate regenerations (film thickness ~100 nm).

2.2.5. Studies of molecular organization and morphology in surface-confined PT thin films.

Although efforts to use surface-confined polymerization have resulted in substantial improvement of the efficiency of the polymerization as well as the surface density and thickness of the resulting thin films, little was known about bulk mesoscale structure and organization of the polymer in such films. In order to gain a deeper understanding of the possible anisotropic organization and chain alignment of polymer molecules in surface-confined thin films, as well as the influence of polymerization conditions on this organization, we carried out detailed structural investigation of the PT thin films using a variety of techniques. First, we carried out polarization-dependent ultraviolet photoemission spectroscopy (UPS) with linearly polarized

light from a synchrotron source. In order to increase the probing depth, photons with increased energy (85 eV) were used in this study, which allowed probing the layer of about 3 nm deep from the film surface.

For the UPS studies, two samples of PT thin films were prepared on semiconducting indium tin oxide (ITO) substrates. Sample 1 (approximately 20 nm thick based on the stylus profilometry measurements) was prepared using a 6 h polymerization time, and sample 2 (thickness approximately 40 nm) was polymerized for 72 h; in both cases, in order to simplify the data analysis, no surface Ni(II) catalytic initiator regeneration (as described above) was used. In the UPS experiments, the incidence angle of the synchrotron light was changed while the emission was collected normal to the surface (Figure 5.3A in the Experimental Section). In sample 1, the intensity enhancement of the PT valence band (maximum at ~7 eV) in the p-polarized light was indicative of anisotropic orientation of the polymer's transition dipole which coincides with the direction of the PT conjugated backbone (Figure 10A, left graph). Considering the high anisotropy of the stretched polymer molecule, the observed intensity enhancement in the p-polarized light revealed some degree of alignment of the surface-immobilized PT brushes. To determine the preferred orientation angle of the anisotropically aligned polymer chains, we studied the dependence of the intensity of the PT valence band on the emission angle α upon irradiation with (s+p)-polarized light (Figure 5.3B shows a schematic experimental setup, and central graph in Figure 2.10A shows actual experimental data). A plot of the intensity of the valence band maximum *vs.* α showed a broad maximum between 10° and 20°, and a peak at 30° (Figure 2.10A, right graph). Considering the significant contribution of the PT valence band orbitals into the averaged photoemission intensities (the photoemission direction coincides with the molecule's transition dipole), the presence of a signal between α 10°

and 20° indicated that the film contained some fraction of the stretched PT chain segments with a tilt angle between 10° and 20° to the surface normal, i.e. very close to the upright orientation. However, presence of the additional peak at higher value of the angle α clearly indicated that a

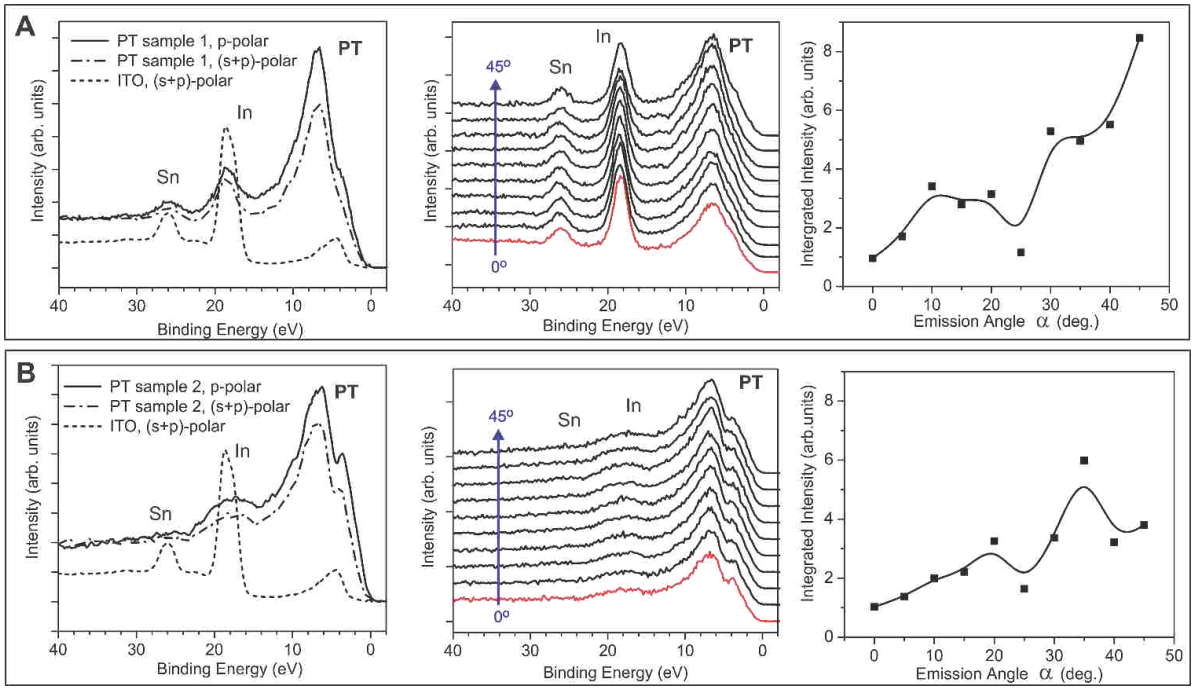

Figure 2.10. Polarization-dependent UPS studies of PT thin-film samples 1 and 2. (A) UPS data for sample 1 (from left to right): UPS spectra acquired at different light polarizations; angular-dependent UPS spectra collected for (s+p)-polarized incident light (beam energy 85 eV, the emission angle α was changed in 5° increments from 0 to 45°); and integrated intensity of the PT polymer valence band maximum (at ~ 7 eV binding energy) *vs.* emission angle α (the area was determined by integration of the valence band peak between Fermi level and 14 eV, with Shirley background subtraction). (B) Data with the same as in (A) experimental setup collected for sample 2.

significant fraction of the PT chain segments was tilted further away from the upright position, closer to the in-plane orientation. The technical limitation of the UPS setup precluded us from looking at the values of the angle α above 45°, but one could not exclude possibility of the presence of even more tilted conjugated segments, especially considering overall large upward

slope of the plot of photoemission intensity *vs.* α. It is important to keep in mind that the photon beam in UPS experiments could only probe relatively low depth near the film surface (about 3 nm), and thus contribution of the deeper layers positioned further away from the film surface to the observed signal would be much smaller. From the initial analysis of these UPS data, it appears that in the sample 1 thin film, some fraction of the PT chain segments showed close to upright orientation (in agreement with the strong signals at α 10-20°), but, at the same time, a large fraction of the chain segments was gradually bending and tilting away from the upright orientation.

In agreement with this structural picture, the thicker sample 2 (thickness approximately 40 nm by stylus profilometry) exhibited a smaller polarization dependence with the p-polarized light (Figure 2.10B). The signal at lower values of angle α (corresponding to the near-upright orientation of the polymer segments) was much weaker compared to sample 1; instead, an intense peak was found between 20 and 45°. As UPS data predominantly reflected the structure and composition of the near-surface layer of the film, it appears that a large fraction of the π-conjugated polymer segments near the surface of the thicker film were oriented along the direction at approximately 40° to the surface normal. Furthermore, considering high-angle limitation of the UPS experimental setup, it is possible that some polymer segments were oriented at even larger angles, closer to the in-plane alignment. Taking into account low probing depth of UPS, and comparing data for the samples 1 and 2, it appears likely that a relatively small fraction of the PT chain segments showed predominantly upright orientation, however, majority of the polymer chains experienced significant tilting and deviation from the upright orientation, with predominant orientation closer to in-plane direction. As UPS could not probe the entire cross-section of the films, it was impossible to determine if there was any uniformity in

the alignment of surface-confined polymer chains (i.e. formation of crystalline domains) or the polymer chains in the bulk of the film were completely randomly oriented, forming a disordered amorphous film.

In the previous experiments on revealing quasi-"living" character of surface-confined polymerization using neutron reflectometry (NR) on selectively deuterated PT film, we concluded that those data supported both the general propagation of the growing polymer chains in the direction normal to the film surface, and uniformity of the resulting polymer chains alignment (*vide supra*). Thus, we decided to carry out additional NR measurements as it can deliver across-the-film profile and thus perfectly supplement UPS studies. A surface-confined PT thin film with an approximate thickness of 50 nm was prepared on a quartz substrate by polymerization of non-deuterated Grignard monomer **4** for 24 h without intermediate Ni(II) surface catalyst regeneration, and the neutron reflectivity data were acquired upon reflecting neutron beam from the polymer/air interface. Figure 2.11A shows the experimental neutron reflectivity curve along with the theoretical model curve which gave the best fit. The scattering length density (SLD) profile based on the fitting model is shown in Figure 2.11B. Remarkably, we found that the film was characterized by constant scattering length density (SLD) of approximately 2.2×10^{-6} Å^{-2} across almost the entire film thickness, spanning from quartz substrate to approximately 70% of the film thickness. The mass density of this high-density part of the film calculated from this SLD value was 1.35 g cm^{-3}, which was higher than the density reported for bulk PT prepared by chemical oxidation of thiophene (1.18 g cm–3),81 but lower than the density obtained from single-crystal X-ray data of octhithiophene (1.58 g cm^{-3}).[82] Since it is expected that mass density of "crystalline" polymer would always be lower than the density

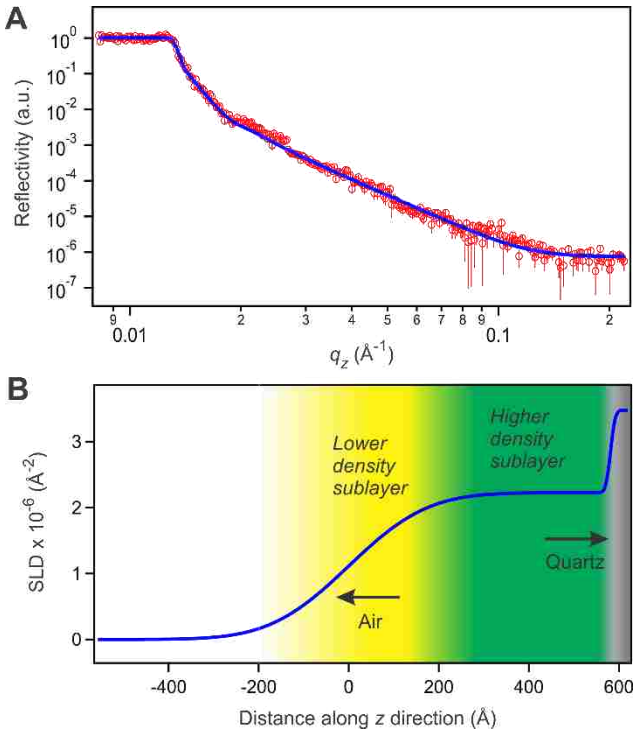

Figure 2.11. Neutron reflectometry study of a 50 nm thick PT film prepared by surface-initiated polymerization on a quartz substrate. (A) Reflectivity data for the film (red circles) and best fit to the data (blue solid line). (B) Scattering length density (SLD) profile based on the best-fit data (single-layer model) presented in A shows two-sublayer stratification in the PT film.

of the corresponding small-molecule crystal, one can safely assume that the bulk of the surface-confined PT film showed uniform morphology and was predominantly formed by closely packed PT chains forming crystalline domains with uniform alignment of the polymer chain segments within each individual domain. NR experiments could not provide information on predominant orientation of these crystalline domains; however, based on the results of the polarized UPS experiments, the polymer chains in the bulk of the film were apparently predominantly oriented along the direction with the tilt angle of at least 40° with respect to the surface normal. In contrast, the outermost layer of the film (approximately 15 nm thick) was characterized by SLD gradually decreasing towards the film surface, with a diffuse film-air interface. Lower SLD

values reflected decreasing mass density in this part of the film, possibly due to the less tight packing of the PT domains and increasing amorphous character near the film surface.

Grazing incidence wide-angle and small-angle X-ray scattering (GIWAXS and GISAXS, respectively) are powerful techniques to study the structure and morphology of thin films of semiconducting polymers, and have been widely used in research of P3HT and related polymers and their blends for photovoltaic applications.[83] The GIWAXS data in Figure 2.12A were acquired using an approximately 40 nm thick PT film prepared on a quartz substrate by surface-initiated polymerization for 72 h without intermediate Ni(II) surface catalytic initiator regeneration (similar to PT sample 2 in the UPS studies, and the sample used in the NR studies described above). The sample showed three distinct arcs at q_z = 1.41 Å^{-1} (d = 4.47 Å), q_z = 1.61 Å^{-1} (d = 3.90 Å), and q_z = 1.94 Å^{-1} (d = 3.24 Å) (Figure 2.12B). The intensity of the arcs maximized in the q_y = 0 plane which clearly indicated the anisotropic nature of the film. The observed GIWAXS pattern was very similar to the previously reported X-ray diffraction pattern of crystalline PT[84, 85] as well as of unsubstituted thiophene oligomers,[86-89] and indicated a highly planar, predominantly extended conformation of the tightly packed surface-confined PT chains. In particular, the observed *d*-spacing pattern was almost identical to the pattern reported by Lahav et al. for β-polymorph of crystalline sexithiophene in Langmuir film (q_{xy} 1.38, 1.63, and 1.97 Å^{-1}).[89] In Lahav's work, using Langmuir technique resulted in uniform alignment of the sexithiophene long molecular axes along the direction normal to the film surface. Similar upright alignment of PT chains in our case would produce Bragg diffraction rods extending along the q_z direction, however experimentally we observed diffraction arcs with a maximum in intensity near the q_z axis (i.e. with the maximum at q_y = 0). The only way to explain this observation was to suggest that the PT chains in the film were packed in the same way as in the

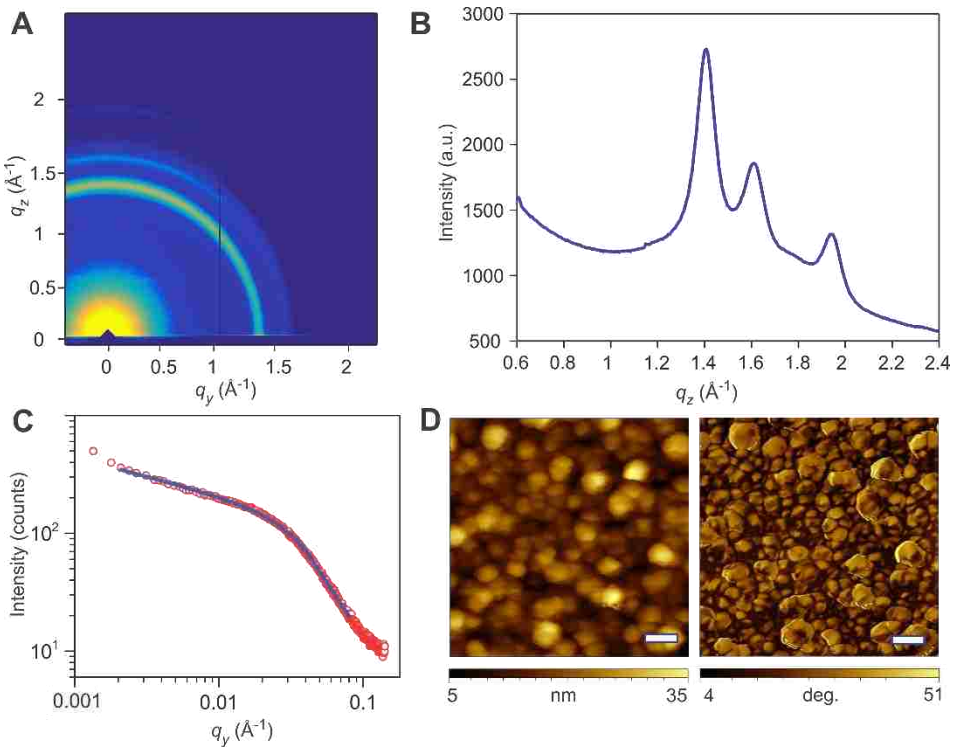

Figure 2.12. (A) Two-dimensional GIWAXS image of a 40 nm thick PT film prepared by surface-initiated polymerization on a quartz substrate. (B) Vertical linecut of the GIWAXS data of the film in A. (C) GISAXS horizontal line trace for the 40 nm thick PT film in (A) (red circles) and fitting these data using a modified Guinier-Porod model (blue trace). (D) Tapping-mode AFM images for the PT film in (A) (left image – topography, right image – phase), scale bars correspond to 100 nm.

β-phase of crystalline sexithiophene, but aligned predominantly parallel to the film surface with herringbone (face-to-edge) packing of the neighboring planarized PT chains within individual crystalline domains. The herringbone molecular packing of unsubstituted PT stays in stark contrast to 3-alkyl-substituted PTs where the alkyl substituents induce face-to-face π-stacking of the conjugated chains[90] but is rather common for unsubstituted oligomeric thiophenes.

The predominantly in-plane alignment of the PT chain segments in GIWAXS experiments was in agreement with the conclusions from UPS experiment. Whereas, due to technical limitations of the UPS experimental setup, we could not observe features originating from the in-plane polymer chain orientation (i.e. tilt angle about 90° to the surface normal), we

did observe in those experiments significant deviation of the polymer chains from the out-of-plane (i.e. normal to surface) orientation, especially in the thicker sample similar to the one studied in the X-ray scattering experiments. Importantly, the broad intensity distribution along the diffraction arcs in GIWAXS experiments indicated that, despite some predominance of the in-plane orientation, the overall pattern was consistent with presence of a full spectrum of crystalline orientations, ranging from out-of-plane to in-plane. This distribution of orientations appeared the same throughout the thickness of the film, and did not change with the angle of incidence. We acquired GIWAXS data at various incidence angles (ranging from 0.16° to 0.22°, both below and above the critical angle for PT) which allowed tunable depth analysis across the film (Figure 5.4 in the Experimental Section). We found that incidence angle variation changed only total intensity of the diffraction profile, but produced no significant variation in the position and relative intensity of the individual diffraction peaks. Therefore, it was reasonable to conclude that the film showed relatively uniform mesostructure and polymer chain packing across almost the entirety of its thickness, in agreement with the constant density across the film revealed in the NR studies.

Further information on the structure and morphology of the surface-confined PT film was obtained from GISAXS studies. The horizontal linecut showed a "Guinier knee"[91] feature indicating formation of lateral nanoscale domains within the film (Figure 2.12C). Fitting the scattering data using a combined Porod plus Guinier model (this model assumes that the Porod region extending from the larger-size domains overlaps with the Guinier region of the smaller-size domains,[92] whereas the corresponding Guinier region corresponding to the large domains could not be observed due to the low q-range limitation of the GISAXS instrumental setup), allowed us to estimate the diameter of small-size lateral domains as approximately 3.2 nm. This

value was much smaller than the average size of lateral surface features (40-60 nm) observed upon subsequent AFM studies carried out on the same film (Figure 2.12D). On the other hand, AFM provides information on size and morphology of the surface features of the film whereas the GISAXS study is characteristic of the average size of the well-defined high-density crystalline segments within the bulk of the film. Therefore, GISAXS data likely reflected the average size of individual lateral crystalline domains within the bulk of the film whereas AFM imaging showed surface features resulting from combination of these multiple crystalline domains into larger surface domains.

Combining together the experimental data and conclusions discussed in this section, we propose a working hypothesis on the structure of thin PT films prepared by surface-initiated polymerization. The polymerization occurs as a controlled chain-growth process, with overall propagation of the front of the growing polymer film in the direction normal to the surface, as was demonstrated using polymerization of the deuterium-labeled Grignard monomer discussed above. Although the requirement to accommodate multiple simultaneously growing surface-attached polymer chains might invoke the chain alignment in the direction normal to the surface (as, for example, schematically shown in Figures 2.1 and 2.8), the results of our experiments completely disagree with this conjecture. Instead, surface-confined polymer chains form densely packed crystalline domains with predominant chain orientation close to the in-plane direction, and in addition showing a continuum of different orientations ranging between in-plane and normal to the surface. Although, at first glance, it may appear impossible to combine both experimentally observed controlled quasi-"living" mechanism of surface-initiated polymerization, and the predominant in-plane alignment of the resulting polymer chains, they could be accommodated if one assumes that the polymer chains start initial growing in the in-

plane direction. Indeed, relatively low Ni(II) catalytic initiator surface density (with each molecule of surface-immobilized initiator **3** occupying an area of about 400 $Å^2$) makes it unfavorable for the polymer chains to align in the normal, out-of-plane direction as they would not be able to achieve close interchain packing. Instead, the attractive van der Waals interactions between the surface-confined polymer chains promote chain tilting which allows to achieve close crystalline packing in the in-plane direction and form a high-density polymer film. However, the clusters cannot grow indefinitely in the initial in-plane direction as they will necessarily start interfering with other neighboring surface-growing clusters. Thus, all of the in-plane growing clusters on the surface can only be mutually accommodated if, at some point, the ensembles of polymer chains gradually twist, eventually forming folded loops allowing to continue the in-plane growth in the opposite direction, without interfering with neighboring growing clusters. The schematic structure of the surface-confined PT film according to this model is illustrated in Figure 2.13. As the result of in-plane growth and polymer chain folding, the polymer film is composed of laterally packed crystalline clusters with an average size of 3.2 nm (as was found in the GISAXS experiments) which protrude through the entire cross-section of the film. Each cluster is formed from a few folded polymer chains which show predominant in-plane "herringbone" (edge-to-face) packing of the chain segments between the folds. Indeed, considering the lateral size of such clusters at 3.2 nm, the average polymer segment between two folds must consist of about 7-8 thiophene repeating units. This explains why crystal structure of the polymer found in GIWAXS experiments strongly resembled that of β-phase of sexithiophene. Furthermore, such a structure would be consistent with the electrochemical data on the surface-confined PT film. Indeed, due to sufficient disruption of π-electron conjugation at the sites where an individual polymer chain twists and folds, folding of the polymer chain every

7-8 repeating units would create electronically isolated crystalline packed "oligothiophene" segments (7 or 8 thiophene units each) – which was actually observed in the cyclic voltammetry (CV) studies (where the CV data of PT film resembled that of thin-film thiophene octamer with a large hysteresis, *vide supra*). The formation of folded packed structure also explains the broad range of other orientations found in GIWAXS data, as the wide range of orientations was produced by the out-of-plane fragments of the polymer chains within the folds.

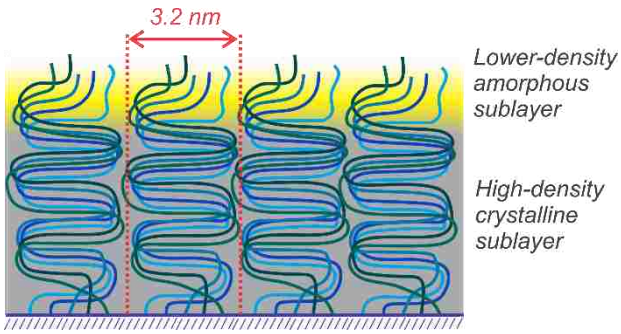

Figure 2.13. Schematic illustration of the proposed PT thin film structure as based on the experimental evidence in this chapter. Surface-confined PT chains bundle together to form folded in-plane packed crystalline domains about 3.2 nm in lateral size. The film consists of these primary domains protruding through the film thickness and densely packed side-by-side. The elements in the image are not up to scale.

The reason for the PT chain to pack in segments of 7-8 repeating units is not clear at this time. It can be simply related to solubility of oligothiophene in the polymerization solvent (THF) as, once the growing chain fragment reaches this critical length, its solubility becomes so low that it has to "crystallize" out of solution. More studies are required to definitely explain this. Overall, this structural model is consistent with controlled, quasi-"living" mechanism of the surface-initiated polymerization, and the relatively smooth surface morphology of the resulting thin films; this is also consistent with finding a sharp deuterated PDT – PT interface in the NR experiments with selectively deuterated films (*vide supra*). On the larger scale, the primary

lateral clusters group in larger size circular domains (40-60 nm in size), which were the typical characteristic of the surface morphology found in AFM experiments (Figure 2.5 and 2.12D). Considering predominantly close to in-plane orientation of PT molecules in this model, the surface-initiated polymerization has to be highly robust and efficient. Indeed, routine preparation of a 40 nm thick PT film would require producing polymer chains in a controlled chain-growth fashion with a degree of polymerization corresponding to a few thousand of thiophene repeating unit – a difficult to accomplish task even for a homogeneous solution polymerization. It may be possible, however, that carrying out externally initiated KCTP in surface-confined fashion somehow increases robustness and controlled character of the polymerization relative to solution polymerization. Clarifying this issue will certainly require additional studies.

Although this working model reasonably explains many of the experimental findings, it remains less certain if formation of the lower-density (and seemingly more amorphous) outermost layer found in the NR experiments happens during surface-initiated polymerization as a result of sufficient lengthening of polymer chains (so the increased entropic contribution can overcome attractive interchain interactions resulting in polymer folding), and thus would be dependent on the total film thickness, or it happens after completion of the polymerization, as a result of stabilizing polymer-solvent interactions. In the latter case, the surface-confined polymer film should always possess a lower-density outer sublayer, whereas in the former case one would expect that lower-thickness surface-confined polymer films would consist of only a single higher-density crystalline layer. Our preliminary GIWAXS and NR studies pointed on the formation of the outer lower-density layer even in thinner films, thus indicating the solvent-affected post-polymerization formation of the outer layer. Also, at this point the success of the

strategy involving combination of surface-initiated polymerization with intermediate regeneration of the Ni(II) surface catalytic initiator in obtaining thicker PT films (*vide supra*) seems to point on this mechanism as well. It appears (at least from the UV/vis absorption spectroscopy data in Figure 2.9) that using a repeated "regeneration" approach can furnish thin films with up to 100 nm thickness which still preserve vibronic features typical for a highly organized polymer film. Additional studies are required to further refine the proposed bulk structural model, and to provide better understanding of the polymerization process and its relation to thin-film structure, as well as to determine other ways to improve control over surface morphology and molecular organization in surface-confined PT thin films.

2.2.6. Preparation of nanopatterned PT thin films by surface-initiated polymerization.

A unique advantage of surface-initiated polymerization is that it allows preparation of nanopatterned surface-immobilized semiconducting polymer thin films. Preparation of uniformly nanopatterned polymer thin films is virtually impossible with current "top-down" paradigm relying on solution processing of pre-synthesized polymers. On the other hand, preparation of such nanopatterned thin films should be relatively straightforward using our surface-initiated *in situ* polymerization approach combined with an appropriate protocol to prepare nanopatterned monolayer of polymerization catalytic initiator **3**. In a proof-of-concept study, we selected particle lithography as a convenient method to prepare such a monolayer. Particle lithography[93] has previously been applied to pattern metals, inorganic materials, alkanethiol self-assembled monolayers (SAMs), organosilane films and polymers.[94-100] Millions of nanostructures can be prepared on surfaces with relatively few defects and high reproducibility to enable patterning large surfaces with well-defined nanostructures.[101-103] Our approach is illustrated in Figure 2.14. First, a close-packed periodic hexagonal array of

monodisperse latex mesoparticles (300 nm diameter) was prepared on the atomically flat Si(111) surface using solution-based assembly. The mesoparticle array served as a surface mask, and the uncovered areas on silicone surface were functionalized with octadecyltrichlorosilane (OTS) using PDMS stamping transfer followed by washing out the latex particles. An example of nanopores produced by particle lithography is shown in Figure 5.1 in the Experimental Section. Although the local roughness of mechanically polished silicon wafers prevented us from distinguishing the pore structures in AFM topography views, the simultaneously acquired lateral force images clearly resolved the circular shapes and hexagonal arrangement of the nanopores.

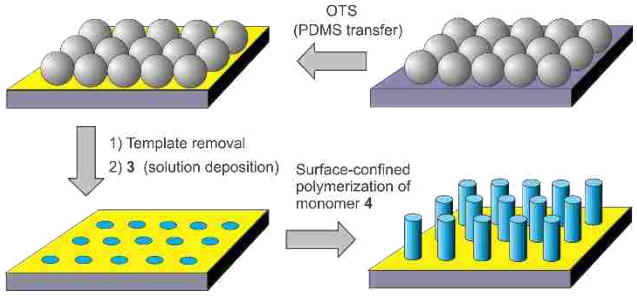

Figure 2.14. Schematic outline of the optimized approach to prepare hexagonally nanopatterned PT thin films via combination of particle lithography and surface-initiated *in situ* polymerization.

Covalent immobilization of the Ni(II) catalytic initiator **3** in the uncovered with OTS areas produced nanopatterned catalytic surface which was used for surface-initiated polymerization of Grignard monomer **4** for 24 h total time to yield hexagonal arrays of PT nanopillars (Figure 2.15).

Covalent immobilization of the Ni(II) catalytic initiator **3** in the uncovered with OTS areas produced nanopatterned catalytic surface which was used for surface-initiated polymerization of Grignard monomer **4** for 24 h total time to yield hexagonal arrays of PT nanopillars (Figure2.15). The long-range order of the PT nanopillars (bright dots in Figure 2.15A)

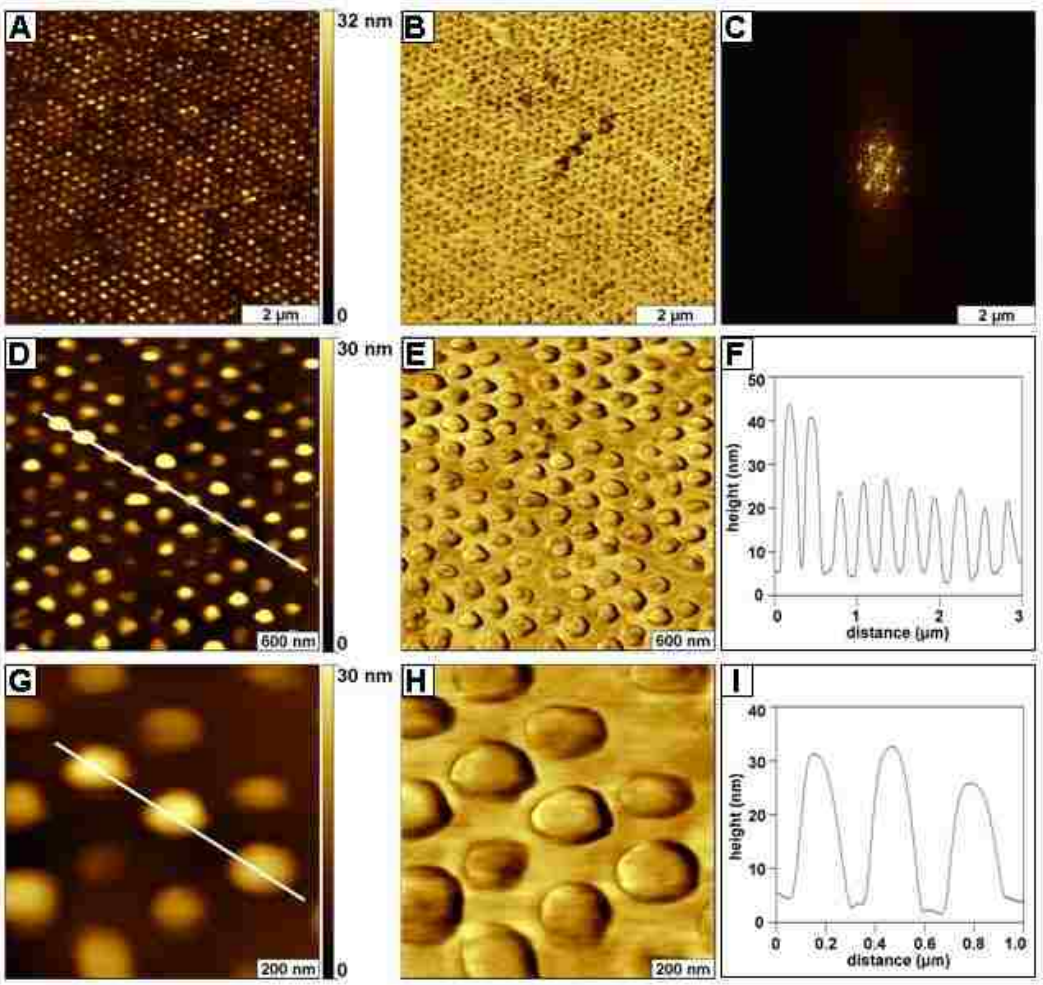

Figure 2.15. Arrays of PT nanocolumns on Si(111) produced by combination of particle lithography and surface-initiated *in situ* polymerization. (A) AFM topography image of the PT surface patterns. (B) Corresponding lateral force image. (C) Two-dimensional FFT spectrum generated from the topograph in A. (D) Zoom-in view (3×3 μm^2) topograph. (E) Corresponding lateral force image for D. (F) Cursor plot for the line in D. (G) High-resolution topograph (1×1 μm^2). (H) Lateral force image for G. (I) Height profile for the line in G.

is shown with a representative 8×8 μm^2 topograph and lateral force image (Figure 2.15B). The regular arrays of PT nanostructures were evident throughout areas of the entire surface, indicating the high-throughput capabilities of particle lithography. The ability to produce large-area PT nanopatterns was also evident from the SEM images of this sample (Figure 5.2 in the Experimental Section). A plot acquired from two-dimensional fast Fourier transform (FFT)

analysis of the 8×8 μm^2 AFM topography image displayed the reciprocal space and periodicity of the nanostructures (Figure 2.15C). The symmetric arrangement of the PT patterns can be viewed more clearly in the successive zoom-in views (3×3 μm^2) of topography and simultaneously acquired lateral force images shown in Figures 2.15D and E, respectively. A line profile (Figure 2.15F) across ten PT nanostructures showed heights ranging from 16 to 38 nm. The center-to-center spacing between nanopatterns measured 289$\pm$3 nm, closely matching the periodicity of the initial latex mesoparticle mask. To obtain perfect nanoscale geometries would require an absolutely flat surface at the atomic level and perfectly symmetric monodisperse latex spheres. In a real situation there are few surfaces that are atomically flat, and the variation in the sizes of latex spheres ranges from 1 to 5%. These small imperfections lead to different pore sizes, which produced the observed variations in height for the nanopillars. Due to the covalent immobilization on the Si surface, the nanopatterned films demonstrated unique stability towards organic solvents. Thus, prolonged ultrasonication of the patterned PT films in commonly used organic solvents such as chloroform and chlorobenzene did not result in any degradation of the nanostructures. This remarkable solvent stability would be particular suitable for further processing of the nanopatterned films, e.g. for spin-casting using solutions of other polymers to make more complex organic devices. This example demonstrated the principle capacity of the combination of particle lithography with efficient surface-initiated polymerization to produce large-area periodically patterned stable PT nanostructures. Further studies on the possibility to control the size of the nanostructures in the surface-confined PT thin films are currently underway.

2.3. Conclusions

Controlled Kumada catalyst transfer polymerization occurring by the chain-growth mechanism became an established method for the synthesis of a wide variety of semiconducting polymers in solution. A possibility to carry out this reaction in heterogeneous fashion on surfaces could make it a valuable tool for the preparation of surface-confined semiconducting polymer films directly from small-molecule monomers. We developed and described a simple and efficient approach to the preparation of surface-immobilized monolayer of catalytic Ni(II) initiator, and demonstrated using it for efficient surface-initiated polymerization to form covalently attached PT thin films with thicknesses up to 100 nm. Our demonstration that this reaction occurs by controlled (quasi-"living") chain-growth mechanism can, in principle, open venues toward controlled preparation of various copolymer and block copolymer thin films with precisely defined molecular composition. The surface-initiated polymerization is also not limited to polythiophenes but can be used to prepare surface-attached thin films of other important semiconducting polymers. We are currently studying using this method to prepare a broader variety of semiconducting polymer and block copolymer films. What makes the surface-confined polymerization truly unique is that it allows preparation of thin films with ordered morphology and uniform alignment of the polymer chains in the bulk of the crystalline polymer film – a property which may result in performance improvement of electronic and optoelectronic devices based on these films. Our extensive structural studies utilizing polarized UPS and X-ray and neutron scattering techniques revealed complex structure and organization of the surface-confined PT thin films; further experiments are still needed to gain better understanding of the film structure, as well as its dependence on various experimental factors. Finally, we demonstrated how the efficient surface-initiated polymerization, combined with nanoscale

surface lithography, can be used in the preparation of large-area uniformly nanopatterned PT thin films. Overall, this initial study will help in further development of surface-confined controlled chain-growth polymerization as a unique synthetic tool for engineering of new electronic and optoelectronic materials based on thin films of semiconducting polymers.

2.4. References

(1) Nelson, J. Organic Photovoltaic Films. *Curr. Opin. Solid State Mater. Sci.* **2002**, *6*, 87-95.

(2) Peet, J.; Kim, J. Y.; Coates, N. E.; Ma, W. L.; Moses, D.; Heeger, A. J.; Bazan, G. C. Efficiency Enhancement in Low-Bandgap Polymer Solar Cells by Processing with Alkane Dithiols. *Nat. Mater.* **2007**, *6*, 497-500.

(3) Lee, J. K.; Ma, W. L.; Brabec, C. J.; Yuen, J.; Moon, J. S.; Kim, J. Y.; Lee, K.; Bazan, G. C.; Heeger, A. J. Processing Additives for Improved Efficiency from Bulk Heterojunction Solar Cells. *J. Am. Chem. Soc.* **2008**, *130*, 3619-3623.

(4) Wang, W.; Wu, H.; Yang, C.; Luo, C.; Zhang, Y.; Chen, J.; Cao, Y. High-Efficiency Polymer Photovoltaic Devices from Regioregular-Poly(3-hexylthiophene-2,5-diyl) and [6,6]-Phenyl-C_{61}-Butyric Acid Methyl Ester Processed with Oleic Acid Surfactant. *Appl. Phys. Lett.* **2007**, *90*, 183512.

(5) Li, G.; Shrotriya, V.; Huang, J.; Yao, Y.; Moriarty, T.; Emery, K.; Yang, Y. High-Efficiency Solution Processable Polymer Photovoltaic Cells by Self-Organization of Polymer Blends. *Nat. Mater.* **2005**, *4*, 864-868.

(6) Park, L. Y.; Munro, A. M.; Ginger, D. S. Controlling Film Morphology in Conjugated Polymer:Fullerene Blends with Surface Patterning. *J. Am. Chem. Soc.* **2008**, *130*, 15916-15926.

(7) Niu, Q.; Zhou, Y.; Wang, L.; Peng, J.; Wang, J.; Pei, J.; Cao, Y. Enhancing the Performance of Polymer Light-Emitting Diodes by Integrating Self-Assembled Organic Nanowires. *Adv. Mater.* **2008**, *20*, 964-969.

(8) Abbel, R.; Grenier, C.; Pouderoijen, M. J.; Stouwdam, J. W.; Leclère, P. E. L. G.; Sijbesma, R. P.; Meijer, E. W.; Schenning, A. P. H. J. White-Light Emitting Hydrogen-Bonded Supramolecular Copolymers Based on π-Conjugated Oligomers. *J. Am. Chem. Soc.* **2009**, *131*, 833-843.

(9) Zhang, Y.; Huang, F.; Chi, Y.; Jen, A. K.-Y. Highly Efficient White Polymer Light-Emitting Diodes Based on Nanometer-Scale Control of the Electron Injection Layer Morphology Through Solvent Processing. *Adv. Mater.* **2008**, *20*, 1565-1570.

(10) Yang, J.-S.; Swager, T. M. Porous Shape Persistent Fluorescent Polymer Films: an Approach to TNT Sensory Materials. *J. Am. Chem. Soc.* **1998**, *120*, 5321-5322.

(11) Naddo, T.; Che, Y.; Zhang, W.; Balakrishnan, K.; Yang, X.; Yen, M.; Zhao, J.; Moore, J. S.; Zang, L. Detection of Explosives with a Fluorescent Nanofibril Film. *J. Am. Chem. Soc.* **2007**, *129*, 6978-6979.

(12) Marshall, N.; Sontag, S. K.; Locklin, J. Surface-Initiated Polymerization of Conjugated Polymers. *Chem. Commun.* **2011**, *47*, 5681-5689.

(13) Alonzi, M.; Lanari, D.; Marrocchi, A.; Petrucci, C.; Vaccaro, L. Synthesis of Polymeric Semiconductors by a Surface-Initiated Approach. *RCS Adv.* **2013**, *3*, 23909-23923.

(14) Bousquet, A.; Awada, H.; Hiorns, R. C.; Dagron-Lartigau, C.; Billon, L. Conjugated-Polymer Grafting on Inorganic and Organic Substrates: a New Trend in Organic Electronic Materials. *Prog. Polym. Sci.* **2014**, *39*, 1847-1877.

(15) Murugan, P.; Krishnamurthy, M.; Jaisankar, S. N.; Samanta, D.; Mandal, A. B. Controlled Decoration of the Surface with Macromolecules: Polymerization on a Self-Assembled Monolayer (SAM). *Chem. Soc. Rev.* **2015**, *44*, 3212-3243.

(16) Beryozkina, T.; Boyko, K.; Khanduyeva, N.; Senkovskyy, V.; Horecha, M.; Oertel, U.; Simon, F.; Stamm, M.; Kiriy, A. Grafting of Polyfluorene by Surface-Initiated Suzuki Polycondensation. *Angew. Chem. Int. Ed.* **2009**, *48*, 2695-2698.

(17) Huddleston, N. E.; Sontag, S. K.; Bilbrey, J. A.; Sheppard, G. R.; Locklin, J. Palladium-Mediated Surface-Initiated Kumada Catalyst Polycondensation: a Facile Route Towards Oriented Conjugated Polymers. *Macromol. Rapid Commun.* **2012**, *33*, 2115-2120.

(18) Kang, S.; Ono, R. J.; Bielawski, C. W. Controlled Catalyst Transfer Polycondensation and Surface-Initiated Polymerization of a *p*-Phenyleneethynylene-Based Monomer. *J. Am. Chem. Soc.* **2013**, *135*, 4984-4987.

(19) Awada, H.; Bousquet, A.; Dagron-Lartigau, C.; Billon, L. Surface-Initiated Polymerization of A-A/B-B Type Conjugated Monomers by Palladium-Catalyzed Stille Polycondensation: Towards Low Band Gap Polymer Brushes. *RCS Adv.* **2015**, *5*, 78436-78440.

(20) Yang, L.; Sontag, S. K.; LaJoie, T. W.; Li, W.; Huddleston, N. E.; Locklin, J.; You, W. Surface-Initiated Poly(3-methylthiophene) as a Hole-Transport Layer for Polymer Solar Cells with High performance. *ACS Appl. Mater. Interfaces* **2012**, *4*, 5069-5073.

(21) Boon, F.; Moerman, D.; Laurencin, D.; Richeter, S.; Guari, Y.; Mehdi, A.; Dubois, P.; Lazzaroni, R.; Clément, S. Synthesis of TiO_2–Poly(3-hexylthiophene) Hybrid Particles through Surface-Initiated Kumada Catalyst-Transfer Polycondensation. *Langmuir* **2014**, *30*, 11340-11347.

(22) Doubina, N.; Jenkins, J. L.; Paniagua, S. A.; Mazzio, K. A.; MacDonald, G. A.; Jen, A. K.-Y.; Armstrong, N. R.; Marder, S. R.; Luscombe, C. K. Surface-Initiated Synthesis of Poly(3-methylthiophene) from Indium Tin Oxide and its Electrochemical Properties. *Langmuir* **2012**, *28*, 1900-1908.

(23) McCullough, R. D. The Chemistry of Conducting Polythiophenes. *Adv. Mater.* **1998**, *10*, 93-116.

(24) Roncali, J. Conjugated Poly(thiophenes): Synthesis, Functionalization, and Applications. *Chem. Rev.* **1992**, *92*, 711-738.

(25) *P3HT Revisited – from Molecular Scale to Solar Cell Devices*; Ludwigs, S., Ed.; Advances in Polymer Science, vol. 265; Springer: Berlin, Heidelberg, 2014.

(26) Osaka, I.; McCullough, R. D. Advances in Molecular Design and Synthesis of Regioregular Polythiophenes. *Acc. Chem. Res.* **2008**, *41*, 1202-1214.

(27) Zhao, G.; He, Y.; Li, Y. 6.5% Efficiency of Polymer Solar Cells Based on Poly(3-hexylthiophene) and Indene-C_{60} Bisadduct by Device Optimization. *Adv. Mater.* **2010**, *22*, 4355-4358.

(28) Dang, M. T.; Hirsch, L.; Wantz, G. P3HT:PCBM, Best Seller in Polymer Photovoltaic Research. *Adv. Mater.* **2011**, *23*, 3597-3602.

(29) Sivula, K.; Ball, Z. T.; Watanabe, N.; Fréchet, J. M. J. Amphiphilic Diblock Copolymer Compatibilizers and Their Effect on the Morphology and Performance of Polythiophene:Fullerene Solar Cells. *Adv. Mater.* **2006**, *18*, 206-210.

(30) Chen, D.; Nakahara, A.; Wei, D.; Nordlund, D.; Russell, T. P. P3HT/PCBM Bulk Heterojunction Organic Photovoltaics: Correlating Efficiency and Morphology. *Nano Lett.* **2011**, *11*, 561-567.

(31) Brinkmann, M.; Rannou, P. Effect of Molecular Weight on the Structure and Morphology of Oriented Thin Films of regioregular Poly(3-hexylthiophene) Grown by Directional Epitaxial Solidification. *Adv. Funct. Mater.* **2007**, *17*, 101-108.

(32) Etzold, F.; Howard, I. A.; Forler, N.; Cho, D. M.; Meister, M.; Mangold, H.; Shu, J.; Hansen, M. R.; Müllen, K.; Laquai, F. The Effect of Solvent Additives on Morphology and Excited-State Dynamics in PCPDTBT:PCBM Photovoltaic Blends. *J. Am. Chem. Soc.* **2012**, *134*, 10569-10583.

(33) He, M.; Zhao, J.; Han, W.; Yang, Y.; Qiu, F.; Lin, Z. Self-Assembly of All-Conjugated Poly(3-alkylthiophene) Diblock Copolymer Nanostructures from Mixed Selective Solvents. *ACS Nano* **2010**, *4*, 3241-3247.

(34) Dimitrakopoulos, C. D.; Malenfant, P. R. L. Organic Thin Film Transistors for Large Area Electronics. *Adv. Mater.* **2002**, *14*, 99-117.

(35) Kim, Y.; Cook, S.; Tuladhar, S. M.; Choulis, S. A.; Nelson, J.; Durrant, J. R.; Bradley, D. D. C.; Giles, M.; McCulloch, I.; Ha, C.-S.; Ree, M. A Strong Regioregularity Effect in Self-Organizing Conjugated Polymer Films and High-Efficiency Polythiophene:Fullerene Solar Cells. *Nat. Mater.* **2006**, *5*, 197-203.

(36) Jeffries-El, M.; McCullough, R. D. Regioregular polythiophenes. In: *Handbook of Conducting Polymers, 3rd ed.*; Skotheim, T. A., Reynolds, J. R., Eds.; CRC Press: Boca Raton, 2007; Vol. 1, 9-1–9-49.

(37) Manceau, M.; Rivaton, A.; Gardette, J. L.; Guillerez, S.; Lemaître, N. The Mechanism of Photo- and Thermooxidation of Poly(3-hexylthiophene) (P3HT) Reconsidered. *Polym. Degrad. Stab.* **2009**, *94*, 898-907.

(38) Chambon, S.; Rivaton, A.; Gardette, J. L.; Firon, M.; Lutsen, L. Aging of a Donor Conjugated Polymer: Photochemical Studies of the Degradation of Poly[2-methoxy-5-(3',7'-dimethyloctyloxy)-1,4-phenylenevinylene]. *J. Polym. Sci., Part A: Polym. Chem.* **2007**, *45*, 317-331.

(39) Adhikari, B.; Majumdar, S. Polymers in Sensor Applications. *Prog. Polym. Sci.* **2004**, *29*, 699-766.

(40) Guimard, N. K.; Gomez, N.; Schmidt, C. E. Conducting Polymers in Biomedical Engineering. *Prog. Polym. Sci.* **2007**, *32*, 876-921.

(41) Ma, H.; Yip, H.-L.; Huang, F.; Jen, A. K.-Y. Interface Engineering for Organic Electronics. *Adv. Funct. Mater.* **2010**, *20*, 1371-1388.

(42) Audebert, P.; Miomandre, F. Electrochemistry of conducting polymers. In: *Handbook of Conducting Polymers, 3rd ed.*; Skotheim, T. A., Reynolds, J. R., Eds.; CRC Press: Boca Raton, 2007; Vol. 1, 18-1–18-40.

(43) Loewe, R. S.; Khersonsky, S. M.; McCullough, R. D. A Simple Method to Prepare Head-to-Tail Coupled, Regioregular Poly(3-alkylthiophenes) Using Grignard Metathesis. *Adv. Mater.* **1999**, *11*, 250-258.

(44) Loewe, R. S.; Ewbank, P. C.; Liu, J.; Zhai, L.; McCullough, R. D. Regioregular, Head-to-Tail Coupled Poly(3-alkylthiophenes) Made Easy by the GRIM Method: Investigation of the Reaction and the Origin of Regioselectivity. *Macromolecules* **2001**, *34*, 4324-4333.

(45) Chen, T.-A.; Wu, X.; Rieke, R. D. Regiocontrolled Synthesis of Poly(3-alkylthiophenes) Mediated by Rieke Zinc: Their Characterization and Solid-State Properties. *J. Am. Chem. Soc.* **1995**, *117*, 233-244.

(46) Sheina, E. E.; Liu, J.; Iovu, M. C.; Laird, D. W.; McCullough, R. D. Chain Growth Mechanism for Regioregular Nickel-Initiated Cross-Coupling Polymerizations. *Macromolecules* **2004**, *37*, 3526-3528.

(47) Iovu, M. C.; Sheina, E. E.; Gil, R. R.; McCullough, R. D. Experimental Evidence for the Quasi-"Living" Nature of the Grignard Metathesis (GRIM) for the Synthesis of Regioregular Poly(3-alkylthiophenes). *Macromolecules* **2005**, *38*, 8649-8656.

(48) Yokoyama, A.; Miyakoshi, R.; Yokozawa, T. Chain-Growth Polymerization for Poly(3-hexylthiophene) with a Defined Molecular Weight and a Low Polydispersity. *Macromolecules* **2004**, *37*, 1169-1171.

(49) Miyakoshi, R.; Yokoyama, A.; Yokozawa, T. Catalyst-Transfer Polycondensation. Mechanism of Ni-Catalyzed Chain-Growth Polymerization Leading to Well-Defined Poly(3-hexylthiophene). *J. Am. Chem. Soc.* **2005**, *127*, 17542-17547.

(50) Senkovskyy, V.; Khanduyeva, N.; Komber, H.; Oertel, U.; Stamm, M.; Kuckling, D.; Kiriy, A. Conductive Polymer Brushes of Regioregular Head-to-Tail Poly(3-alkylthiophenes) via Catalyst Transfer Surface-Initiated Polycondensation. *J. Am. Chem. Soc.* **2007**, *129*, 6626-6632.

(51) Khanduyeva, N.; Senkovskyy, V.; Beryozkina, T.; Bocharova, V.; Simon, F.; Nitschke, M.; Stamm, M.; Crötzschel, R.; Kiriy, A. Grafting of Poly(3-hexylthiophene) from Poly(4-bromostyrene) Films by Kumada Catalyst-Transfer Polycondensation: Revealing of the Composite Films Structure. *Macromolecules* **2008**, *41*, 7383-7389.

(52) Khanduyeva, N.; Senkovskyy, V.; Beryozkina, T.; Horecha, M.; Stamm, M.; Uhrich, C.; Riede, M.; Leo, K.; Kiriy, A. Surface Engineering Using Kumada Catalyst-Transfer Polycondensation (KCTP): Preparation and Structuring of Poly(3-hexylthiophene)-Based Graft Copolymer Brushes. *J. Am. Chem. Soc.* **2009**, *131*, 153-161.

(53) Kiriy, A.; Senkovskyy, V.; Sommer, M. Kumada Catalyst-Transfer Polycondensation: Mechanism, Opportunities, and Challenges. *Macromol. Rapid Commun.* **2011**, *32*, 1503-1517.

(54) Sontag, S. K.; Sheppard, G. R.; Usselman, N. M.; Marshall, N.; Locklin, J. Surface-Confined Nickel-Mediated Cross-Coupling Reactions: Characterization of Initiator Environment in Kumada Catalyst-Transfer Polycondensation. *Langmuir* **2011**, *27*, 12033-12041.

(55) Sontag, S. K.; Marshall, N.; Locklin, J. Formation of Conjugated Polymer Brushes by Surface-Initiated Catalyst-Transfer Polycondensation. *Chem. Commun.* **2009**, 3354-3356.

(56) Bryan, Z. J.; McNeil A. J. Conjugated Polymer Synthesis via Catalyst-Transfer Polycondensation (CTP): Mechanism, Scope, and Applications. *Macromolecules* **2013**, *46*, 8395-8405.

(57) Chavez, C. A.; Choi, J.; Nesterov, E. E. One-Step Simple Preparation of catalytic Initiators for Catalyst-Transfer Kumada Polymerization: Synthesis of Defect-Free Polythiophenes. *Macromolecules* **2014**, *47*, 506-516.

(58) Kurth, D. G.; Bein, T. Surface Reactions on Thin Layers of Silane Coupling Agents. *Langmuir* **1993**, *9*, 2965-2973.

(59) Chong, A. S. M.; Zhao, X. S. Functionalization of SBA-15 with APTES and Characterization of Functional Materials. *J. Phys. Chem. B* **2003**, *107*, 12650-12657.

(60) Bilbrey, J. A.; Sontag, S. K.; Huddleston, N. E.; Allen, W. D.; Locklin, J. On the Role of Disproportionation Energy in Kumada Catalyst-Transfer Polycondensation. *ACS Macro Lett.* **2012**, *1*, 995-1000.

(61) Hsu, S. L.; Signorelli, A. J.; Pez, G. P.; Baughman, R. H. Highly Conductive Iodine Derivatives of Polyacetylene: Raman, XPS, and X-ray Diffraction Studies. *J. Chem. Phys.* **1978**, *69*, 106-111.

(62) Couturaud, B.; Mas, A.; Robin, J. J. Surface-Initiated Reversible Addition-Fragmentation Chain Transfer Polymerization from "Clickable" Polypropylene Surface Modified by Iodine Plasma Activation. *Eur. Polym. J.* **2015**, *70*, 276-285.

(63) *Handbook of X-ray Photoelectron Spectroscopy*; Chastain, J, King, R. C. Jr., Eds.; Physical Electronics, Inc.: Eden Prairie, 1995.

(64) Biesinger, M. C.; Payne, B. P.; Grosvenor, A. P.; Lau, L. W. M.; Gerson, A. R.; Smart, R. S. C. Resolving Surface Chemical States in XPS Analysis of First Row Transition Metals, Oxides and Hydroxides: Cr, Mn, Fe, Co and Ni. *Appl. Surf. Sci.* **2011**, *257*, 2717-2730.

(65) Biesinger, M. C..; Payne, B. P.; Lau, L. W. M.; Gerson, A.; Smart, R. S. C. X-ray Photoelectron Spectroscopic Chemical State Quantification of Mixed Nickel Metal, Oxide and Hydroxide Systems. *Surf. Interface Anal.* **2009**, *41*, 324-332.

(66) Grosvenor, A. P.; Biesinger, M. C.; Smart, R. S. C.; McIntyre, N. S. New Interpretations of XPS Spectra of Nickel Metal and Oxides. *Surf. Sci.* **2006**, *600*, 1771-1779.

(67) Kim, Y.; Cook, S.; Tuladhar, S. M.; Choulis, S. A.; Nelson, J.; Durrant, J. R.; Bradley, D. D. C.; Giles, M.; McCulloch, I.; Ha, C.-S.; Ree, M. A Strong Regioregularity Effect in Self-Organizing Conjugated Polymer Films and High-Efficiency Polythiophene:Fullerene Solar Cells. *Nat. Mater.* **2006**, *5*, 197-203.

(68) Grenier, C. R. G.; Pisula, W.; Joncheray, T. J.; Müllen, K.; Reynolds, J. R. Regiosymmetric Poly(dialkylphenylenedioxythiophene)s: Electron-Rich, Stackable π-Conjugated Nanoribbons. *Angew. Chem. Int. Ed.* **2007**, *46*, 714-717.

(69) Kim, S.-S.; Na, S.-I.; Jo, J.; Tae, G.; Kim, D.-Y. Efficient Polymer Solar Cells Fabricated by Simple Brush Painting. *Adv. Mater.* **2007**, *19*, 4410-4415.

(70) Roncali, J.; Garnier, F. Poly Mono-, Bi-, and Trithiophene: Effect of Oligomer Chain Length on the Polymer Properties. *Synth. Met.* **1986**, *15*, 323-331.

(71) Hillman, A. R.; Swann, M. J. Spectroscopic Studies of the Growth and Potential Cycling of Polybithiophene Films. *Electrochim. Acta* **1988**, *33*, 1303-1312.

(72) Alkan, S.; Cutler, C. A.; Reynolds, J. R. High Quality Electrochromic Polythiophenes via $BF_3 \cdot Et_2O$ Electropolymerization. *Adv. Funct. Mater.* **2003**, *13*, 331-336.

(73) Zotti, G.; Zecchin, S.; Vercelli, B.; Berlin, A.; Grimoldi, S.; Pasini, M. C.; Raposo, M. M. M. Electrochemical, Magnetic, and Electrical Properties of α,ω-Capped Sexithiophene Films. 1. Neutral-Polaron and Polaron-Bipolaron Conductivities. *Chem. Mater.* **2005**, *17*, 6492-6502.

(74) Zotti, G.; Schiavon, G.; Berlin, A.; Pagani, G. Thiophene Oligomers as Polythiophene Models. 2. Electrochemistry and in Situ ESR of End-Capped Oligothienyls in the Solid State. Evidence for π-Dimerization of Hexameric Polarons in Polythiophene. *Chem. Mater.* **1993**, *5*, 620-624.

(75) Lösche, M.; Schmitt, J.; Decher, G.; Bouwman, W. G.; Kjaer, K. Detailed Structure of Molecularly Thin Polyelectrolyte Multilayer Films on Solid Substrates as Revealed by Neutron Reflectometry. *Macromolecules* **1998**, *31*, 8893-8906.

(76) Kharlampieva, E.; Kozlovskaya, V.; Ankner, J. F.; Sukhishvili, S. A. Hydrogen-Bonded Polymer Multilayers Probed by Neutron Reflectivity. *Langmuir* **2008**, *24*, 11346-11349.

(77) Pinto, J. C.; Whiting, G. L.; Khodabakhsh, S.; Torre, L.; Rodríguez, A. B.; Dalgliesh, R. M.; Higgins, A. M.; Andreasen, J. W.; Nielsen, M. N.; Geoghegan, M.; Huck, W. T. S.; Sirringhaus, H. Organic Thin Film Transistors with Polymer Brush gate Dielectrics Synthesized by Atom Transfer Radical Polymerization. *Adv. Funct. Mater.* **2008**, *18*, 36-43.

(78) Keum, J. K.; Browning, J. F.; Xiao, K.; Shao, M.; Halbert, C. E.; Hong, K. Morphological Origin for the Stratification of P3HT:PCBM Blend Film Studied by Neutron Reflectometry. *Appl. Phys. Lett.* **2013**, *103*, 223301.

(79) Chen, H.; Peet, J.; Hu, S.; Azoulay, J.; Bazan, G.; Dadmun, M. The Role of Fullerene Mixing Behavior in the Performance of Organic Photovoltaics: PCBM in Low-Bandgap Polymers. *Adv. Funct. Mater.* **2014**, *24*, 140-150.

(80) A similar approach based on the active surface catalyst "re-initiation" was recently described by Locklin: Huddleston, N. E.; Roy, A.; Bilbrey, J. A.; Zhao, Y.; Locklin, J. Functionalization of Reactive End Groups in Surface-Initiated Kumada Catalyst-Transfer Polycondensation. *Macromol. Symp.* **2015**, *351*, 27-36.

(81) Gumus, O. Y.; Unal, H. I.; Erol, O.; Sari, B. Synthesis, Characterization, and Colloidal Properties of Polythiophene/Borax Conducting Composite. *Polym. Compos.* **2011**, *32*, 418-426.

(82) Fichou, D.; Bachet, B.; Demanze, F.; Billy, I.; Horowitz, G.; Garnier, F. Growth and Structural Characterization of the Quasi-2D Single Crystal of α-Octithiophene. *Adv. Mater.* **1996**, *8*, 500-504.

(83) Müller-Buschbaum, P. The Active Layer Morphology of Organic Solar Cells Probed with Grazing Incidence Scattering Techniques. *Adv. Mater.* **2014**, *26*, 7692-7709.

(84) Brückner, S.; Porzio, W. The Structure of Neutral Polythiophene. An Application of the Rietveld Method. *Makromol. Chem.* **1988**, *189*, 961-967.

(85) Yamamoto, T.; Morita, A.; Miyazaki, Y.; Maruyama, T.; Wakayama, H.; Zhou, Z.; Nakamura, Y.; Kanbara, T. Preparation of π-Conjugated Poly(thiophene-2,5-diyl), Poly(*p*-phenylene), and Related Polymers Using Zerovalent Nickel Complexes. Linear Structure and Properties of π-Conjugated Polymers. *Macromolecules* **1992**, *25*, 1214-1223.

(86) Porzio, W.; Destri, S.; Mascherpa, M.; Brückner, S. Structural Aspects of Oligothienyl Series from X-ray Powder Diffraction Data. *Acta Polymer.* **1993**, *44*, 266-272.

(87) Servet, B.; Ries, S.; Trotel, M.; Alnot, P.; Horowitz, G.; Garnier, F. X-ray Determination of the Crystal Structure and Orientation of Vacuum Evaporated Sexithiophene Films. *Adv. Mater.* **1993**, *5*, 461-464.

(88) Horowitz, G.; Bachet, B.; Yassar, A.; Lang, P.; Demanze, F.; Fave, J.-L.; Garnier, F. Growth and Characterization of Sexithiophene Single Crystals. *Chem. Mater.* **1995**, *7*, 1337-1341.

(89) Isz, S.; Weissbuch, I.; Kjaer, K.; Bouwman, W. G.; Als-Nielsen, J.; Palacin, S.; Ruaudel-Teixier, A.; Leiserowitz, L.; Lahav, M. Crystalline Mono- and Multilayer Self-Assemblies of Oligothiophenes at the Air-Water Interface. *Chem. Eur. J.* **1997**, *3*, 930-939.

(90) Dudenko, D.; Kiersnowski, A.; Shu, J.; Pisula, W.; Sebastiani, D.; Spiess, H. W.; Hansen, M. R. A Strategy for Revealing the Packing in Semicrystalline π-Conjugated Polymers: Crystal Structure of Bulk Poly-3-hexyl-thiophene (P3HT). *Angew. Chem. Int. Ed.* **2012**, *51*, 11068-11072.

(91) Szarko, J. M.; Rolczynski, B. S.; Lou, S. J.; Xu, T.; Strzalka, J.; Marks, T. J.; Yu. L.; Chen, L. X. Photovoltaic Function and Exciton/Charge Transfer Dynamics in a Highly Efficient Semiconducting Copolymer. *Adv. Funct. Mater.* **2014**, *24*, 10-26.

(92) Beaucage, G. Approximations Leading to a United Exponential/Power-Law Approach to Small-Angle Scattering. *J. Appl. Cryst.* **1995**, *28*, 717-728.

(93) Haynes, C. L.; Van Duyne, R. P. Nanosphere Lithography: a Versatile Nanofabrication Tool for Studies of Size-Dependent Nanoparticle Optics. *J. Phys. Chem. B* **2001**, *105*, 5599-5611.

(94) Tessier, P.; Velev, O. D.; Kalambur, A. T.; Lenhoff, A. M.; Rabolt, J. F.; Kaler, E. W. Structured Metallic Films for Optical and Spectroscopic Applications via Colloidal Crystal Templating. *Adv. Mater.* **2001**, *13*, 396-400.

(95) Jiang, P.; Bertone, J. F.; Colvin, V. L. A Lost-Wax Approach to Monodisperse Colloids and Their Crystals. *Science* **2001**, *291*, 453-457.

(96) McLellan, J. M.; Geissler, M.; Xia, Y. N. Edge Spreading Lithography and Its Application to the Fabrication of Mesoscopic Gold and Silver Rings. *J. Am. Chem. Soc.* **2004**, *126*, 10830-10831.

(97) Li, J.-R.; Garno, J. C. Elucidating the Role of Hydrosilation for Nanopatterning Organosilanes via Particle Lithography. *Nano Lett.* **2008**, *8*, 1916-1922.

(98) Briseno, A. L.; Han, S. B.; Rauda, I. E.; Zhou, F. M.; Toh, C. S.; Nemanick, E. J.; Lewis, N. S. Electrochemical Polymerization of Aniline Monomers Infiltrated into Well-Ordered Truncated Eggshell Structures of Polyelectrolyte Multilayers. *Langmuir* **2004**, *20*, 219-226.

(99) Choi, D.-G.; Jang, S. G.; Yu, H. K.; Yang, S.-M. Two-Dimensional Polymer Nanopattern by Using Particle-Assisted Soft Lithography. *Chem. Mater.* **2004**, *16*, 3410-3413.

(100) Marquez, M.; Patel, K.; Carswell, A. D. W.; Schmidtke, D. W.; Grady, B. P. Synthesis of Nanometer-Scale Polymeric Structures on Surfaces from Template Assisted Admicellar Polymerization: A Comparative Study with Protein Adsorption. *Langmuir* **2006**, *22*, 8010-8016.

(101) Cai, Y.; Ocko, B. M. Large-Scale Fabrication of Protein Nanoarrays Based on Nanosphere Lithography. *Langmuir* **2005**, *21*, 9274-9279.

(102) Valsesia, A.; Colpo, P.; Silvan, M. M.; Meziani, T.; Ceccone, G.; Rossi, F. Fabrication of Nanostructured Polymeric Surfaces for Biosensing Devices. *Nano Lett.* **2004**, *4*, 1047-1050.

(103) Weekes, S. M.; Ogrin, F. Y.; Murray, W. A. Fabrication of Large-Area Ferromagnetic Arrays Using Etched Nanosphere Lithography. *Langmuir* **2004**, *20*, 11208-11212.

CHAPTER 3. PREPARATION OF ALL-CONJUGATED DIBLOCK COPOLYMER FILMS BY SURFACE-INITIATED KUMADA CATALYST TRANSFER POLYMERIZATION (SI-KCTP) AND STUDY OF THEIR OPTOELECTONIC PROPERTIES

3.1. Introduction

All-conjugated polymers, which are composed of dissimilar blocks (e.g. electron rich or electron deficient blocks), have been an important subject of research because of the potentieal possibility to control optoelectronic properties (such as absorption, emission, and charge transport, etc.), phase separation, and crystallinity.[1-7] Particularly, in organic photovoltaics (OPVs), controlling optical characteristics of an active layer plays a crucial role. For instance, alternating copolymers composed of donor and acceptor moieties can create a new electronic transition that extents absorption band up to the near IR region, thus increasing number of absorbed photons and therefore improving device's performance.[6,8,9] In addition, donor-acceptor type all-conjugated block copolymers can be used to disign ITO-free or all-polymer solar cells by replacing inorganic oxide or/and metal electrodes. This could deliver a potential platform for future flexible devices.[10-12] Another important key feature of the block copolymers is distinguishable phase separation on the surface, which originally arises from immiscibility or crystallizability difference between the blocks. As explained in the chapter 1.3, manipulating the exciton pathway to have minimum diffusion length is associated with BHJ solar cell performance. If one can fabricate a periodic nanostructured morphology using the phase separation ability of block copolymers, which displays a certain interface distance of less than a few tens nanometer (maximum diffusion length of excitons generated by light is around 10 nm[13], see Figure 1.5B in the chapter 1.3 for the ideal case) as well as a proper direction,[2,14] high total efficiency of OPV would be achieved through by reducing migration length of photogenerated exitons and diminishing rate of nongeminate exciton recombination.[15-18] However, to date,

tremendous amount of efforts to achieve an effective phase separation with the block copolymers for OPVs utilized simple solution-based processing, such as spin castings, roll-to-roll castings, or inkjet printings, the methods that only target control of weak intermolecular forces between polymer chains, leading a large amount of disorder (see Figure 1.5C in the chapter 1.3 for the real structure of device). Although a few attempts have succeeded to design the required structures with some degree of control,[19-21] accurate control of the phase separation in order to achieve the ideal structure for high device performance still remains the most difficult challenge.

On the other hand, surface-initiated polymerization can be an alternative method to try to tackle these issues. Covalently attached polymer chains that stretch from the bottom to the top electrode under a certain angle to the surface normal can potentially minimize migration length of excitons and also possibly reduce recombination rate to increase total efficiency.[22,23] In addition, polymer thin films covalently anchored on the surface can show superior in physical/chemical stability over traditional films made by solution-based methods.[24] Moreover, from a synthetic standpoint, well-established polymerization techniques for CPs can be simply implemented for the surface-initiated polymerization, so a proper molecular organization to optimize internal optoelectronic process (e.g. exciton separation, light absorption or charge transport) can be easily delivered via controlling molecular weight, polydispersity or molecular structure of repeating units. In this sense, despite a few recent attempts using other metal-catalyzed reactions (e.g., Suzuki[25], Sonogashira[26], and Negishi polymerization[27]) for the surface-initiated polymerization, SI-KCTP remains the most developed method for preparation of CP thin films due to the well-defined nature of the living chain-growth mechanism stated in the chapter 1.

Many impressive achievements have been demonstrated to develop synthetic protocols for SI-KCTP. Kiriy have successively reported preparation of P3HT thin films using a surface bound initiator, Ar-Ni(PPh_3)$_2$-Br.[28,29] Locklin's group introduced a new initiator, Ar-Ni(COD)(PPh_3)$_2$, to build polythiophene (PT) and poly(*p*-phenylene) (PPP) thin film on the gold surface, and investigated an opportunity to use these films in replacing a hole-transporting layer for OPV.[23] These early attempts revealed that the initiators were not efficient in effecting surface-initiated polymerization by chain-growth fashion due to undesired side reactions, resulting in low degree of polymerization as well as lower surface density. Later, Kiriy group introduced a ligand exchange step to afford Ar-Ni(dppp)Br as an initiator,[30] and prepared conjugated microporous polymer thin film to increase specific surface area for potential applications in adsorption or separation.[31] Luscombe group introduced a different approach based on a ligand exchange step to make poly(3-methylthiophene) (P3MT) film on ITO and demonstrated controlled chain-growth mechanism in that case. Interestingly, all these examples have involved homopolymers and no diblock copolymer or more complex polymer thin film has been described to date.

In chapter 2, we described a simple anf efficient preparation of an external catalytic [Ni(0)] initiator. This method does not require complicated ligand exchange step process, that may cause side reactions forcing the polymerization away from the chain-growth way. We used state-of-the-art experiments to demonstrate that our system was very efficient in preparation of relative thick film in a short reaction time, with well-controlled chain-growth mechanism. We also proposed a model structure of the thin film, which included densely packed domains with predominantly in-plane "herringbone" (edge-to-face) packing of the folded PT chains. Another important characteristic of our method was using reactivation with a Ni(dppp)$_2$ solution to

regenerate prematurely terminated catalytic sites, which allowed increase overall efficiency of surface-initiated polymerization. This result prompted us to investigate possibility of fabricating all-conjugated diblock copolymer thin films in order to take advantage of the unique properties of diblock copolymers. Herein, we report an easy and efficient synthetic protocol for the preparation of all-conjugated polythiophene-*b*-poly(*p*-phenylene), PT-*b*-PPP, copolymer thin film, as well as opposite sequence copolymer, poly(*p*-phenylene)-*b*-polythiophene, PPP-*b*-PT, and their optoelectronic properties and structureal characteristics investigated by UV/vis, PL spectroscopy, cyclic voltammetry (CV), X-ray photoelectron spectroscopy (XPS), atomic force microscope (AFM), and stylus profilometry. To the best of our knowledge, there have been no previous reports on preparation of all-conjugated diblock copolymer thin films by surface-initiated polymerization. This method promises to open an efficient synthetic route for a new structural platform for electronic and optoelectronic applications.

3.2. Results and Discussion

3.2.1. Preparation of all-conjugated diblock copolymer thin films.

To prepare a surface anchored external Ni(II) initiator, we used 2-(triethoxysilyl)-5-iodothiophene as a precursor which was reacted with $Ni(dppp)_2$ to yield $(EtO)_3Si$-Th-Ni(dppp)I catalytic initiator (Figure 3.1). Covalent immobilization of this external initiator on quartz surface at 55 ℃ for three days yielded an external initiator for SI-KCTP, as was confirmed in XPS measurement and CV analysis as described in chapter 2. Polymerizations were conducted by adding a required Grignard monomer solution to get a desired block. Scotch tape test and extensive ultrasonicating with various solvents (such as toluene, chloroform, acetone, methanol, and water) were carried out after polymerization to remove physisorbed polymer residues from the film surface. Before carrying out a second polymerization step, the substrate functinalized

with the first block was immersed into a solution of $Ni(dppp)_2$ for "reactivation" in order to regenerate prematurely terminated catalytic sites (Figure 3.1).

An AFM study was undertaken to confirm the formation of surface-initiated conjugated polymer thin films. The AFM image of polythiophene homopolymer (PT) film was obtained after 5 min polymerization time and poly(*p*-phenylene) homopolymer (PPP) film was obtained after polymerization for 12 h. Surface morphologies by topography (Figure 3.2A for PT and C for PPP) for both PT and PPP homopolymer films showed globular features, which were a

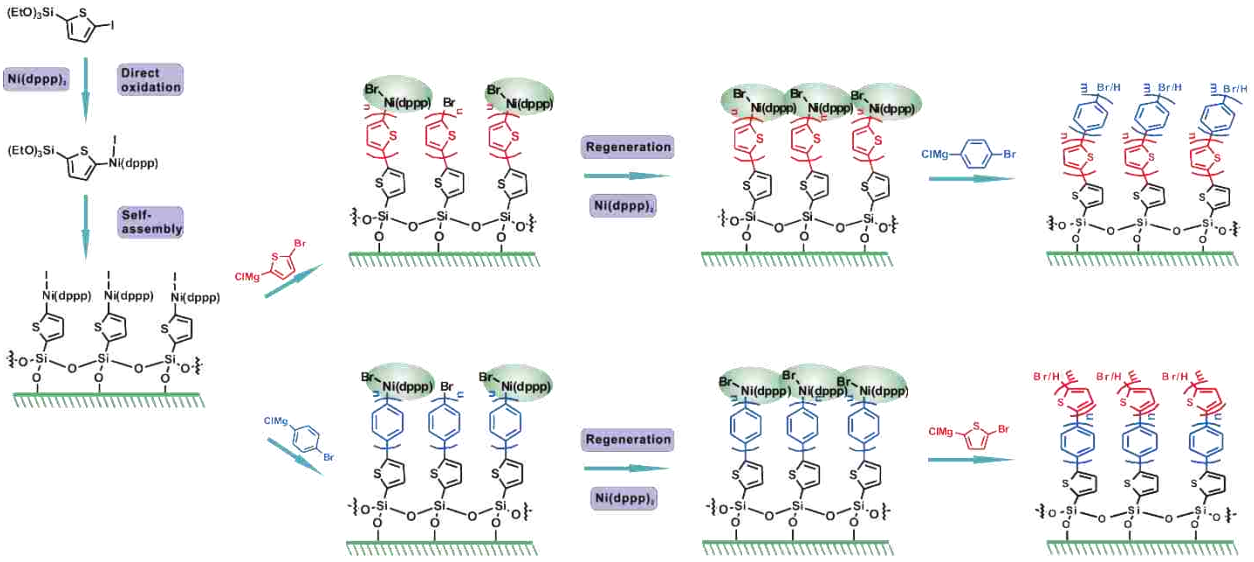

Figure 3.1. The general scheme of SI-KCTP for all-conjugated diblock copolymer thin films with different sequences.

typical morphology of surface-initiated polymer films (as described in chapter 2). Scale range of height in topography mode for each homopolymer film was lower than the thickness of the film measured by the stylus profilometer (thickness of PT was 36 nm and 65 nm for PPP by profilometry.), because holes (dark areas in the topographies) did not actually represent quartx substrate, as was proved by corresponding phase modes. In the case of PT-*b*-PPP diblock

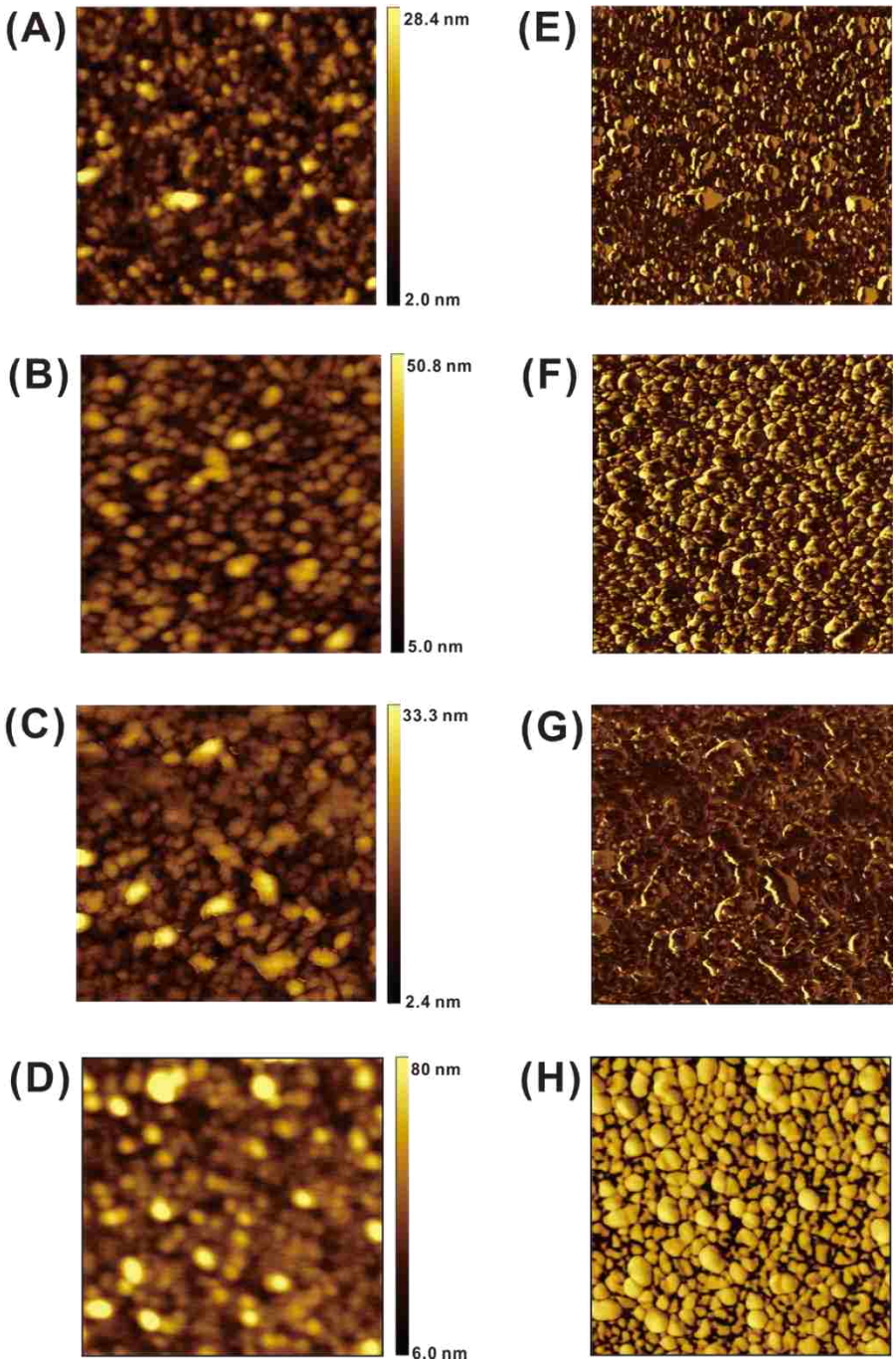

Figure 3.2. AFM images for homopolymer and all-conjugated diblock copolymer thin films. The left column is corresponding to topographies of (A) PT, (B) PT-b-PPP, (C) PPP, and (D) PPP-b-PT thin film, repectively. The right column represents phase modes for (E) PT, (F) PT-b-PPP, (G) PPP, and (H) PPP-b-PT thin film. All images are 1 × 1 μm scale.

copolymer film, it displayed morphology similar to the previous homopolymers (Figure 3.2B). Thickness of the film obtained by profilometer was around 77 nm that was also larger than the scale range of the corresponding topography image, meaning that substrate was covered with continuous copolymer film. For PPP-*b*-PT diblock copolymer film, reaction time was slightly different. In order to avoid side reactions or undesired effects, polymerization time to prepare the first block, PPP, was limited in time 1.5 h, in which the polymerization was assumed to remain a "living" chain-growth process. Subsequent reactivation was carried out, followed by second polymerization for PT with reaction time 1 h (see details in the Experimental section). The surface morphology of the PPP-*b*-PT showed similar features as PT-*b*-PPP film pointing out a densely covered surface-initiated polymer film. Scale range of height for the both diblock copolymer thin films significantly increased relative to each corresponding homopolymer film, thus indicating that the second polymerization was indeed successful.

Based on film thinkness vs. polymerization time profile (Figure 3.3), polymerization for each homopolymer proceeded in controlled chain-growth fashion with first order kinetic rate until consuming most of monomers. The polymerization for PT occurred rapidly, finishing in 20 min and yielding 66 nm thick film. In the case of PPP, although polymerization followed chain-growth mechanism until 2 h, the rate of polymerization was significantly slower than that of PT. It should be noticed that the optimized polymerization condition to prepare poly(p-phenylene), PPP, involve using dppe as a ligand for Ni(II) catalytic initiator and LiCl as an additive to suppress homocoupling reaction.[32] With our reaction condition (using dppp as a ligand instead of dppe and no LiCl as an additive), extensive homo-coupling between monomers and chain-transfer reactions could happen during the polymerization for PPP, introducing precipitations over the substrate. As polymerization proceeded, this precipitation would cover the substrate by

physisorption, which would hamper both the initial surface-initiated polymerization as well as the subsequent polymerization (for polythiophene, PT). This phenomenon could result in more unreacted homopolymer thin film, PPP, over the formation of all-conjugated diblock copolymer film, PPP-*b*-PT. In order to minimize the drawback, we used 1-bromo-4-iodobenzene to prepared Grignard monomer for PPP, due to the lower reactivity of aryl bromides in the homocoupling, followed by successively added thiophene Grignard monomer solution to prepare the second block with 1.5 h polymerization time. However, despite this attempt, we still observed small amount of precipitation of PPP which affected its optoelectronic properties (see below) as well as slow reaction rate. On the other hand, in the PT case, no precipitation was found even after extended polymerization time, implying that polymerization predominantly occurred on the surface.

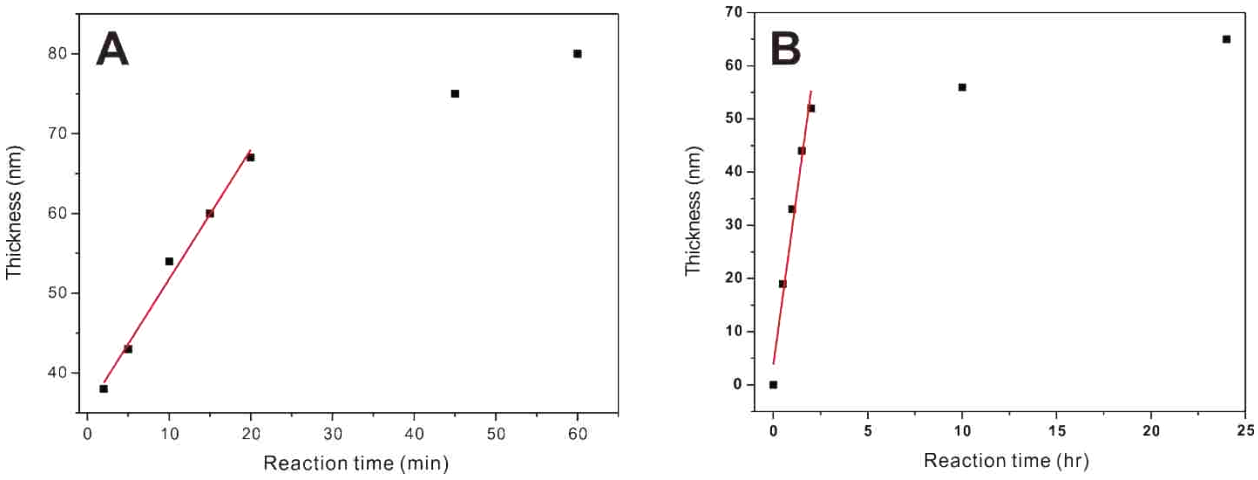

Figure 3.3. Thickness of each homopolymer thin film with reaction time measured by profilometer. (A) polythiophene thin film and (B) poly(*p*-phenylene) thin film prepared by SI-KCTP. Red lines represent linear fitting for each homopolymer thin film in a time range of controlled-living growth polymerization.

3.2.2. Spectroscopic and electrochemical properties of all-conjugated diblock copolymer thin films.

Figure 3.4 shows UV/vis spectra of homopolymer and diblock copolymer thin films. In order to make clear quantitative comparison, polymerization time for all first blocks in the diblock copolymer films was same as the time for the homopolymers (e.g., 5 min for PT and 1.5 h for PPP). Polymerization time for the PPP block in PT-*b*-PPP film was also 1.5 h, however preparation of the PT block in the PPP-*b*-PT film was extended to 1 h. PT homopolymer film absorption was represented by a band with a maximum at around 505 nm, with well-defined vibronic structures at around 550 nm and 600 nm that typically originate from increased molecular organization.[33,34] λ_{max} of the PPP homopolymer film absorption band was at 390 nm with a vibronically structured shoulder. UV/vis spectra for both block copolymer films resulted from a simple summation of each constituent homopolymer with similar characteristic λ_{max} and well-defined vibronic structures of the absorption band. However, λ_{max} corresponding to the PPP part of the PT-*b*- PPP block copolymer film showed a hypsochromic shift. This indicated the

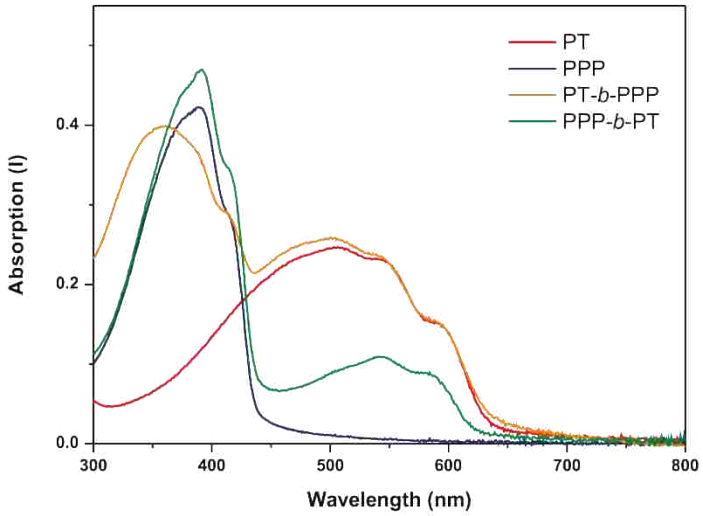

Figure 3.4. UV/vis spectra of homopolymer and all conjugated diblock copolymer thin films.

PPP block was likely less extended than in the homopolymer film, PPP, obtained in the same time, indicating possible oliogomeric nature of this block. Miyakoshi et al.[32] and Wu et al.[35] previously reported that sequence of polymerization was a key factor for the block copolymerization. They mentioned that Ni catalytic initiators had tendency to stay on a more electron rich moiety relative to the less electron-rich one. Since thiophene ring is slightly more electron rich than *p*-phenylene ring, Ni initiators would form a complex with poly thiophene block, and it would be difficult for the Ni active center to migrate toward the second block, resulting either in slow or no polymerization. Thus, the polymerization to form the second, PPP, block might be impeded. Although this tendency might have existed in this polymerization, the polymerization to form the PT-*b*-PPP film seemed to be reasonably successful confirmed by futher characterization experiments (CV, PL, and AFM). On the other hand, the PPP-*b*-PT thin film displayed the same λ_{max} while retaining vibronic structure in the region corresponding to the PPP absorption band.. Meanwhile, the PT absorption band showed substantially lower optical density as well as suppressed λ_{max} at around 505 nm. As mentioned above, small amount of precipitation of PPP at the end of polymerization could have hampered polymerization of PT by blocking access to the active sites. In addition, this could be also due to steric issue, as upon first block formation on the surface, aggregation of the polymer chains would make active centers less accessible for subsequent polymerization, thus further decreasing the polymerization rate down. Indeed, the effect of this factor could explain oligomeric nature of the second block, PPP, in PT-*b*-PPP, because we could observe higher optical density and thickness (not shown here) by increasing reaction time for the second polymerization.

These trends were consistent with the result of CV studies. CV data for the diblock copolymer films are presented in Figure 3.5A (for CV data for homopolymer films, see Figure

5.5 in the Experimental Section). Oxidation and reduction peaks for the copolymer films could be represented by simple summation of similar peaks for each homopolymer film as were UV/vis spectra. Oxidation peak at 0.8 V and reduction peak at 0.15 V were associated with PT block, indicating irreversible redox process. PPP block contributed at 1.3 V for oxidation peak and 0.8 V for reduction peak that also pointed on irreversible redox process. Oxidation and reduction peaks corresponding to PT block in the PPP-b-PT film were significantly depressed compared to those of PT-b-PPP film, likely because of the slow or impeded polymerization of PT block caused by the factors mentioned above. The oxidation and reduction peak current as a function of scan rate was recorded in Figure 5B. The linearity was expected of conjugated polymer films covalently bound to an electrode.

Since all-conjugated diblock copolymers consisted of two distinct blocks in close proximity, Photoexcitation energy transfer (including through space Förster energy transfer by

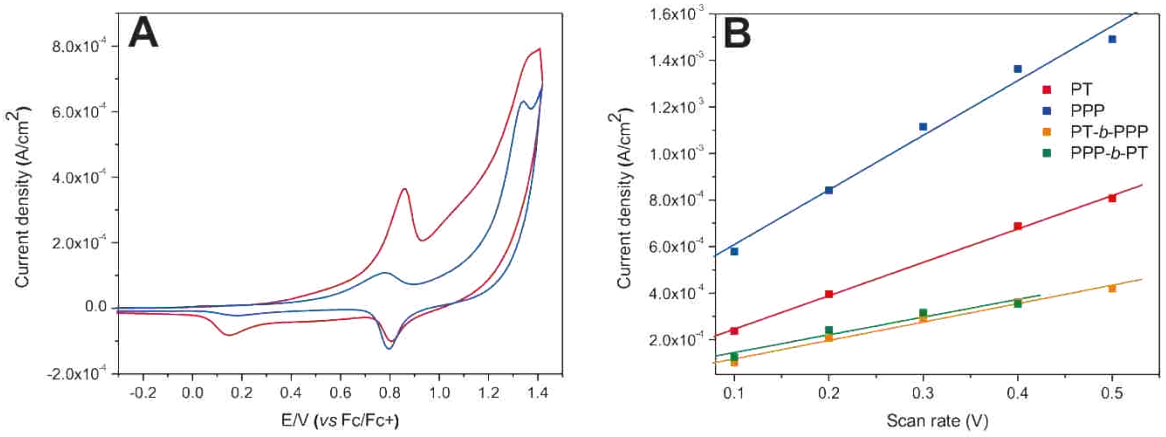

Figure 3.5. (A) Cyclic voltamograms of all-conjugated diblock thin films on ITO acquired in 0.1M Bu_4PNF_6 in acetonitrile with sweep rate 0.1 Vs^{-1}. Red trace represents PT-*b*-PPP and blue trace shows PPP-*b*-PT. (B) Scan rate vs. current density of homopolymer and all-conjugated diblock copolymer thin films. For diblock copolymer films, reduction peaks (rather than oxidation peaks) were used for plotting.

dipole-dipole induced mechanism along with the intrachain FRET) was dominated.[33,36,37] Thus, PL study could offer deeper insight of the structure of polymers to support formation of diblock copolymer. All PL spectra were normalized to make clear quantitative comparison (Figure 3.6). Homopolymer PPP film was excited at 380 nm and showed characteristic vibronically structured PL in the range of 400 - 550 nm, and PT film was excited at 530 nm showed PL band between 600 ~ 800 nm (PL of PT homopolymer film excited at 380 nm presented nearly no luminescence). These PL band for both homopolymers exhibited clear vibronic structure due to well-defined ordered morphology of polymer chains on the surface in spin-cast films fo conjugated polymers.[33,37]

In the case of PT-b-PPP film, there was a strong decrease of the PL intensity of the PPP band because of energy migration from PPP to PT, while simultaneously resulting in PT PL band with broad emission in the range of 500 - 740 nm. The PPP-*b*-PT block copolymer exhibited similar tendency with ever stronger decrase iin PL intensity of PPP band. We assumed that regular morphology of PPP block on the surface increased Förster energy transfer efficiency due to three-dimensional nature of the rough surface. Such aggregation provided an efficient energy transfer by separate overlap of similar energy levels along polymer chains (intrachain) as well as interchain.[4] Besides FRET associated with diblock copolymer chains on the surface, mixed homopolymer chains on the surface could also contribute to Förster energy transfer due to the proximity between homopolymer chains. This mixed homopolymer film can be a result of some side reactions. Locklin group[38] suggested that dispropotionation reaction between adjacent Ni(II) catalytic centers could happen during polymerization, which would leave dormant chains for further polymerization (Figure 3.7B). Even though we did not use a long alkyl linker at the catalytic initiator, it is obvious that formation of long polymer chains provides enough flexibility

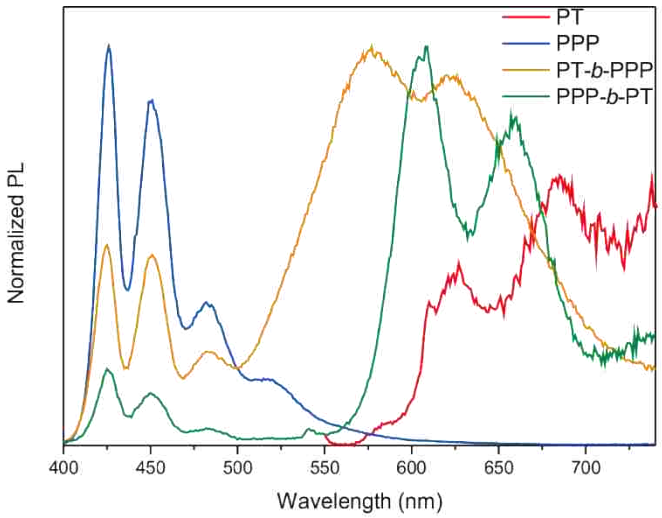

Figure 3.6. Photoluminescence spectra of homopolymer and all-conjugated diblock copolymer thin films. PT film was exited at 530 nm, other films were excited at 380 nm.

for the chains to tilt toward each other for dispropotionation to occur. This undesired side reaction can generate a mixed block within the block copolymer film with dormant homopolymer chains.

The other possible reaction to form dormant chains is chain transfer reaction that transfers Ni(II) catalytic initiator to a Grignard monomer in solution, leaving halogen atom at the end of surface-immobilized chain (Figure 3.7A). This side reaction would generated insoluble oligomers or polymers, which were not observed in the case of PT and PT-*b*-PPP thin film polymerization, but were detected in the case of PPP for both homopolymer and diblock copolymer films. Although we tried to limit polymerization times to where the reaction would remain within a range of robust chain-growth mechanism and produced very small amount of precipitations, we still should consider the chain transfer that could create "imperfect" (or "defecteus") diblock copolymer films. Thus, we immersed the substrate after the first block polymerization into a $Ni(dppp)_2$ solution for "reactivation" step to regenerate active Ni(II)

catalytic sites (Figure 3.1). In chapter 2, we demonstrated that reaction of halide terminated chains with a $Ni(dppp)_2$ solution allowed conversion of halogen group back to Ni(II) catalytic initiator which allowed to prepared PT films with the high thickness relative to the films prepared without regeneration step.

The last process (Figure 3.7C) can happen due to steric congestion leaving active sites imbedded within the first polymer block and available for the second polymerization. All three processes may happen either at same time or independently but since we did not introduce solubilizing groups to the monomers. A simple solution based analysis after degrafting polymer from the substrate was not possible. Therefore, we decided to use XPS to study interface between the block in more detail.

3.2.3. XPS measurement: Evidence for "defect" free all-conjugated diblock copolymer thin films.

XPS is the most widely used analytical tool for surface chemistry due to its surface-sensitivity, relative simplicity in use and rather straightforward data interpretation.[39] Based on the mechanism of KCTP elucidated in our previous studies, polymer chains would be terminated either with hydrogen or halogen atoms after quenching with methanol.[40] This halogen atom is easily detectable by XPS. In order to discern each homopolymer chains, we used differently halogenated monomers for each polymerization. In particular, we used 2,5-dibromothiophene to generate Grignard monomer for PT and 1,4- diiodobenzene to generate Grignard monomer for PPP. As expected, XPS spectrum ought to show only one corresponding signal for homopolyer films and, if copolymerization was successful in complete overage of the preceding block, diblock copolymer films as well. Otherwise, diblock copolymer films might display both signals, Br and I, because we used different aryl halide monomers for each block. We limited reaction time to less than 5 min for PT and 30 min for PPP in both diblock copolymer film preparations

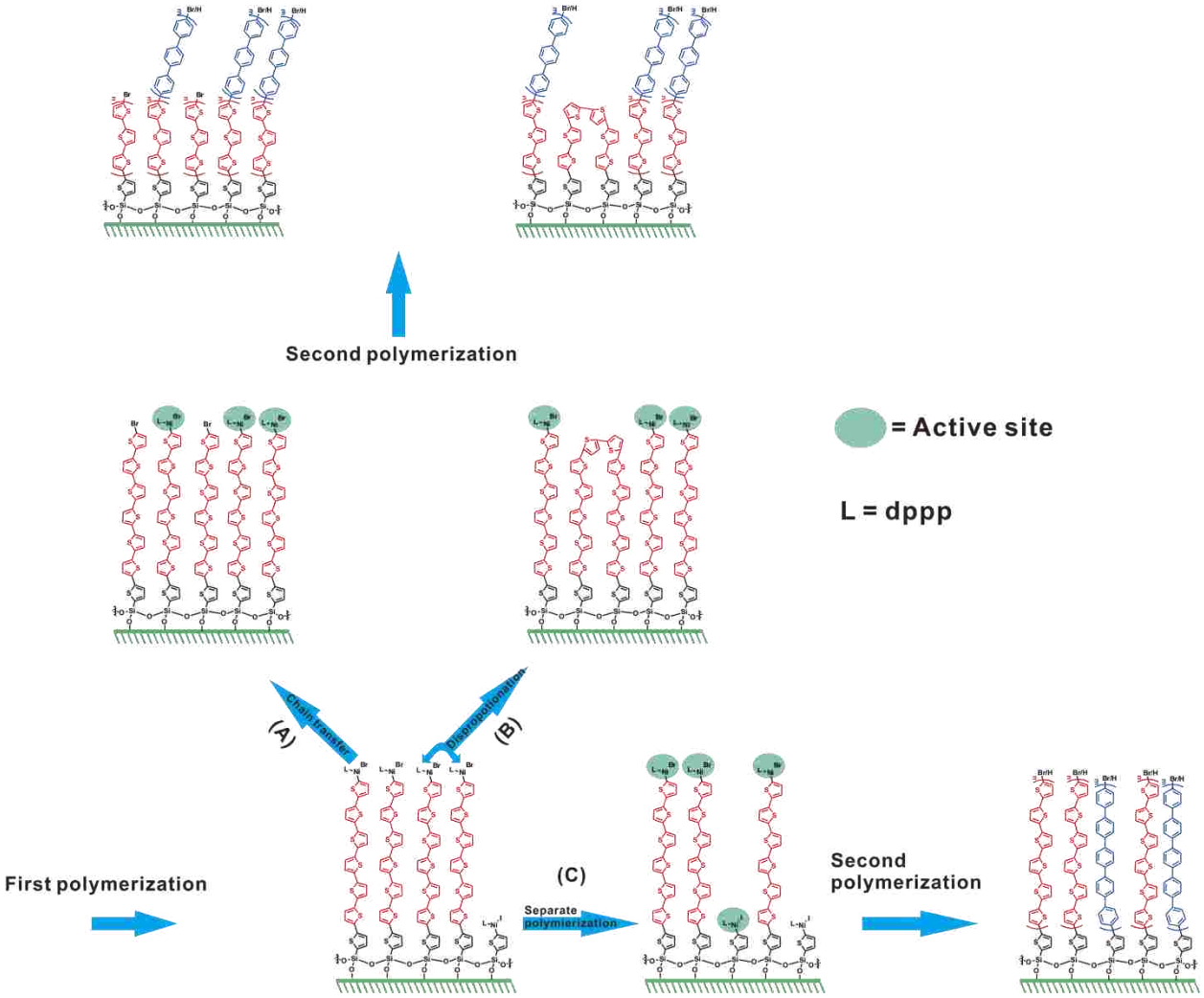

Figure 3.7. Possible pathways to form a mixed polymer thin film. (A) Chain transfer reaction occured by migration of a Ni(II) active center to a monomer solution. (B) Dispropotionation path observed by coupling reaction between adjacent chains. (C) In-block polymerization due to steric congestion during the first polymerization.

because detectable depth limit of ejected photon in XPS without energy loss is usually no more than 10 nm.[41] In order to simplify the study, we did not use reactivation for this experiment. Upon completion fo surface-initiated polymerization, we quenched the substrates by sonicating with methanol. Figure 3.8 shows high-resolution XPS spectra of the thin films. PT and PPP homopolymer films display only bromine and iodine signals, respectively. Only I $4d_{3/2}$ and I $4d_{5/2}$ peaks but no Br 3d peak were detected for PT-*b*-PPP in XPS spectra. This indicates that all

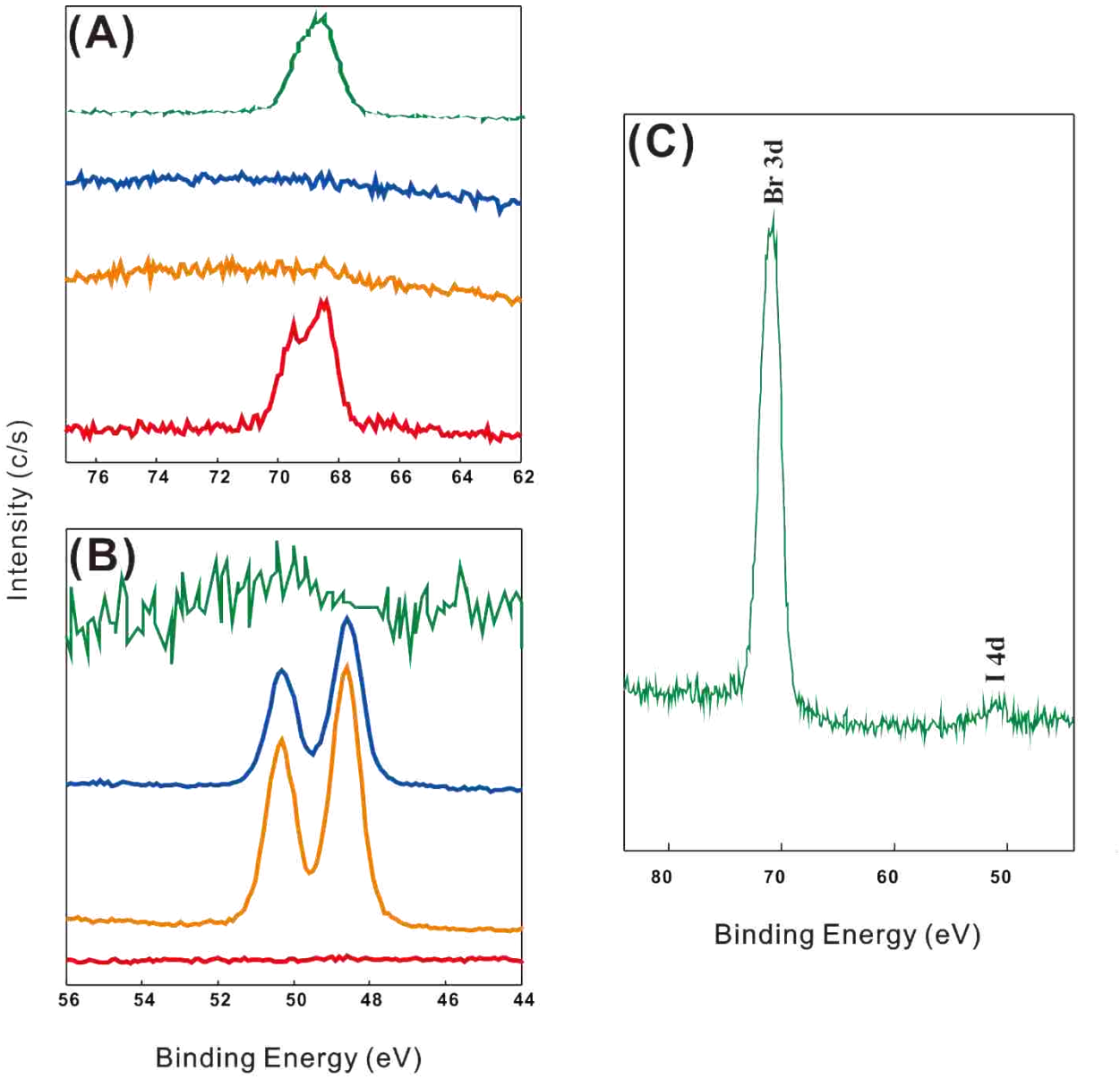

Figure 3.8. High-resolution XPS spectra presenting (A) Br 3d and (B) I 4d regions of PT (red), PT-*b*-PPP (orange), PPP (blue), and PPP-*b*-PT (green) thin films. (C) is a wide range XPS spectrum of PPP-*b*-PT to show the presence of I 4d peak.

PT polymer chains (at least all the chains that had active sites, Ni(II)) have been converted to PT-*b*-PPP diblock copolymer chains after second polymerization with 4-iodophenylmagnesium chloride monomer solution. However, in the case of PPP-*b*-PT diblock copolymer, Br $3d_{3/2}$ and Br $3d_{5/2}$ peaks were observed as well as a small peak corresponding to I 4d (see Figure 3.8C). We

could not determine how many PPP homopolymer chains remained on the surface because absolute quantitative analysis in XPS was not possible without internal or external standard, however, at least, we could conclude that some PPP chains remained as unreacted homopolymers due to side reactions mentioned above. This imperfection of diblock copolymerization in the synthesis of PPP-*b*-PT was consistent with the findings from UV/vis, PL, and CV experiments.

3.3. Conclusions

For the first time, we developed an efficient synthetic protocol for all-conjugated diblock copolymer thin films by SI-KCTP with a new Ni(II) catalytic initiator. The order of polymerization was found to affect the structure of diblock copolymer films. The polymerization for PT-*b*-PPP produced relatively short chains of PPP block compared to homopolymerization because Ni(II) catalytic initiator tended to form complex with a thiophene ring, reducing reaction rate for the subsequent polymerization. In contrast to PT-*b*-PPP film, some PPP chains from the first block did not converted into diblock copolymer chains by subsequent polymerization in the case of PPP-*b*-PT film. We assumed this imperfection might originate from steric hindrance issues. As expected for all-conjugated diblock copolymers in solution, our block copolymer thin films displayed efficientenergy transfer from PPP block to PT block. However, the order of blocks significantly affected energy transfer and PL spectra. The new approach could offer a valuable platform to control optical and electrochemical properties of polymer thin films for future applications.

3.4. References

(1) Darling, S. B. Directing the Self-Assembly of Block Copolymers. *Prog. Polym. Sci.* **2007**, *32*, 1152-1204.

(2) Lee, Y.; Gomez, E. D. Challenges and Opportunities in the Development of Conjugated Block Copolymers for Photovoltaics. *Macromolecules* **2015**, *48*, 7385-7395.

(3) Morse, D. C.; Fredrickson, G. H. Semiflexible Polymers near Interfaces. *Phys. Rev. Lett.* **1994**, *73*, 3235-3238.

(4) Giovanella, U.; Betti, P.; Botta, C.; Destri, S.; Moreau, J.; Pasini, M.; Porzio, W.; Vercelli, B.; Bolognesi, A. All-Conjugated Diblock Copolymer Approach to Improve Single Layer Green Electroluminescent Devices. *Chem.Mater.* **2011**, *23*, 810-816.

(5) Park, C.; Yoon, J.; Thomas, E. L. Enabling Nanotechnology with Self Assembled Block Copolymer Patterns. *Polymer* **2003**, *44*, 6725-6760.

(6) Zhang, Q. T.; Tour, J. M. Alternating Donor/Acceptor Repeat Units in Polythiophenes. Intramolecular Charge Transfer for Reducing Band Gaps in Fully Substituted Conjugated Polymers. *J. Am. Chem. Soc.* **1998**, *120*, 5355-5362.

(7) Tan, Z. a.; Tang, R.; Zhou, E.; He, Y.; Yang, C.; Xi, F.; Li, Y. Electroluminescence and Photovoltaic Properties of Poly(P-Phenylene Vinylene) Derivatives with Dendritic Pendants. *J.Appl. Polym. Sci.* **2008**, *107*, 514-521.

(8) Havinga, E. E.; Tenhoeve, W.; Wynberg, H. A New Class of Small Band-Gap Organic Polymer Conductors. *Polym. Bull.* **1992**, *29*, 119-126.

(9) Havinga, E. E.; Tenhoeve, W.; Wynberg, H. Alternate Donor-Acceptor Small-Band-Gap Semiconducting Polymers - Polysquaraines and Polycroconaines. *Synt. Met.* **1993**, *55*, 299-306.

(10) Forrest, S. R. The Path to Ubiquitous and Low-Cost Organic Electronic Appliances on Plastic. *Nature* **2004**, *428*, 911-918.

(11) Günes, S.; Neugebauer, H.; Sariciftci, N. S. Conjugated Polymer-Based Organic Solar Cells. *Chem. Rev.* **2007**, *107*, 1324-1338.

(12) Brabec, C. J.; Sariciftci, N. S.; Hummelen, J. C. Plastic Solar Cells. *Adv. Funct. Mater.* **2001**, *11*, 15-26.

(13) Stubinger, T.; Brutting, W. Exciton Diffusion and Optical Interference in Organic Donor-Acceptor Photovoltaic Cells. *J. Appl. Phys.* **2001**, *90*, 3632-3641.

(14) Yu, X.; Yang, H.; Wu, S.; Geng, Y.; Han, Y. Microphase Separation and Crystallization of All-Conjugated Phenylene–Thiophene Diblock Copolymers. *Macromolecules* **2012**, *45*, 266-274.

(15) Brochon, C.; Sary, N.; Mezzenga, R.; Ngov, C.; Richard, F.; May, M.; Hadziioannou, G. Synthesis of Poly(Paraphenylene Vinylene)—Polystyrene-Based Rod-Coil Block Copolymer by Atom Transfer Radical Polymerization: Toward a Self-Organized Lamellar Semiconducting Material. *J. Appl. Polym. Sci.* **2008**, *110*, 3664-3670.

(16) Hiorns, R. C.; Iratçabal, P.; Bégué, D.; Khoukh, A.; De Bettignies, R.; Leroy, J.; Firon, M.; Sentein, C.; Martinez, H.; Preud'homme, H.; Dagron-Lartigau, C. Alternatively Linking Fullerene and Conjugated Polymers. *J. Appl. Polym. Sci. Part A: Polym. Chemistry* **2009**, *47*, 2304-2317.

(17) Guo, C.; Lin, Y.-H.; Witman, M. D.; Smith, K. A.; Wang, C.; Hexemer, A.; Strzalka, J.; Gomez, E. D.; Verduzco, R. Conjugated Block Copolymer Photovoltaics with near 3% Efficiency through Microphase Separation. *Nano Letters* **2013**, *13*, 2957-2963.

(18) Schwartz, B. J.; RH, F.; RW, G.; AB, H.; JH, B.; RN, M. Conjugated Polymers as Molecular Materials: How Chain Conformation and Film Morphology Influence Energy Transfer and Interchain Interactions. *Annu. Rev. Phys. Chem.* **2003**, *54*, 141-172.

(19) Krebs, F. C.; Fyenbo, J.; Jorgensen, M. Product Integration of Compact Roll-to-Roll Processed Polymer Solar Cell Modules: Methods and Manufacture Using Flexographic Printing, Slot-Die Coating and Rotary Screen Printing. *J. Mater. Chem.* **2010**, *20*, 8994-9001.

(20) Polino, G.; Shanmugam, S.; Bex, G. J. P.; Abbel, R.; Brunetti, F.; Di Carlo, A.; Andriessen, R.; Galagan, Y. Photonic Flash Sintering of Ink-Jet-Printed Back Electrodes for Organic Photovoltaic Applications. *ACS Appl. Mater. Interfaces* **2016**, *8*, 2325-2335.

(21) Kim, B. G.; Jeong, E. J.; Chung, J. W.; Seo, S.; Koo, B.; Kim, J. A Molecular Design Principle of Lyotropic Liquid-Crystalline Conjugated Polymers with Directed Alignment Capability for Plastic Electronics. *Nat. Mater.* **2013**, *12*, 659-664.

(22) Marshall, N.; Sontag, S. K.; Locklin, J. Surface-Initiated Polymerization of Conjugated Polymers. *Chem. Commun. (Camb)* **2011**, *47*, 5681-5689.

(23) Yang, L.; Sontag, S. K.; LaJoie, T. W.; Li, W.; Huddleston, N. E.; Locklin, J.; You, W. Surface-Initiated Poly(3-Methylthiophene) as a Hole-Transport Layer for Polymer Solar Cells with High Performance. *ACS Appl. Mater. Interfaces* **2012**, *4*, 5069-5073.

(24) Barbey, R.; Lavanant, L.; Paripovic, D.; Schüwer, N.; Sugnaux, C.; Tugulu, S.; Klok, H.-A. Polymer Brushes Via Surface-Initiated Controlled Radical Polymerization: Synthesis, Characterization, Properties, and Applications. *Chem. Rev.* **2009**, *109*, 5437-5527.

(25) Elmalem, E.; Kiriy, A.; Huck, W. T. S. Chain-Growth Suzuki Polymerization of N-Type Fluorene Copolymers. *Macromolecules* **2011**, *44*, 9057-9061.

(26) Kang, S.; Ono, R. J.; Bielawski, C. W. Controlled Catalyst Transfer Polycondensation and Surface-Initiated Polymerization of a P-Phenyleneethynylene-Based Monomer. *J. Am. Chem. Soc.* **2013**, *135*, 4984-4987.

(27) Tkachov, R.; Senkovskyy, V.; Beryozkina, T.; Boyko, K.; Bakulev, V.; Lederer, A.; Sahre, K.; Voit, B.; Kiriy, A. Palladium-Catalyzed Chain-Growth Polycondensation of Ab-Type Monomers: High Catalyst Turnover and Polymerization Rates. *Angew. Chem. Int. Ed.* **2014**, *53*, 2402-2407.

(28) Khanduyeva, N.; Senkovskyy, V.; Beryozkina, T.; Bocharova, V.; Simon, F.; Nitschke, M.; Stamm, M.; Grötzschel, R.; Kiriy, A. Grafting of Poly(3-Hexylthiophene) from Poly(4-Bromostyrene) Films by Kumada Catalyst-Transfer Polycondensation: Revealing of the Composite Films Structure. *Macromolecules* **2008**, *41*, 7383-7389.

(29) Senkovskyy, V.; Khanduyeva, N.; Komber, H.; Oertel, U.; Stamm, M.; Kuckling, D.; Kiriy, A. Conductive Polymer Brushes of Regioregular Head-to-Tail Poly(3-Alkylthiophenes) Via Catalyst-Transfer Surface-Initiated Polycondensation. *J. Am. Chem. Soc.* **2007**, *129*, 6626-6632.

(30) Senkovskyy, V.; Tkachov, R.; Beryozkina, T.; Komber, H.; Oertel, U.; Horecha, M.; Bocharova, V.; Stamm, M.; Gevorgyan, S. A.; Krebs, F. C.; Kiriy, A. "Hairy" Poly(3-Hexylthiophene) Particles Prepared Via Surface-Initiated Kumada Catalyst-Transfer Polycondensation. *J. Am. Chem. Soc.* **2009**, *131*, 16445-16453.

(31) Senkovskyy, V.; Senkovska, I.; Kiriy, A. Surface-Initiated Synthesis of Conjugated Microporous Polymers: Chain-Growth Kumada Catalyst-Transfer Polycondensation at Work. *ACS Macro Letters* **2012**, *1*, 494-498.

(32) Miyakoshi, R.; Shimono, K.; Yokoyama, A.; Yokozawa, T. Catalyst-Transfer Polycondensation for the Synthesis of Poly(P-Phenylene) with Controlled Molecular Weight and Low Polydispersity. *J. Am. Chem. Soc.* **2006**, *128*, 16012-16013.

(33) Grenier, C. R. G.; Pisula, W.; Joncheray, T. J.; Müllen, K.; Reynolds, J. R. Regiosymmetric Poly(Dialkylphenylenedioxythiophene)S: Electron-Rich, Stackable Π-Conjugated Nanoribbons. *Angew. Chem. Int. Ed.* **2007**, *46*, 714-717.

(34) Kim, Y.; Cook, S.; Tuladhar, S. M.; Choulis, S. A.; Nelson, J.; Durrant, J. R.; Bradley, D. D. C.; Giles, M.; McCulloch, I.; Ha, C.-S.; Ree, M. A Strong Regioregularity Effect in Self-Organizing Conjugated Polymer Films and High-Efficiency Polythiophene:Fullerene Solar Cells. *Nat. Mater.* **2006**, *5*, 197-203.

(35) Wu, S.; Bu, L.; Huang, L.; Yu, X.; Han, Y.; Geng, Y.; Wang, F. Synthesis and Characterization of Phenylene-Thiophene All-Conjugated Diblock Copolymers. *Polymer* **2009**, *50*, 6245-6251.

(36) Giovanella, U.; Botta, C.; Gurioli, M.; Papagni, A.; Tubino, R.; Maiorana, S.; Del Buttero, P.; Alderighi, D.; Kudrna, J. Optical Properties and Photoexcitations of an Organic Blue Emitter Embedded in a Polymeric Active Matrix. *J. Appl. Phys.* **2002**, *91*, 6511-6515.

(37) List, E. J. W.; Creely, C.; Leising, G.; Schulte, N.; Schlüter, A. D.; Scherf, U.; Müllen, K.; Graupner, W. Excitation Energy Migration in Highly Emissive Semiconducting Polymers. *Chem. Phys. Lett.* **2000**, *325*, 132-138.

(38) Sontag, S. K.; Sheppard, G. R.; Usselman, N. M.; Marshall, N.; Locklin, J. Surface-Confined Nickel Mediated Cross-Coupling Reactions: Characterization of Initiator Environment in Kumada Catalyst-Transfer Polycondensation. *Langmuir* **2011**, *27*, 12033-12041.

(39) Hsu, S. L.; Signorelli, A. J.; Pez, G. P.; Baughman, R. H. Highly Conducting Iodine Derivatives of Polyacetylene: Raman, Xps and X-Ray Diffraction Studies. *J. Chem. Phys.* **1978**, *69*, 106-111.

(40) Chavez, C. A.; Choi, J.; Nesterov, E. E. One-Step Simple Preparation of Catalytic Initiators for Catalyst-Transfer Kumada Polymerization: Synthesis of Defect-Free Polythiophenes. *Macromolecules* **2014**, *47*, 506-516.

(41) Werner, W. S. M. Electron Transport in Solids for Quantitative Surface Analysis. *Surf. Interface Anal.* **2001**, *31*, 141-176.

CHAPTER 4. POLY(3,4-ETHYLENEDIOXITHIOPHENE) (PEDOT) THIN FILMS AS A HOLE TRANSPORTING LAYER FOR ITO-FREE DEVICES PREPARED BY SURFACE-INITIATED KUMADA CATALYST TRNASFER POLYMERIZATION

4.1. Introduction

Poly(3,4-ethylenedioxithiophene) (PEDOT) has been attracting significant attention of the researchers in organic electronics field because of its unique optoelectronic properties. Conductivity of the pristine bulk PEDOT, which is a black and insoluble powder, lies in the range from 1 to 100 S cm^{-1},[1] depending on the preparation conditions. The PEDOT films prepared by electropolymerization on the metal electrodes display much higher conductivity ranging from 100 to 400 S cm^{-1}, with exact value of conductivity depending on the particular dopant.[2] Temperature dependence of the conductivity places PEDOT somewhat on the metallic side, and it is often referred to as "synthetic metal".[3] A number of applications based on the PEDOT's high conductivity have been reported, such as antielectrostatics,[3,4] bio/chemo sensors,[5,6] organic capacitors,[7,8] etc. Meanwhile, neutral PEDOT has a moderate band gap energy of around 1.7 eV. The band gap value can be readily manipulated by adding substituents, or modifying the ethylene dioxide unit and/or thiophene unit. Among the most common derivatives are 3,4-propylenedioxithiophene (ProDOT),[2,9] 3,4-butylenedioxithiophene (BuDOT),[10,11] 3,4-butanesulfonic acid functionalized EDOT (EDOTS),[12] 3,4-ethylenedithiathiophene (EDTT),[13] etc. (Figure 4.1). These derivatives would be potential candidates for electrochromic and other electronic applications.[14,15]

Like other CPs, bulk PEDOT powder is nearly insoluble in any organic or aqueous solvents, which limits further detailed structural and properties studies, as well as potential applications. In addition, PEDOT has a low oxidation potential, which facilitates turning the

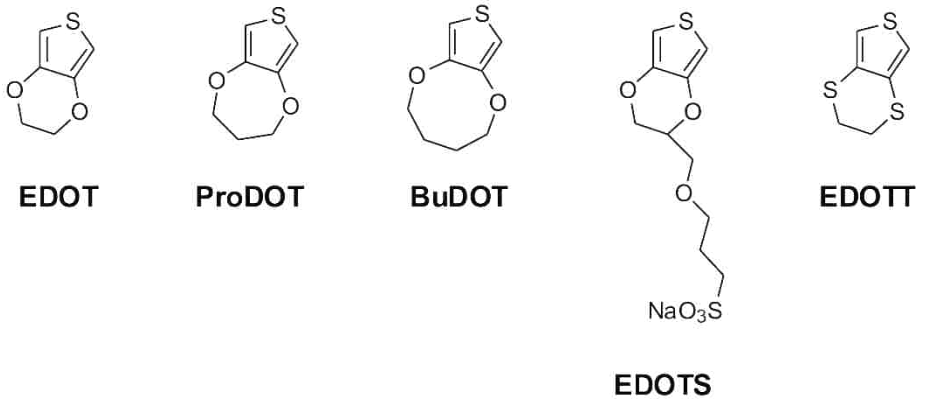

Figure 4.1. Representative examples of EDOT derivatives studied in literatures.

polymer into an oxidized state and significantly reduces stability of any devices based on the polymer. Consequently, many efforts have been attempted to increase solubility of PEDOT. One of the most popular methods to address the solubility issue is to polymerize EDOT with a counteranion monomer, resulting in a dispersion solution with a polymeric counteranion, such as polystyrene sulfonate (PSS),[16,17] or sulfated poly(b-hydroxyether) (S-PSE).[18] Particularly, to date, PEDOT:PSS is one of the most well-known and commercially available semiconducting polymers. The aqueous PEDOT:PSS dispersion dramatically alters mechanical/chemical properties as well as opto-electronic nature of a spin-casted film. For example, the dispersion itself has a dark blue color, but the casted film is transparent with high transmissivity, i.e., more than 90% transmittance is in the visible range. The spin-casted film shows high thermal stability up to 1000 ℃ for several hours, and displays moderate conductivity, ranging from 1 to 10 S cm^{-1}.[19] The work function of the PEDOT:PSS film matches well to organic donor materials, bridging energy barrier between the metal anodes and the donor components.[20] Additionally, PEDOT:PSS spin-casted film on ITO can improve smoothness of the rough surface and therefore diminish possibility of local shorting in the ultrathin layer, thus enhancing overall device performance.[20,21]

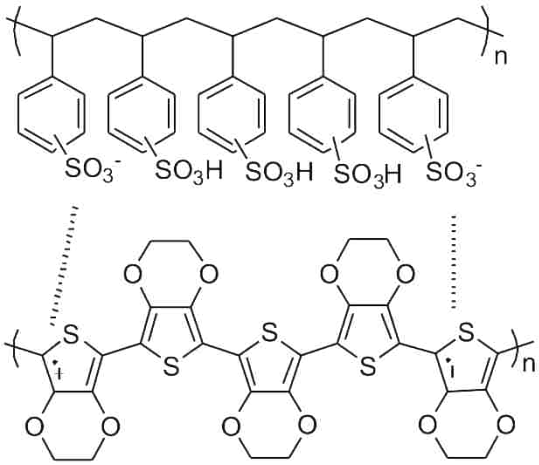

Figure 4.2. PEDOT:PSS molecular structure (BAYTRON P). The dash lines indicate ionic interaction between PEDOT and PSS.

Considering all these advantages, it is not surprising that PEDOT:PSS has become the most widely used component as a hole transporting layer for organic electronic applications.

Despite the excellent features of PEDOT:PSS, inherent acidic nature of this material is a substantial drawback because it renders degradation of the ITO or the organic donor layers. The typical molar ratio in PEDOT:PSS is about 0.8:1, i.e. there are excessive sulfonic acid groups to provide negative charge to make it as an non-stoichiometric soluble polymer electrolyte system.[22] The presence of free sulfonic acid groups makes PEDOT:PSS rather corrosive, which often leads to problems associated with destructive action of PSS on ITO or other donor materials. In addition, the overall excessive negative charge can facilitate quenching the holes generated by absorption light, i.e. the film can display unfavorable hole-blocking ability, resulting in decreasing the overall device performance. Consequently, general lifetime of organic electronic devices made with PEDOT:PSS as a hole transporting layer could be as little as 600 h,[23] which is too low for most applications. And the moderate conductivity further lowered by the PSS component would be another drawback. Therefore, a large number of studies have attempted to circumvent this issue by carrying out direct deposition of the PEDOT layer on a

target surface, using electrochemical polymerization,[24] oxidative chemical vapor deposition (oCVD),[25] and radical polymerization.[26] Unfortunately, none of these methods can provide accurate control over PEDOT film deposition, due to uncertain mechanism, variable kinetics,[27] which all resulted in low film quality and insufficient transporting characteristics. Additionally, some of the suggested reactions require harsh or difficult to achieve conditions such as ultra-high vacuum, high temperature,[25] etc.

On the other hand, surface-initiated Kumada catalyst transfer polymerization (SI-KCTP) of EDOT monomer is an alternative approach to grow PEDOT film on surfaces for using it as a hole transporting layer. Indeed, a similar concept has been investigated by the Locklin group[28] who prepared poly(3-methylthiophene) (P3MT) film on ITO as a hole transporting layer (P3MT/ITO) using SI-KCTP. They demonstrated that P3MT/ITO system was stable against air, moisture, and light for over one month, with only slightly less efficiency than a device made with using traditional PEDOT:PSS. In this chapter, we describe our concept to implement SI-KCTP with an external catalytic initiator developed in our lab to prepare a surface-confined PEDOT layer, and investigate the possibility to use surface-confined PEDOT to replace PEDOT:PSS for a hole transporting layer in electronic devices, as well as replacement of ITO as anode material (Figure 4.3).

4.2. Results and discussion

We chose to use 2,5-dibromo-EDOT as a starting monomer to synthesize PEDOT polymer brush on the surface. $(EtO)_3$Si-Th-Ni(dppp)I, a Ni(II) external catalytic initiator complex, was first immobilized on quartz surface. In order to prepare the required Grignard monomer for surface-initiated polymerization, the turbo Grignard reagent (*i*-PrMgCl·LiCl) was used because of low reactivity of 2,5-dibromo-EDOT towards Mg-halogen exchange (see Experimental section for

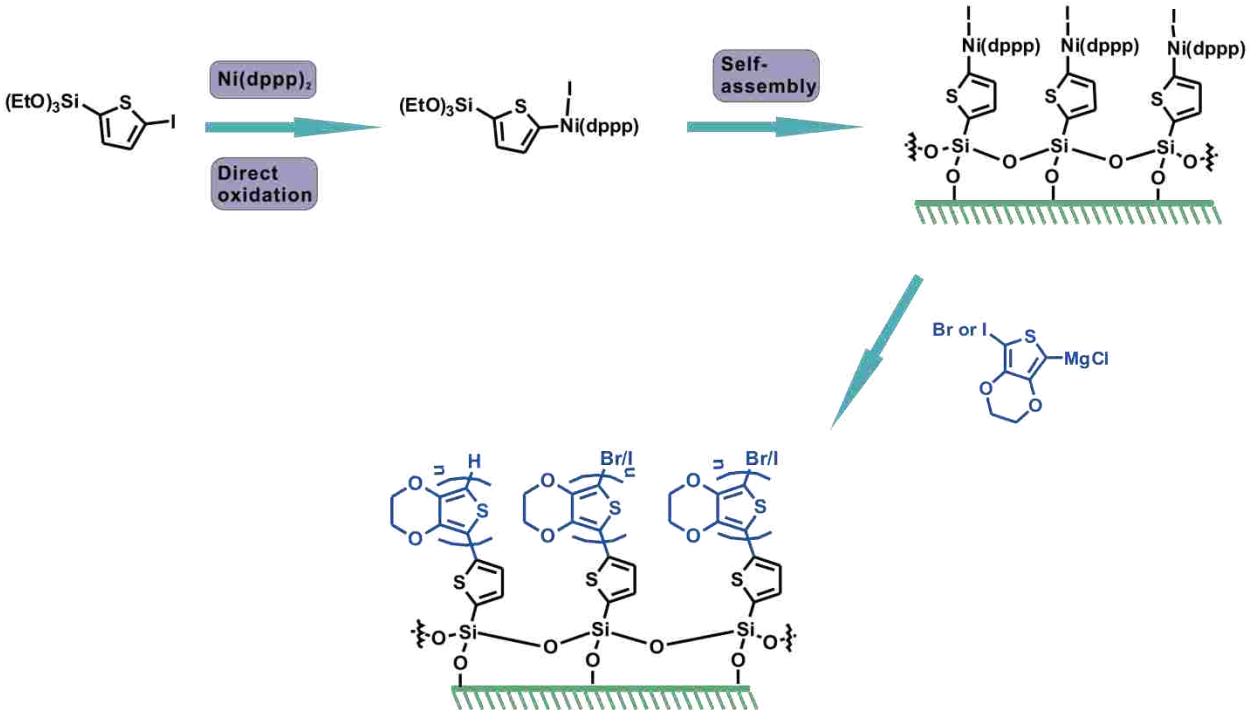

Figure 4.3. General scheme of using SI-KCTP to prepare surface-confined PEDOT films.

details). Then, the surface-initiated polymerization was carried out at a relatively high temperature, 60 ℃, with vigorous stirring for 3 days, resulting in a dark blue color film of PEDOT on the quartz surface. A sequential sonication with different solvents (chloroform, acetone, methanol, and water) over 50 min was performed to remove physisorbed polymers or other organic by-products. Although using high temperature might likely result in less robust chain-growth mechanism of surface-initiated polymerization (which was reflected in the relatively large amount of solution-formed insoluble PEDOT), our attempts to perform polymerization at lower temperature, below 60 ℃, were not successful.

Infrared (IR) spectroscopy was used to confirm formation of the surface-confined PEDOT film (Figure 4.4). Major features in the IR spectrum were consistent with the characteristic peaks attributed to PEDOT film described in literature.[29] The band at 1460 cm^{-1} was assigned to C=C

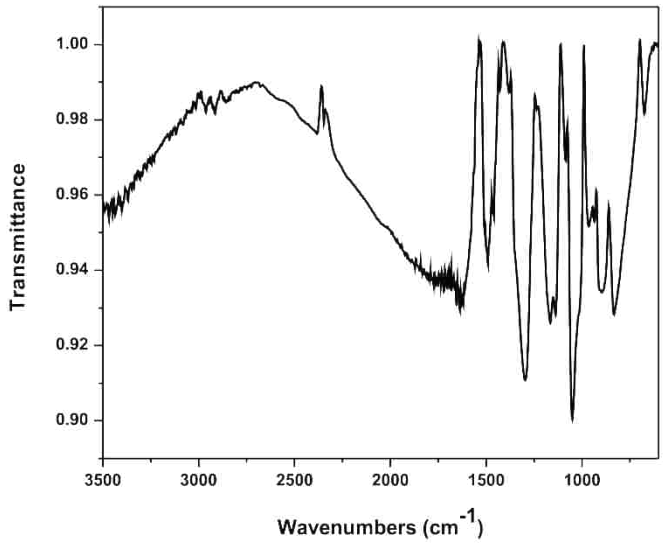

Figure 4.4. IR spectrum of the PEDOT film prepared by surface-initiated polymerization on quartz at 60 ℃ for 3 days.

stretching of the thiophene ring. The band corresponding to C-O stretching on the ethylenedioxide fragment appeared at 1051 cm^{-1} and 1165 cm^{-1}. Presence of CH_2 bending of the ethylene part was confirmed by the bands at 1300 cm^{-1} and 1491 cm^{-1}. Most of these peaks were very sharp, and some strong peaks at around 900 - 800 cm^{-1} were overlapped with the peaks which could be assigned to the EDOT monomer or oligomer. Hence, it was likely that a substantial fraction of the EDOT oligomers or even the monomers might be present in the film, implying overall low degree of polymerization. However, due to the limitation of IR spectroscopy and the inconsistency of the obtained IR spectrum with those previously reported for PEDOT, additional structural evidence was required to confirm formation of the PEDOT polymer brush.

UV/vis spectrum in Figure 4.5A (black trace) shows spectrum of the PEDOT film prepared by surface-initiated polymrization. The broad absorption band with λ_{max} 550 nm and

spanning to 720 nm is a typical UV/vis spectral band characteristic of an undoped PEDOT film fabricated by electrochemical polymerization, but with roughly 50 nm blue shift relative to the λ_{max} reported in literature.[29] The bandgap E_g^{opt} of 1.7 eV determined by the onset of an absorption band was in the range of a typical PEDOT bandgap values. However, we found no fine vibronic structure of the absorption band which is typically expected for the undoped PEDOT film and other CP films. Furthermore, the optical density of the film was very low compared to that of PT films prepared by surface-initiated polymerization in similar experimental conditions (generally showing optical absorbance of more than 0.8). We suggested that both features indicated low degree of polymerization as well as lower surface density and poor chain alignment in the film. In addition, a noticeable shoulder at around 350 nm could also indicate presence of relatively short oligomers in the film.[29] The procedure involving

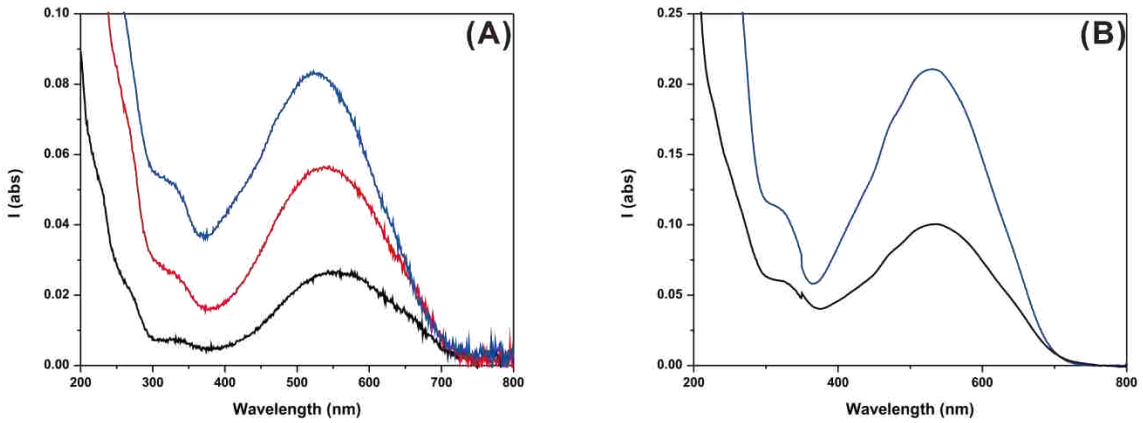

Figure 4.5. UV/vis spectra of PEDOT films on quartz substrate. (A) black trace: a PEDOT film prepared by surface-initiated polymerization using Grignard monomer obtained from 2,5-dibromo-EDOT (the polymerization was carried out at 60 ℃ for 3 days), red trace: the film prepared using Ni(II) catalytic initiator regeneration procedure applied to the previous PEDOT film, blue trace: the film made starting with 2,5-diiodo-EDOT to prepare Grignard monomer (the surface-initiated polymerization was carried out at 60 ℃ for 3 days). (B) temperature dependence of the polymerization utilizing Grignard monomer prepared from 2,5-diiodo-EDOT: the polymerization carried out at 50 ℃ for 3 days (black trace), and at 40 ℃ for 1 day (blue trace).

intermediate regeneration of the active Ni(II) catalytic initiator (described in detail in Chapter 2) was tested to support these assumptions. After the initial surface-initiated polymerization, the polymer film was immersed into a $Ni(dppp)_2$ solution to reactivate Br-terminated polymer chains, which was followed by further polymerization in the same conditions. As shown in figure 4.5A (red trace), the intensity of both absorption bands at 350 nm and 550 nm increased approximately twice relative to the original spectrum. As it was discussed in chapters 2 and 3, it is clear that several side reactions, such as disproportionation or chain transfer reaction, can readily happen, especially at the high temperature used for surface-initiated polymerization in the PEDOT preparation. These side reactions likely caused early termination of the polymerization and therefore resulted in a low degree of polymerization, leaving a mixture of surface-confined polymer brushes of different lengths.

AFM studies of the PEDOT surface-confined film revealed a non-uniform rough surface morphology (Figure 4.6). The surface consisted of small globular-like domains that represenedt a typical surface morphology of polymer films prepared by surface-initiated polymerization (see Chapter 2). However, the height of the surface features showed very broad variation, with an average height of the features at around 40 nm and with large RMS value of 9.5 nm meaning a highly uneven surface.

To better understand electrochemical characteristics of the PEDOT films, we carried out CV studies (Figure 4.7). One quasi-reversible redox peak was observed at $E_{1/2}$ -0.75 V, and an intense non-reversible oxidation peak -0.3 V (vs. Fc/Fc^+ reference electrode). The CV curve did not show significant change during several voltage sweepings, implying that the PEDOT film was stable towards electrochemical processes. The intense non-reversible oxidation peak

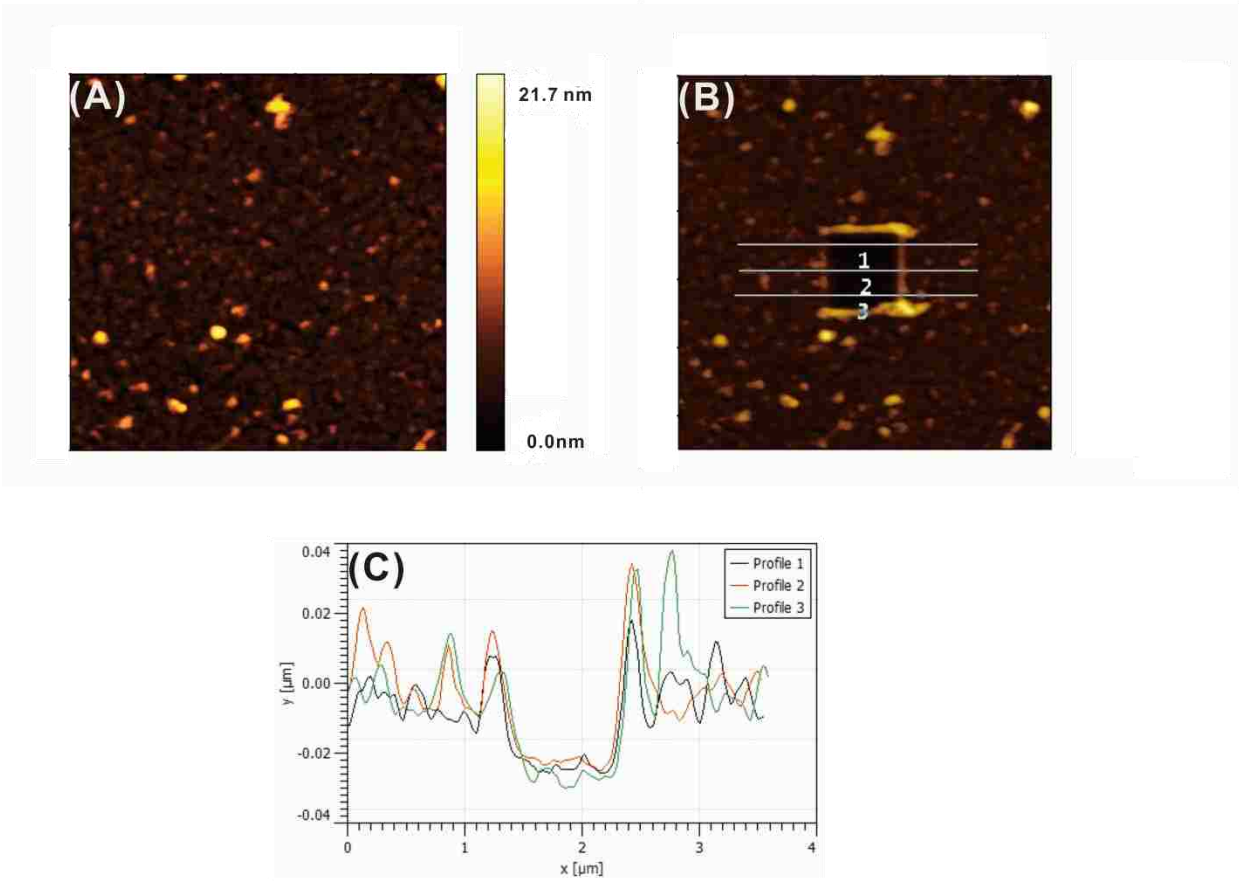

Figure 4.6. (A) AFM topography of the PEDOT film; (B) and (C) – line analysis using nanoshaving procedure. Each profiles in (C) correspond to the indicated lines in (B). All images are 5 × 5 µm in size.

indicated faster electron transfer process than could be observed in an oligomer film, due to the presence of well-defined PEDOT chains, whereas a less intense corresponding reduction peak spanned over more broad potential range therefore indicating a slow reduction process. This slow reduction process pointed out that the doped PEDOT film could act as a potential hole transporting layer. The presence of a quasi-reversible redox peak at -0.75 V might be an indication of a long range molecular ordering of the PEDOT chains. Unlike the broad reduction peak at -0.1 V, the smaller reduction peak at -0.75 V was observed as a rather sharp peak. On the basis of the bandgap energy obtained from the onset of UV/vis spectral band (1.7 eV) and

HOMO level from the intense irreversible oxidation peak in the CV, calculated HOMO (E_{HOMO} = -[$E_{oxi,\ onset}$ + 5.1]eV)[30] and LUMO ($E_{LUMO} = E_g^{opt} + E_{HOMO}$) energy levels of the film were -4.8 eV and -3.1 eV, respectively. The HOMO energy of the film was substantially close to the work function value of the O_2 plasma treated ITO, -5.0 eV,[21] which also suggested that the film could be a good replacement for ITO as an organic electrode.

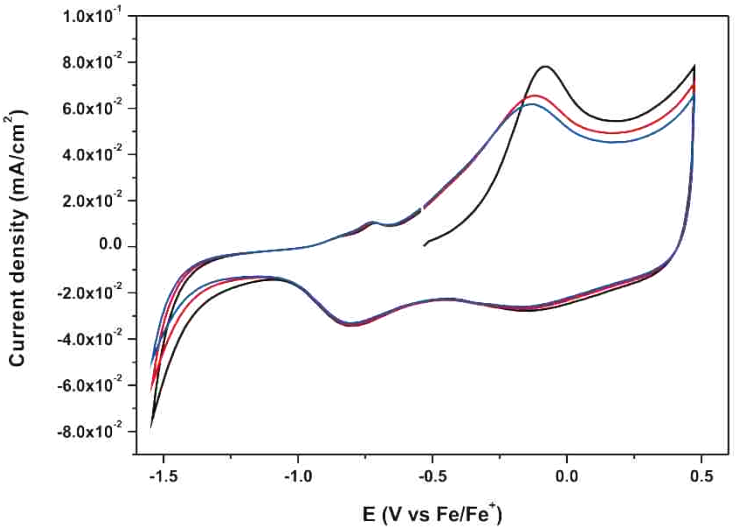

Figure 4.7. Cyclic voltammetry (CV) studies of the surface-confined PEDOT film on ITO surface. Data were acquired versus ferrocene external standard in 0.1 M Bu_4NPF_6 in CH_2Cl_2, with sweep rate 0.1 V s^{-1}. Black trace is the first scan. Red and blue traces represent second and third scan, respectively.

In order to further optimize polymerization condition, we tested a different monomer and attempted temperature variation. To increase reactivity of the Grignard monomer, we used 2,5-diiodoEDOT to prepare the corresponding Grignard monomer, and carried out surface-initiated polymerization at the same temperature, 60 ℃. As can be seen in figure 4.6A (blue line), even with less polymerization time, optical absorbance of the polymer film prepared using iodo-Grignard monomer was substantially higher than that of the PEDOT film prepared using 2,5-dibromoEDOT-based monomer, even with using the Ni(II) catalyst regeneration procedure,

while the small blue shift of λ_{max} was also noticed. This substantial increase in the optical absorbance along with the blue shift might indicate that more polymeric chains existed on the surface, although with lower conjugation length of the individual chains. Simultaneously, the absorbance at the shorter wavelength also increased, possibly indicating that the polymerization produced higher fraction of oligomeric chains. We assumed that this was due to the high reactivity of iodo-monomer towards both propagation and disproportionation in the surface-initiated polymerization. The higher reactivity in propagation resulted in increasing polymer chain length, and possibly higher polymer surface density, whereas the higher efficiency in disproportionation reaction resulted in higher polydispersity of the surface-confined polymer chains, which could be responsible for the lower effective conjugation length.

We found that surface-initiated polymerization showed strong temperature dependence (figure 4.5B). Although one would predict lower polymerization reaction rate at lower temperature, lowering temperature would also result in the decrease of the rate of side reactions (such as disproportionation and chain-transfer) which could potentially lead to the higher degree of polymerization at longer reaction time. The surface-initiated polymerization with iodo-EDOT Grignard monomer at 50 ℃ for 3 days produced PEDOT films with slightly higher optical absorbance. Interestingly, carrying out the same reaction at 40 ℃ for only one day yielded PEDOT film with more than twice higher optical absorbance at λ_{max}, supporting our assumption of more robust chain-growth polymerization at lower temperature. However, we also observed increasing the optical absorption of the short wavelength band corresponding to EDOT oligomers. This proved that formation of oligomeric chains was still occurring on the surface because of the disproportionation and chain-transfer side reactions. It appears that optimizing reaction conditions in order to obtain high-quality PEDOT film requires fine balancing between

various factors responsible for the polymerization and disproportionation processes, and currently we are further investigating these factors.

Doping with halogens has been generally used to increase conductivity of CPs. As it was mentioned above, one of the reasons for the popularity of PEDOT:PSS for organic electronics is high conductivity in the doped state resulting from the presence of PSS. Thus, we conducted a doping test for the surface-confined PEDOT film using iodine vapor, upon monitoring both spectroscopic and conductive properties of the film. UV/vis absorption spectra were acquired before and after iodine doping (Figure 4.8). After exposure of the film to iodine vapor for one day, both near-IR polaron and bipolaron absorption bands became dominant, and the film turned to transparent sky-blue color. In good agreement with previous studies, formation of polaron and bipolaron states upon iodine doping was an indication of high conductivity of the sample. In addition, high transmittance in the visible region was an essential requirement for using this film

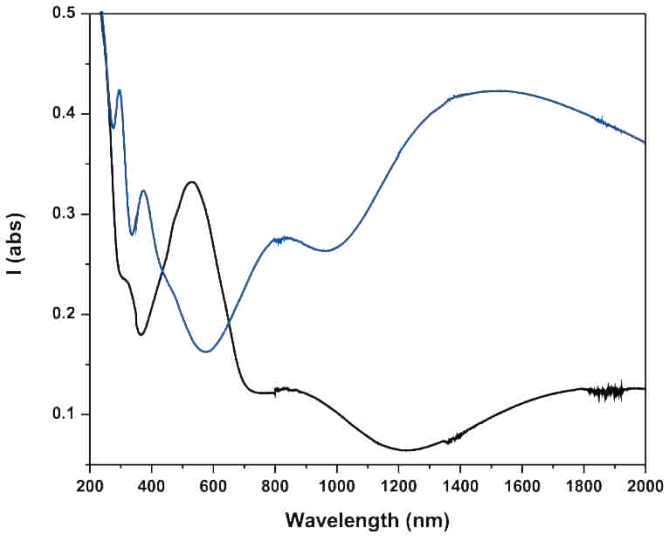

Figure 4.8. UV/vis spectra of the PEDOT films before (black trace) and after (blue trace) doping by exposure to iodine vapor for 1 day.

for light-transparent organic electrodes.

Electrical conductivity 4-point probe measurements (table 4.1) for the PEDOT films were carried out to test conductivity which was determined assuming 40 nm thickness of the film as derived from nanoshaving experiment (figures 4.6B and C). Before doping, average conductivity of the film was 1.66×10^{-4} S cm^{-1}. After the iodine doping, conductivity became two orders of magnitude higher, up to 3.47×10^{-2} S cm^{-1}. This value was very similar to the conductivity of germanium.

Table 4.1. 4-point probe conductivity measurements of the PEDOT films on quartz substrate before and after doping with iodine vapor.[a, b]

before exposure to I_2					
R (ohm)	Resistivity (Ω cm)[c]	Conductivity (S cm^{-1})[d]	Thickness (μm)[e]	Average conductivity (S cm^{-1})	STD
2.80E+09	1.12E+04	8.93E-05	0.04	1.66E-04	0.003866
1.25E+09	5.00E+03	2.00E-04			
1.51E+09	6.04E+03	1.66E-04			
1.32E+09	5.28E+03	1.89E-04			
1.31E+09	5.24E+03	1.91E-04			
1.24E+09	4.96E+03	2.02E-04			
1.71E+09	6.84E+03	1.46E-04			
2.14E+09	8.56E+03	1.17E-04			
1.25E+09	5.00E+03	2.00E-04			
1.54E+09	6.16E+03	1.62E-04			
after exposure to I_2					
R (ohm)	Resistivity (Ω cm)[c]	Conductivity (S cm^{-1})[d]	Thickness (μm)[e]	Average conductivity (S cm^{-1})	STD
5.63E+06	2.25E+01	4.44E-02	0.04	3.47E-02	1.19649
1.03E+07	4.12E+01	2.43E-02			
1.16E+07	4.64E+01	2.16E-02			
5.60E+06	2.24E+01	4.46E-02			

Table 4.1. continue

R (ohm)	Resistivity (Ω cm)[c]	Conductivity (S cm^{-1})[d]	Thickness (μm)[e]	Average conductivity (S cm^{-1})	STD
4.76E+06	1.90E+01	5.25E-02	0.04	3.47E-02	1.19649
6.02E+06	2.41E+01	4.15E-02			
9.65E+06	3.86E+01	2.59E-02			
7.75E+06	3.10E+01	3.23E-02			
5.84E+06	2.34E+01	4.28E-02			
1.44E+07	5.76E+01	1.74E-02			

[a] the film was prepared on quartz using polymerization at 40 °C for 1 day of Grignard monomer synthesized from 2,5-diiodo-EDOT; [b] 10 random measurements on each film was performed; [c] resistivity (Ω cm) = R × thickness; [d] conductivity (S cm^{-1}) = 1/resistivity; [e] The thickness was determined from the line analysis of AFM nanoshaving experiments (figure 4.6B and C) for all measurements.

4.3. Conclusions

Using surface-initiated KCTP, we prepared PEDOT thin films on quartz and ITO substrates. Due to the low reactivity of 5-bromo-2-(3,4-ethylenedioxythienyl)magnesium chloride monomer, high temperature and long reaction time were required for the polymerization, which resulted in less robust chain-growth mechanism, and dominance of chain-termination processes, essentially leading to low degree of polymerization. Various experiments pointed out that the surface-confined PEDOT film was composed of a mixture of oligomeric and polymeric chains of various length, with rather high polydispersity. Despite the seemingly disordered nature of the surface-confined PEDOT film, experimentally determined energy levels (HOMO, LUMO, and bandgap) and electrochemical studies (CV and 4-probe conductivity) suggested that the iodine-doped film could potentially replace PEDOT:PSS in various electronic devices. To further optimize surface-initiated polymerization conditions, polymerization of a Grignard monomer derived from 2,5-diiodo-EDOT was studied at different temperatures. Although this monomer showed some promise in achieving higher degree of polymerization, detrimental side reactions

were still not completely suppressed resulting in the formation of a substantial amount of oligomeric EDOT chains as was reflected in the optical and electrochemical properties of the polymer film. At the moment, we are attempting further optimization of the polymerization process to improve the quality of PEDOT thin films. In addition, we will study formation of the PEDOT thin films on flexible polymeric substrates, as required for the preparation of flexible organic electronic devices.

4.4. References

(1) Heywang, G.; Jonas, F. Poly(Alkylenedioxythiophene)S—New, Very Stable Conducting Polymers. *Adv. Mater.* **1992**, *4*, 116-118.

(2) Dietrich, M.; Heinze, J.; Heywang, G.; Jonas, F. Electrochemical and Spectroscopic Characterization of Polyalkylenedioxythiophenes. *J. Electroanal. Chem.* **1994**, *369*, 87-92.

(3) Groenendaal, L.; Jonas, F.; Freitag, D.; Pielartzik, H.; Reynolds, J. R. Poly(3,4-Ethylenedioxythiophene) and Its Derivatives: Past, Present, and Future. *Adv. Mater.* **2000**, *12*, 481-494.

(4) Akoudad, S.; Roncali, J. Electrochemical Synthesis of Poly(3,4-Ethylenedioxythiophene) from a Dimer Precursor. *Synt. Met.* **1998**, *93*, 111-114.

(5) Mohan, K.; Donavan, K. C.; Arter, J. A.; Penner, R. M.; Weiss, G. A. Sub-Nanomolar Detection of Prostate-Specific Membrane Antigen in Synthetic Urine by Synergistic, Dual-Ligand Phage. *J. Am Chem. Soc.* **2013**, *135*, 7761-7767.

(6) Malmström, J.; Nieuwoudt, M. K.; Strover, L. T.; Hackett, A.; Laita, O.; Brimble, M. A.; Williams, D. E.; Travas-Sejdic, J. Grafting from Poly(3,4-Ethylenedioxythiophene): A Simple Route to Versatile Electrically Addressable Surfaces. *Macromolecules* **2013**, *46*, 4955-4965.

(7) Ghosh, S.; Inganäs, O. Conducting Polymer Hydrogels as 3d Electrodes: Applications for Supercapacitors. *Adv. Mater.* **1999**, *11*, 1214-1218.

(8) Larmat, F.; Reynolds, J. R.; Qiu, Y.-J. Polypyrrole as a Solid Electrolyte for Tantalum Capacitors. *Synt. Met.* **1996**, *79*, 229-233.

(9) Winter, I.; Reese, C.; Hormes, J.; Heywang, G.; Jonas, F. The Thermal Ageing of Poly(3,4-Ethylenedioxythiophene). An Investigation by X-Ray Absorption and X-Ray Photoelectron Spectroscopy. *Chem. Phys.* **1995**, *194*, 207-213.

(10) Kumar, A.; Welsh, D. M.; Morvant, M. C.; Piroux, F.; Abboud, K. A.; Reynolds, J. R. Conducting Poly(3,4-Alkylenedioxythiophene) Derivatives as Fast Electrochromics with High-Contrast Ratios. *Chem. of Mater*. **1998**, *10*, 896-902.

(11) Welsh, D. M.; Kumar, A.; Morvant, M. C.; Reynolds, J. R. Fast Electrochromic Polymers Based on New Poly(3,4-Alkylenedioxythiophene) Derivatives. *Synt. Met.* **1999**, *102*, 967-968.

(12) Stéphan, O.; Schottland, P.; Le Gall, P.-Y.; Chevrot, C.; Mariet, C.; Carrier, M. Electrochemical Behaviour of 3, 4-Ethylenedioxythiophene Functionalized by a Sulphonate Group. Application to the Preparation of Poly(3, 4-Ethylenedioxythiophene) Having Permanent Cation-Exchange Properties. *J. Electroanal. Chem.* **1998**, *443*, 217-226.

(13) Wang, C.; Schindler, J. L.; Kannewurf, C. R.; Kanatzidis, M. G. Poly(3,4-Ethylenedithiathiophene). A New Soluble Conductive Polythiophene Derivative. *Chem.Mater*. **1995**, *7*, 58-68.

(14) Akoudad, S.; Roncali, J. International Conference on Science and Technology of Syntheticelectrogenerated Poly(Thiophenes) with Extremely Low Bandgap. *Synt. Met.* **1999**, *101*, 149.

(15) J. Irvin, D.; J. DuBois Jr, C.; R. Reynolds, J. Dual P- and N-Type Doping in an Acid Sensitive Alternating Bi(Ethylenedioxythiophene) and Pyridine Polymer. *Chem. Commun.* **1999**, 2121-2122.

(16) Aleshin, A. N.; Williams, S. R.; Heeger, A. J. Transport Properties of Poly(3,4-Ethylenedioxythiophene)/Poly(Styrenesulfonate). *Synt. Met.* **1998**, *94*, 173-177.

(17) Lefebvre, M.; Qi, Z.; Rana, D.; Pickup, P. G. Chemical Synthesis, Characterization, and Electrochemical Studies of Poly(3,4-Ethylenedioxythiophene)/Poly(Styrene-4-Sulfonate) Composites. *Chem.Mater*. **1999**, *11*, 262-268.

(18) Sakmeche, N.; Aeiyach, S.; Aaron, J.-J.; Jouini, M.; Lacroix, J. C.; Lacaze, P.-C. Improvement of the Electrosynthesis and Physicochemical Properties of Poly(3,4-Ethylenedioxythiophene) Using a Sodium Dodecyl Sulfate Micellar Aqueous Medium. *Langmuir* **1999**, *15*, 2566-2574.

(19) Jonas, F.; Krafft, W.; Muys, B. Poly(3, 4-Ethylenedioxythiophene): Conductive Coatings, Technical Applications and Properties. *Macromol. Symp.* **1995**, *100*, 169-173.

(20) Günes, S.; Neugebauer, H.; Sariciftci, N. S. Conjugated Polymer-Based Organic Solar Cells. *Chem. Rev.* **2007**, *107*, 1324-1338.

(21) Park, H.; Howden, R. M.; Barr, M. C.; Bulovic, V.; Gleason, K.; Kong, J. Organic Solar Cells with Graphene Electrodes and Vapor Printed Poly(3,4-Ethylenedioxythiophene) as the Hole Transporting Layers. *ACS Nano* **2012**, *6*, 6370-6377.

(22) Ghosh, S.; Rasmusson, J.; Inganäs, O. Supramolecular Self-Assembly for Enhanced Conductivity in Conjugated Polymer Blends: Ionic Crosslinking in Blends of Poly(3,4-Ethylenedioxythiophene)-Poly(Styrenesulfonate) and Poly(Vinylpyrrolidone). *Adv. Mater.* **1998**, *10*, 1097-1099.

(23) Lloyd, M. T.; Peters, C. H.; Garcia, A.; Kauvar, I. V.; Berry, J. J.; Reese, M. O.; McGehee, M. D.; Ginley, D. S.; Olson, D. C. Influence of the Hole-Transport Layer on the Initial Behavior and Lifetime of Inverted Organic Photovoltaics. *Sol. Energy Mater. Sol. Cells* **2011**, *95*, 1382-1388.

(24) Pei, Q.; Zuccarello, G.; Ahlskog, M.; Inganäs, O. Electrochromic and Highly Stable Poly(3,4-Ethylenedioxythiophene) Switches between Opaque Blue-Black and Transparent Sky Blue. *Polymer* **1994**, *35*, 1347-1351.

(25) Howden, R. M.; Flores, E. J.; Bulović, V.; Gleason, K. K. The Application of Oxidative Chemical Vapor Deposited (Ocvd) Pedot to Textured and Non-Planar Photovoltaic Device Geometries for Enhanced Light Trapping. *Org. Electron.* **2013**, *14*, 2257-2268.

(26) Sadekar, A. G.; Mohite, D.; Mulik, S.; Chandrasekaran, N.; Sotiriou-Leventis, C.; Leventis, N. Robust Pedot Films by Covalent Bonding to Substrates Using in Tandem Sol-Gel, Surface Initiated Free-Radical and Redox Polymerization. *J. Mater. Chem.* **2012**, *22*, 100-108.

(27) Heinze, J.; Frontana-Uribe, B. A.; Ludwigs, S. Electrochemistry of Conducting Polymers—Persistent Models and New Concepts. *Chem. Rev.* **2010**, *110*, 4724-4771.

(28) Yang, L.; Sontag, S. K.; LaJoie, T. W.; Li, W.; Huddleston, N. E.; Locklin, J.; You, W. Surface-Initiated Poly(3-Methylthiophene) as a Hole-Transport Layer for Polymer Solar Cells with High Performance. *ACS Appl. Mater. Interfaces* **2012**, *4*, 5069-5073.

(29) Tran-Van, F.; Garreau, S.; Louarn, G.; Froyer, G.; Chevrot, C. Fully Undoped and Soluble Oligo(3,4-Ethylenedioxythiophene)S: Spectroscopic Study and Electrochemical Characterization. *J. Mater. Chem.* **2001**, *11*, 1378-1382.

(30) Cardona, C. M.; Li, W.; Kaifer, A. E.; Stockdale, D.; Bazan, G. C. Electrochemical Considerations for Determining Absolute Frontier Orbital Energy Levels of Conjugated Polymers for Solar Cell Applications. *Adv. Mater.* **2011**, *23*, 2367-2371.

5. EXPERIMENTAL SECTION

5.1. General Procedures

All reactions were performed under an atmosphere of dry nitrogen (unless mentioned otherwise). Melting points were determined in open capillaries and are uncorrected. Column chromatography was performed on silica gel (Sorbent Technologies, 60 Å, 40-63 μm) slurry packed into glass columns. Tetrahydrofuran (THF), ether, dichloromethane, toluene, acetonitrile, and hexanes were dried by passing through activated alumina using a PS-400 Solvent Purification System from Innovative Technology, Inc. The water content of the solvents was periodically controlled by Karl Fischer titration (using a DL32 coulometric titrator from Mettler Toledo). All other solvents (HPLC or anhydrous grade) were used as received. Tetrabutylammonium hexafluorophosphate for electrochemical measurements was obtained from Aldrich and used after recrystallization from ethanol. Isopropylmagnesium chloride (2.0 M solution in THF) was purchased from Acros Organics, all other reagents and solvents were obtained from Aldrich and Alfa Aesar and used without further purification. Organometallic reagents were titrated with salicylaldehyde phenylhydrazone prior to use.[1] Indium tin oxide (ITO) coated glass slides (25×75×1.1 mm polished float glass, 8-12 Ohm/sq. surface resistivity) were purchased from Delta Technologies, Ltd. 75×25 mm^2 sized polished rectangular quartz slides were purchased from Chemglass. Silicon (111) wafers were purchased from Virginia Semiconductor Inc. Monodisperse latex mesospheres (300 nm diameter) were supplied by Thermo Scientific. UV-Visible spectra were recorded on a Varian Cary 50 and Agilent Cary 5000 spectrophotometers. Thickness of polymer films on quartz substrates was determined by scratching the film surface with a razor blade, and acquiring an across-the-scratch depth profile using Bruker Dektak XT stylus profiler. Scanning Electron Microscopy images were acquired

with Hitachi S-3600N microscope. ^{1}H NMR spectra were recorded at 400 MHz , and ^{13}C NMR – at 100 MHz, and are reported in ppm downfield from tetramethylsilane; ^{31}P NMR spectra were obtained at 162 MHz and are reported in ppm relative to 80% aqueous H_3PO_4 as external standard. Electrochemical and spectroelectrochemical measurements were performed using an Autolab PGSTAT 302 potentiostat from Eco Chemie. The experiments were carried out using a three-electrode system with a thin polymer film on ITO as a working electrode, $Ag/AgNO_3$ non-aqueous reference electrode, and a Pt gauze counter electrode. The reference electrode was checked against ferrocene standard every time before and after the experiments were performed, and the measured potentials were reported against the Fc/Fc^+ redox potential value. All experiments were carried out in 0.1 M Bu_4NPF_6 solution in CH_2Cl_2 as supporting electrolyte. High resolution mass spectra were obtained at the LSU Department of Chemistry Mass Spectrometry Facility.

5.2. Atomic Force Microscopy

Samples were characterized with a model 5500 atomic force microscope (AFM) equipped with Picoscan v5.3.3 software (Agilent Technologies, Chandler, AZ). Images were acquired using contact mode in ambient conditions. Oxide-sharpened silicon nitride cantilevers with force constants ranging from 0.1 to 0.5 N/m were used for imaging (Veeco Probes, Santa Barbara, CA). Digital images were processed with Gwyddion open source software (version 2.9), which is supported by the Czech Metrology Institute.[4]

5.3. X-ray Photoelectron Spectroscopy (XPS)

The XPS experiments were carried out using PHI *VersaProbe II* instrument equipped with a monochromatic Al K(alpha) source. Instrument base pressure was ca. 8×10^{-10} Torr.

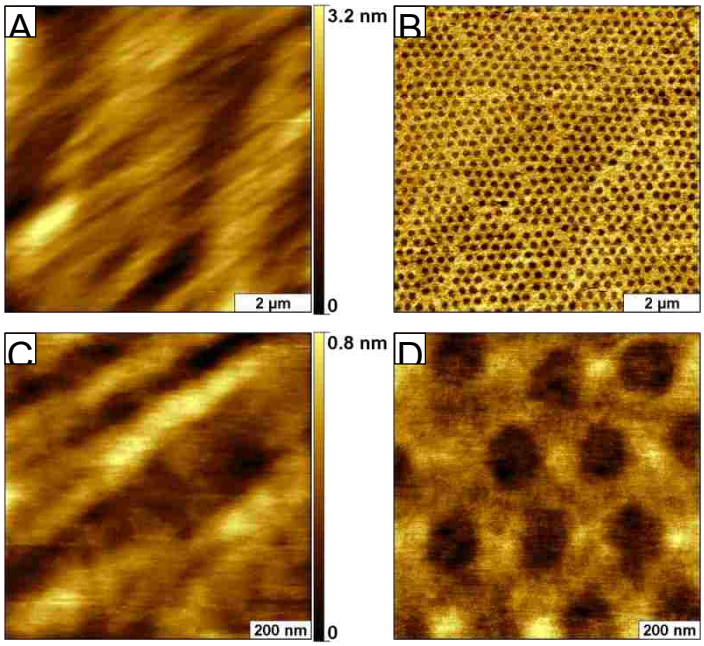

Figure 5.1. By combining particle lithography with contact printing, an array of circular pores of uncovered Si/SiO_2 substrate was prepared within an OTS film using 300 nm latex masks. (A) In a wide area AFM topograph (8×8 μm^2) the pores cannot be resolved. (B) The corresponding lateral force image clearly reveals the periodic array of pore nanostructures. (C) At higher magnification (1×1 μm^2) the topography image still does not resolve the nanopatterns. (D) The spacing and dimensions of the pores can be clearly viewed in the lateral force frame.

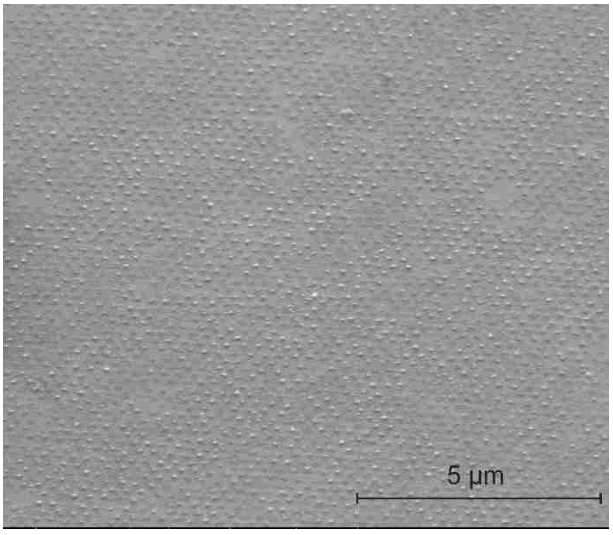

Figure 5.2. Scanning Electron Microscopy image of nanopatterned PT thin film on Si(111) substrate showing large-area hexagonal patterning with PT nanopillars.

The X-ray power of 50 W at 15 kV was used for all experiments with 200 micron beam size at the X-ray incidence and take off angles of 45°. The instrument work function was calibrated to give a binding energy (BE) of 84.0 eV for Au $4f_{7/2}$ line for metallic gold and the spectrometer dispersion was adjusted to give a BE's of 284.8 eV, 932.7 eV and of 368.3 eV for the C 1*s* line of adventitious (aliphatic) carbon presented on the non-sputtered samples, Cu $2p_{3/2}$ and Ag $3d_{5/2}$ photoemission lines, respectively. The patented PHI dual charge neutralization system was used on all samples. The high resolution I 3*d* and Ni 2*p* spectra were taken with a minimum of 10-60 s scans using 0.1 eV steps and 23.5 eV pass energy. Signal above background measurement and Shirley background subtraction was made using *MultiPak* v9.0 PHI software. At the ultimate *Versa Probe II* instrumental resolution the temperature spread (at 14/86%) of the metallic silver Fermi edge was less than 120 meV. All XPS spectra were recorded using PHI software *SmartSoft –XPS* v2.0 and processed using PHI *MultiPack* v9.0 and/or *CasaXPS* v.2.3.14. The relative sensitivity factors from *MultiPack* library were used to determine atomic percentages. Peaks were fitted using GL line shapes a combination of Gaussians and Lorentzians. Wherever possible, conclusions were drawn from the number of resolved signals for a given element, so as to minimize reliance on absolute binding energies for the nonconductive molecular materials. A given sample was examined at 5-6 different spots on the mounted specimen to assure that consistent, reproducible results were obtained.

5.4.Ultraviolet Photoemission Spectroscopy (UPS)

The UPS measurements were performed at the LSU Center for Advanced Microstructures and Devices (CAMD) using the 3 m toroidal grating monochromator (3 m TGM) beamline. The UHV chamber was equipped with an energy analyzer with an angular acceptance of ±1° and a combined (including the monochromator) energy resolution of 150 meV or better. The base

Table 5.1. Fitting parameters for I 3*d* and Ni 2*p* high-resolution XPS spectra in Figure 2.2.

Trace/ Sample	Transitions		Position, eV	Position separation, eV	FWHM, eV	% Gauss	Area	% Area	Chi Squared
Violet trace in Figure 2.2A	I $3d_{5/2}$		618.64	0.0	1.81	80	1986	46.51	2.32
	I $3d_{3/2}$		630.07	11.42	2.03	80	1701	39.84	
Red trace in Figure 2.2A	I $3d_{5/2}$	Dark yellow trace	618.95	0.0	1.78	80	1916	26.53	1.36
	I $3d_{3/2}$		630.36	2.00	1.5	100	2320	32.12	
	I $3d_{5/2}$	Purple trace	620.97	11.5	1.75	92	1193	16.51	1.13
	I $3d_{3/2}$		632.46	13.5	1.54	82	1794	24.84	
Green trace in Figure 2.2A	I $3d_{5/2}$		621.36	0.00	1.54	83	4099	57.99	2.69
	I $3d_{3/2}$		632.85	11.49	1.49	81	2970	42.01	
Red trace in Figure 2.2B	Ni $2p_{3/2}$	Blue trace	855.74	0.00	2.96	80	3999	22.99	1.48
	Shake up	Green trace	861.04	5.3	6.96	95	4506	23.9	
	Ni $2p_{1/2}$	Blue trace	874.50	18.76	4.05	100	2652	14.00	
	Shake up	Green trace	876.58	20.85	8.47	80	7940	42.00	
Violet trace in Figure 2.2B	Ni $2p_{3/2}$	Blue trace	856.05	0.00	2.58	80	14423	31.549	2.18
	Shake up	Green trace	861.40	5.35	5.96	80	14248	31.16	
	Ni $2p_{1/2}$	Blue trace	873.82	17.77	3.12	100	7406	16.2	
	Shake up	Green trace	879.72	23.68	5.99	100	9648	21.1	

pressure of the UPS chamber was ~5×10^{-10} mbar. All the photoemission spectra were taken with incident photon energy of 85 eV. The emitted photoelectrons were collected with an analyzer movable in-plane with surface normal and the incident photon beam. The Fermi level position was established from a copper piece in electrical contact with the sample. The valence band features binding energies are reported with respect to this Fermi level. All the measurements were carried out at ambient temperature.

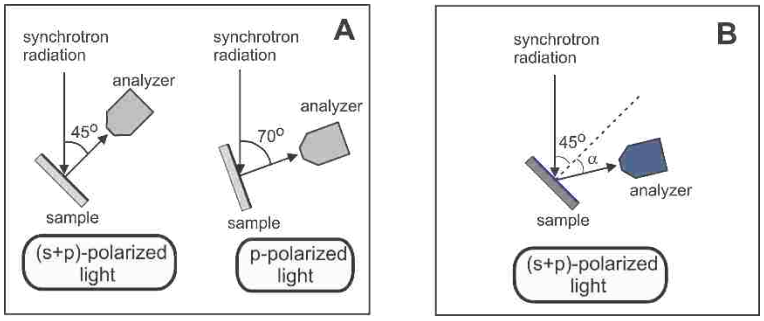

Figure 5.3. Schematics of polarization-dependent UPS studies of PT thin-film samples. (A) Normal emission geometry setup for (s+p)- and p-polarized light in the UPS studies. (B) Experimental setup for emission angle-dependent UPS spectroscopy utilizing (s+p)-polarized incident light.

5.5. Grazing Incidence X-ray Scattering

Grazing incidence X-ray scattering measurements were performed at beamline 8-ID-E of the Advanced Photon Source at Argonne National Laboratory.[5] An X-ray wavelength of λ = 1.6868 Å was used. The area detector, a Pilatus 1M (Dectris, Switzerland) pixel array detector, was positioned 204 mm from the sample for GIWAXS and 2165 mm from the sample for GISAXS. In both geometries, the sample was measured under ambient conditions and the scattering measured at two different detector heights for a range of incident angles, θ = 0.16° to 0.22° and exposure times of 10 s (GIWAXS) or 20 s (GISAXS). Combining corresponding images eliminated rows of inactive pixels between the detector modules and verified that the samples were not damaged by the synchrotron beam. The acquired data (as two-dimensional

images) were further treated and analyzed using *GIXSGUI* software package.[6] Fitting of the GISAXS data using a combined Porod plus Guinier model was performed with MATLAB.

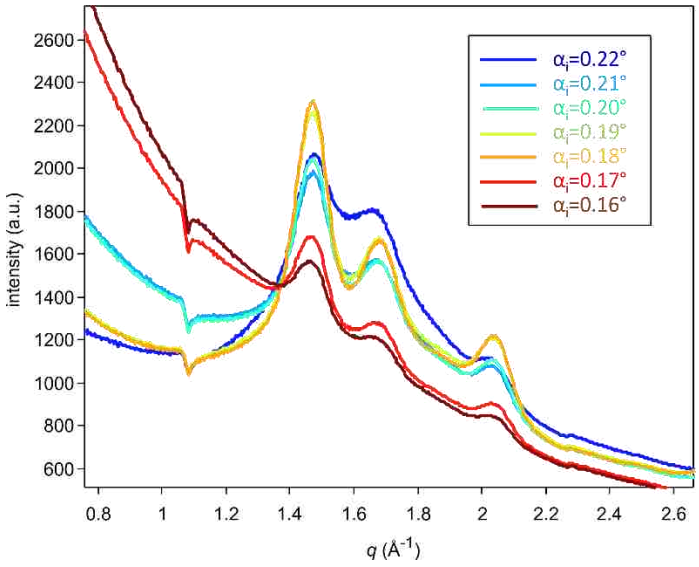

Figure 5.4. One-dimensional linecuts of GIWAXS images (integrated along the arcs between angle ϕ 0 to 90°) acquired at various incidence angles α_i of X-ray beam for the surface-confined PT thin film in Figure 2.12.

5.6. Neutron Reflectometry

Neutron reflectivity measurements were performed at the Spallation Neutron Source Liquids Reflectometer (SNS-LR, Beamline 4B) at the ORNL. The reflectivity data were collected using a sequence of 3.25-Å -wide continuous wavelength bands (selected from 2.63 Å < λ < 16.63 Å) and incident angles (ranging over 0.60° < θ < 2.71°), where λ is the neutron wavelength and θ is the scattering angle. Using these settings, the momentum transfer, $q = (4\pi \sin \theta/\lambda)$, was varied over a range of 0.008 Å^{-1} < q < 0.22 Å^{-1}. Reflectivity curves were assembled by combining seven different wavelength and angle data sets together, maintaining a constant sample footprint and relative instrumental resolution of $\delta q/q = 0.023$ by varying the incident-beam apertures.

The reduced data consisted of absolute neutron reflectivity (*R*) *vs.* neutron momentum transfer *q*. *Layers*[7] and *Motofit*[8] software were used to fit the measured reflectivity curves, providing the reflectivity of a model scattering length density profile, which can be analyzed to determine the structure of the thin films. One or two layers were used to model the depth profiles of the films. The scattering length density, thickness, and roughness of each layer was freely varied in the fitting procedure. The quality of fit was gauged by minimizing χ^2 between data and model reflectivity curves.

5.7. Synthetic Details

5.7.1. Synthesis and preparation of the polymer thin films in Chapter 2

5.7.1.1. 2-Triethoxysilyl-5-iodothiophene 2

A solution of isopropyl magnesium chloride (3.3 ml of 2.0 M solution in THF, 6.6 mmol) was added dropwise to a stirred solution of 2.0 g (6.0 mmol) of 2,5-diiodothiophene in 20 ml of THF at 0 ℃. The reaction mixture was stirred for 1.5 h at this temperature and then the temperature was lowered to –78 ℃, and 1.8 g (1.8 ml, d = 1.01 g ml^{-1}, 9.0 mmol) of chlorotriethoxysilane was added dropwise, and the reaction mixture was allowed to warm to room temperature overnight. The resulting solution was precipitated into hexanes, the solids were filtered, and the filtrate was concentrated in vacuo, and subjected to Kugelrohr distillation (ca. 85 ℃ at 10 mTorr,) to afford **2** as a colorless oil (1.1 g, 50%). It was dissolved in 15 ml of toluene to make a 0.2 M stock solution which was kept at –30 ℃ in an inert atmosphere glovebox. ^{1}H NMR ($CDCl_3$) δ 7.28 (d, *J* = 4 Hz, 1H), 7.1 (d, *J* = 4 Hz, 1H), 3.84 (q, *J* = 8 Hz, 6H), 1.21 (t, *J* = 8 Hz, 9H).

5.7.1.2. Bis[1,3-bis(diphenylphosphino)propane]nickel(0) ($Ni(dppp)_2$)

It was prepared following the literature procedure.[2]

5.7.1.3. Preparation of catalytic initiator 3

A mixture of 44.2 g (0.05 mmol) of $Ni(dppp)_2$ and 0.125 ml of 0.2 M solution of **2** (0.025 mmol) in 10 ml of toluene was stirred at 45 ℃ for 24 h to afford a nominally 2.5 mM solution of the catalytic initiator **3**. *Due to the air-sensitive nature of compounds involved, all procedures were performed inside an inert atmosphere glovebox.*

5.7.1.4. Cleaning and activation of substrates

Quartz substrates Rectangular quartz slides (approx. 1.1×2.5 cm^2) were ultrasonicated sequentially for 10 min in acetone, chloroform, methanol, and deionized water. The pre-cleaned slides were placed into Piranha solution (a mixture of conc. H_2SO_4 and 30 % H_2O_2 (7:3)) and ultrasonicated for 30 min. After rinsing with copious amount of deionized water, substrates were dried in N_2 flow at room temperature for 24 h, and then activated using mild O_2 plasma for 5 min just before using. (***NOTE:*** *extreme care must be taken when dealing with piranha solutions as they can detonate when contacted with organic compounds!*)

ITO-glass substrates Rectangular ITO-covered glass slides (approx. 1.1×2.5 cm^2) were ultrasonicated for 10 min in chloroform, acetone, methanol, and deionized water. The pre-cleaned slides were subjected to an RCA-type cleaning procedure by keeping in a water – 30% H_2O_2 – 30% aqueous NH_3 (5:1:1) mixture at 70 ℃ for 1 h. The substrates were then rinsed with copious amount of deionized water and dried in N_2 flow at room temperature for 12 h, and then activated using mild O_2 plasma for 5 min.

Si(111) wafer Pieces of boron-doped polished wafers of Si(111) were cut into 1×1 cm^2 squares and placed in Piranha solution (a mixture of conc. H_2SO_4 and 30 % H_2O_2 (7:3)). Next, silicon substrates were rinsed with copious amount of deionized water and dried in ambient air.

(***NOTE:*** *extreme care must be taken when dealing with piranha solutions as they can detonate when contacted with organic compounds!*)

5.7.1.5. Preparation of surface-immobilized monolayer of catalytic initiator 3 (Direct method)

Activated substrate slides were immersed into a 2.5 mM solution of **3** placed in 20 ml scintillation vials and kept at 55 ℃ for 60 h followed by gentle rinsing with toluene, and then used for surface-confined polymerization. *Due to the air-sensitive nature of compounds involved, all procedures were performed inside an inert atmosphere glovebox.*

5.7.1.6. Preparation of surface-immobilized monolayer of catalytic initiator 3 (Indirect method)

Activated substrate slides were immersed into a 2.5 mM solution of **2** in toluene (placed in 20 ml scintillation vials) and kept at 55 ℃ for 60 h followed by gentle rinsing with toluene. Then, the substrates with monolayer of **2** were transferred to another 20 ml vial with a 5 mM solution of $Ni(dppp)_2$ in toluene and kept at 40 ℃ for 1 day. The resulting substrates were rinsed with toluene and then used for surface-confined polymerization. *Due to the air-sensitive nature of compounds involved, all procedures were performed inside an inert atmosphere glovebox.*

5.7.1.7. Surface-confined polymerization of Grignard monomer 4

Due to sensitivity of the polymerization process to moisture and oxygen, the entire polymerization procedure should be carried out in an inert atmosphere glovebox. A solution of isopropylmagnesium chloride (0.26 ml of 2.0 M solution in THF, 0.525 mmol) was added dropwise to a stirred solution of 0.121 g (0.5 mmol) of 2,5-dibromothiophene in 10 ml of THF at 0 ℃, and the resulting solution was stirred for 1 h to yield a nominally 50 mM solution of Grignard monomer **4**. A substrate with a monolayer of catalytic initiator **3** (prepared either by method B or by method A as described above) was then placed in the Grignard monomer **4** solution (in a 20 ml scintillation vial) and kept at room temperature for the specified amount time

(6-72 h) to allow for polymerization. The substrate with the surface-confined PT film was then quenched with methanol and then cleaned by subsequent ultrasonication in chloroform, acetone, methanol, and water, and dried in flow of nitrogen.

5.7.1.8. Surface-confined *in situ* polymerization with regeneration of Ni(II) catalytic center (a typical procedure)

The initial surface-confined polymerization was performed as described above, with the polymerization time varying between 6 and 12 h. The substrates were then rinsed with toluene, and placed in a 5 mM solution of $Ni(dppp)_2$ in toluene (10 ml in 20 ml scintillation vials) where they were kept at 40 ℃ for 20 h. The regenerated substrates were rinsed with copious amount of toluene, and placed in a 50 mM solution of Grignard monomer **4** where they were kept at 40 ℃ for subsequent polymerization (polymerization time varied between 6 and 12 h). This sequence (surface-confined polymerization and catalyst regeneration) can be repeated as many times as required (up to 3). At the end, the substrates were immersed in methanol and ultrasonicated for 10 min. The PT thin films were further washed by subsequent ultrasonication in chloroform, acetone, methanol, and water, and dried in flow of nitrogen.

5.7.1.9. Determination of surface coverage using ferrocene-functionalized monolayers

A solution of isopropylmagnesium chloride (0.21 ml of 2.0 M solution in THF, 0.42 mmol) was added dropwise to a stirred solution of 0.144 g (0.4 mmol) of 2-ferrocenyl-5-bromothiophene (prepared as described in ref. 3) in 10 ml of THF at 0 ℃. The resulting solution was additionally stirred for 1 h. ITO/glass substrates with the monolayer of initiator **3** were placed in the resulting solution of Grignard compound **5** at 60 ℃ and kept there for 20 h. The resulting substrates were then immersed in methanol and washed subsequently with chloroform and acetone upon ultrasonication for 10 min. The cyclic voltammetry studies were carried out

using a three-electrode set up described in General Procedures section with monolayer-modified ITO/glass working electrode (electrode area ~1.13 cm^2), $Ag/AgNO_3$ non-aqueous reference electrode, and a Pt gauze counter electrode in 0.1 M Bu_4NPF_6 solution in CH_2Cl_2 as supporting electrolyte.

The surface coverage density was estimated based on the measured area of the redox peak of ferrocene. The value was corrected by the corresponding data for the bare ITO electrode. Assuming the ferrocene oxidation/reduction being a one-electron process, the surface density was estimated using the formula:

$$\Gamma = \frac{Q}{F}$$

where Q is the redox peak area (C cm^{-2}), and F is Faraday constant (96500 C mol^{-1}).

5.7.1.10. Spectroelectrochemical experiments

These were conducted using a rectangular quartz cuvette (path length 1 cm) with a PT-modified ITO/glass working electrode placed inside the cuvette, Pt gauze counter electrode attached around the walls inside the cuvette with a rectangular hole against the sample, and Ag/Ag^+ non-aqueous working electrode which was checked against Fc/Fc^+ standard immediately before and after measurements. The supporting electrolyte was 0.1 M Bu_4NPF_6 in CH_2Cl_2. Absorption spectra were recorded in 0.1 V potential increments using Agilent Cary 5000 spectrometer.

5.7.1.11. Tetraiodothiophene

A solution of thiophene (16.8 g, 0.2 mol), iodine (89.4 g, 0.35 mol), and iodic acid (31.0 g, 0.18 mol) in a mixture of water (80 ml), acetic acid (170 ml), carbon tetrachloride (65 ml), and sulfuric acid (4.5 ml) placed in a 1 L flask was stirred upon reflux at 120 °C for one week. After the mixture was cooled down to room temperature, the red solid was filtered and washed

successively with water and 5% aqueous $Na_2S_2O_3$ solution until the color of the solid turned to yellow. Then, the solid was dried in air and recrystallized from 1,4-dioxane to give 103.0 g (88%) of tetraiodothiophene as yellow crystalline material. ^{13}C NMR (DMSO-d_6) δ 108.04 (s, 2C), 90.78 (s, 2C).

5.7.1.12. Tetradeuterothiophene

Tetraiodothiophene (110.5 g, 0.188 mol) was added to a mixture of D_2O (137.7 g, 6.88 mol), acetic anhydride (78.0 g, 0.76 mol), and zinc dust (89.6 g, 1.37 mol), and the mixture was briefly stirred at 0 ℃, allowed to warm to room temperature, and then the mixture was refluxed at 120 ℃ for one day. After allowing to cool to room temperature, the resulting mixture was distilled at reduced pressure (10 mm Hg) at room temperature, and the distillate was collected in an externally cooled receiving flask. The distillate formed two layers, and the top aqueous layer was removed using a pipet, and organic layer was neutralized with Na_2CO_3 and dried over Na_2SO_4. This produced 12.8 g (78%) of tetradeuterothiophene as a colorless liquid. ^{13}C NMR ($CDCl_3$) δ 126.64 (t, J = 26 Hz, 2C), 124.94 (t, J = 26 Hz, 2C).

5.7.1.13. 2,5-Dibromothiophene-D_2

A solution of NBS (60.0 g, 0.337 mol) in 25 ml of DMF was added dropwise over a 10 min period to a stirred solution of tetradeuterothiophene (12.0 g, 0.135 mol) in 100 ml of DMF at room temperature, and the resulting solution was heated to 75 ℃ for 1 day. The reaction mixture was quenched with ice water and extracted with chloroform. The organic extract was neutralized with $Na_2S_2O_3$ and washed with water. The organic phase was dried over Na_2SO_4, concentrated in vacuo, and the crude product was purified by column chromatography on silica gel with hexanes as an eluent to give 26.5 g (80%) of 2,5-dibromothiophene-D_2 as a colorless liquid. ^{13}C NMR ($CDCl_3$) δ 130.28 (t, J = 26 Hz, 2C), 111.65 (s, 2C).

5.7.1.14. Surface-confined polymerization

Due to sensitivity of the polymerization process to moisture and oxygen, the entire polymerization procedure was carried out in an inert atmosphere glovebox. A solution of isopropylmagnesium chloride (0.26 ml of 2.0 M solution in THF, 0.525 mmol) was added dropwise to a stirred solution of 0.121 g (0.5 mmol) of 2,5-dibromothiophene in 10 ml of THF at 0 ℃, and the resulting solution was stirred for 1 h to yield a nominally 50 mM solution of Grignard monomer **4**. A solution of Grignard monomer **4**-D_2 was prepared following the same procedure starting with 0.123 g (0.5 mmol) of 2,5-dibromothiophene-D_2. A substrate with a monolayer of catalytic initiator **3** was then placed in a solution of Grignard monomer **4**-D_2 (in a 20 ml scintillation vial) and kept at room temperature for 1 h. The substrate was then gently rinsed with toluene, and placed in a solution of Grignard monomer **4** (in a 20 ml scintillation vial) where it was kept 6 h to afford stratified PDT/PT thin film. The film was then quenched with methanol and cleaned by successive ultrasonication with chloroform, acetone, methanol, and water, and dried in flow of nitrogen.

5.7.1.15. Preparation of nanopatterned PT film using combination of particle lithography and surface-confined polymerization

Monodisperse latex mesospheres (300 nm diameter) were washed with deionized water to remove surfactants by centrifugation. A small volume (300 µL) of aqueous latex suspension (1 wt%) was centrifuged at 14000 rpm for 15 min, and the supernatant was decanted. The pellet of latex was resuspended in 300 µL of deionized water. A drop of the latex suspension (30 µL) was deposited on the freshly cleaned Si(111) substrate and dried in air for 2 h. During the drying step, as water was evaporating, the monodisperse latex spheres formed crystalline layers on the substrate, which provided a lithographic mask for patterning organosilanes. Next, a 2×2 cm^2

block of polydimethylsiloxane (PDMS, Sylgard 184, Dow Corning) was prepared for patterning octadecyltrichlorosilane (OTS). A 30 μL volume of a 30% v/v solution of OTS in bicyclohexyl was deposited on the surface of the PDMS block and then dried quickly with a stream of nitrogen. The "inked" PDMS block was placed on top of the masked silicon substrate. The areas of contact between the latex mesospheres and substrate were protected from deposition of OTS. After 1 h, the PDMS block was removed from the sample and the surface was rinsed with deionized water. The mask of latex particles was removed completely by rinsing with ethanol and deionized water several times, using sonication. After removal of the latex mask, a layer of OTS persisted on the surface to define periodic circular pores of uncovered substrate. Surface-immobilization of the Ni(II) catalytic initiator **3** within the uncovered surface was carried out as described above (method B). Subsequent surface-initiated polymerization of Grignard monomer **4** was performed following the procedure described above, with polymerization time 24 h.

5.7.2. Preparation of the diblock copolymer films in Chapter 3

5.7.2.1. Synthesis of diblock copolymer thin films

Due to sensitivity of the polymerization process to moisture and oxygen, the entire polymerization procedure was carried out in an inert atmosphere glovebox. All substrates and surface-immobilized monolayer of catalytic initiator 3 were prepared following the previous procedures in Chapter 2. A solution of isopropylmagnesium chloride (0.26 ml of 2.0 M solution in THF, 0.525 mmol) was added dropwise to a stirred solution of 0.121 g (0.5 mmol) of 2,5-dibromothiophene in 10 ml of THF at 0 ℃, and the resulting solution was stirred for 1 h to yield a nominally 50 mM solution of thiophene Grignard monomer. In order to prepare phenylene Grignard solution, 0.071g of 2-bromoiodobenzene was dissolved in anhydrous THF (0.25 mmol, 10 mM) and stirred at 0 ℃. Then, 0.13 ml isopropyl magnesium (2 M solution in THF, 0.26

mmol) was added by dropwise and stirred for 1 h to prepare a nominally 25 mM solution of phenylene Grignard monomer. For PT-*b*-PPP thin film, a surface-immobilized substrate with the catalytic initiator 3 was immersed into a solution of thiophene Grignard and kept at room temperature for time varying depending on the reaction conditions described in Chapter 3 to produce a polythiophene thin film (except for the kinetic study of homopolymer, all polymerizations to form polythiophene as the first block were carried out for 5 min). After polymerization, the substrate was rinsed with toluene and moved to a 5 mM solution of $Ni(dppp)_2$ in toluene (10 ml in 20 ml scintillation vials) where they were kept at 40 ℃ for 20 h for reactivation. Then the substrate was washed with toluene and placed in a solution of phenylene Grignard monomer for 1 h (for the AFM images, reaction time was overnight). After completing polymerizations, the substrate was quenched by methanol and cleaned by sequential sonications with various solvent (chloroform, acetone, methanol, and DI-water) for 10 min each followed by drying under N_2 atmosphere. To prepare PPP-*b*-PT thin film, a substrate with surface-immobilized monolayer of catalytic initiator **3** was immersed in a prepared solution of phenylene Grignard monomer (10 ml in 20 ml scintillation vials), and kept at room temperature for less than 1.5 h. After polymerization, "reactivation" was carried out. After reactivation, the PPP thin film substrate was rinsed with toluene and immersed in a solution of thiophene Grignard monomer for 1 h to yield PPP-*b*-PT thin film. Quenching and cleaning procedure was same with PT-*b*-PPP thin film mentioned above.

5.7.2.2. Cyclic Voltammetry (CV) studies of diblock copolymer thin films

The cyclic voltammetry studies were carried out using a three-electrode set up described in General Procedures section with a monolayer-modified ITO/glass working electrode,

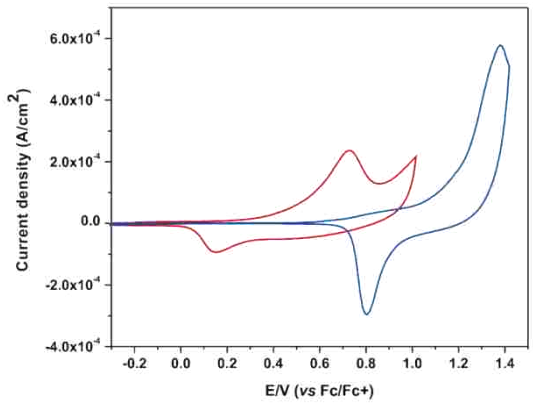

Figure 5.5. Cyclic Votammetry (CV) studies of PT homopolymer thin film (red trace) and PPP homopolymer thin film (blue trace).

$Ag/AgNO_3$ non-aqueous reference electrode, and a Pt gauze counter electrode in 0.1 M Bu_4NPF_6 solution in CH_2Cl_2 as supporting electrolyte. The sweep rate was 0.1 V s^{-1}.

5.7.2.3. XPS measurement of diblock copolymer thin films

The XPS studies were conducted following the procedure described in the General Procedures section. All diblock copolymer thin films were prepared by the same procedure described above except for using 1,4-diiodobenzene to prepare solution of phenylene Grignard monomer.

5.7.3. Preparation of PEDOT thin films

5.7.3.1. Preparing isopropylmagnesium chloride lithium chloride complex (Turbo Grignard solution)

1.7 g of lithium chloride (0.04 mol) was dissolved in 20 ml of isopropylmagnesuim chloride solution (2.0 M solution in THF) with vigorous stirring at room temperature and transferred to a schlenk flask to make 2.0 M solution of “Turbo Grignard”.

5.7.3.2. PEDOT thin films prepared with 2,5-dibromoEDOT and 2,5-diiodoEDOT

Due to sensitivity of the polymerization process to moisture and oxygen, the entire polymerization procedure was carried out in an inert atmosphere glovebox. All substrates and surface-immobilized monolayer of catalytic initiator **3** were prepared following the previous procedures in Chapter 2. A solution of isopropylmagnesium chloride lithium chloride complex (Turbo Grignard, 0.26 ml of 2.0 M solution in THF, 0.525 mmol) was added dropwise to a stirred solution of 0.150 g (0.5 mmol) of 2,5-dibromoEDOT in 10 ml of THF at 0 ℃, and the resulting solution was stirred for 1 h to yield a nominally 50 mM solution of 5-bromo-2-(3,4-ethylenedioxithienyl)magnesium chloride monomer. To make a solution of 5-iodo-2-(3,4-ethylenedioxithienyl)magnesium chloride monomer, 0.197g of 2,5-diiodoEDOT was dissolved in anhydrous THF (0.5 mmol, 10 mM) and stirred at 0 ℃. Then, 0.26 ml isopropylmagnesium chloride (2 M solution in THF, 0.525 mmol) was added dropwise and stirred for 1 h to prepare a nominally 50 mM solution of Grignard monomer. A substrate with surface-immobilized catalytic initiator **3** was immersed into a solution of EDOT Grignard and kept at different temperatures for the time varying depending on the reaction conditions described in Chapter 4 to produce a PEDOT thin film. Quenching and cleaning procedure was followed the same as for the other surface-initiated olymer films describe above.

5.7.3.3. Conductivity measurement of PEDOT films

Conductivity of the PEDOT films was measured by a 4-point probe with Keithley 2400 Sourcemeter. To test conductivity of iodine doped PEDOT thin film, a substrate with PEDOT thin film was kept under iodine vapor in a 20 ml scintillation vial for one day, before carrying out the measurement.

5.8. References

(1) Love, B. E.; Jones, E. G. The Use of Salicylaldehyde Phenylhydrazone as an Indicator for the Titration of Organometallic Reagents *J. Org. Chem.* **1999**, *64*, 3755-3756.

(2) Corain, B.; Bressan, M.; Rigo, P. The Behaviour of Nickel(0) Diphosphine Complexes Towards Unsaturated Organic Compounds *J. Organomet. Chem.* **1971**, *28*, 133-136.

(3) Sontag, S. K.; Sheppard, G. R.; Usselman, N. M.; Marshall, N.; Locklin, J. Surface-Confined Nickel Mediated Cross-Coupling Reactions: Characterization of Initiator Environment in Kumada Catalyst-Transfer Polycondensation *Langmuir* **2011**, *27*, 12033-12041.

(4) Gwyddion 2.9; Czech Metrology Institute: http://gwyddion.net/, 2010.

(5) Jiang, Z.; Li, X.; Strzalka, J.; Sprung, M.; Sun, T.; Sandy, A. R.; Narayanan, S.; Lee, D. R.; Wang, J. The Dedicated High-Resolution Grazing-Incidence X-ray Scattering Beamline 8-ID-E at The Advanced Photon Source *J. Synchrotron Rad.* **2012**, *19*, 627-636.

(6) Jiang, Z. GIXSGUI: A MATLAB Toolbox for Grazing-Incidence X-ray Scattering Data Visualization and Reduction, and Indexing of Buried Three-Dimensional Periodic Nanostructured Films *J. Appl. Cryst.* **2015**, ***48***, 917-926.

(7) *Layers* is an Excel spreadsheet for modeling neutron reflectivity data developed by John F. Ankner at the Oak Ridge National Laboratory.

(8) Nelson, A. Co-refinement of Multiple-Contrast Neutron/X-ray Reflectivity Data Using MOTOFIT *J. Appl. Cryst.* **2006**, *39*, 273-276.

APPENDIX A: PERMISSIONS

Order Completed

Thank you for your order.

This Agreement between Sang Gil Youm ("You") and John Wiley and Sons ("
consists of your license details and the terms and conditions provided by Jo
Copyright Clearance Center.

Your confirmation email will contain your order number for future reference.

Get the printable license.

License Number	3887510504564
License date	Jun 14, 2016
Licensed Content Publisher	John Wiley and Sons
Licensed Content Publication	Angewandte Chemie International Edition
Licensed Content Title	Polymer–Fullerene Composite Solar Cells
Licensed Content Author	Barry C. Thompson,Jean M. J. Fréchet
Licensed Content Date	Nov 28, 2007
Licensed Content Pages	20
Type of use	Dissertation/Thesis
Requestor type	University/Academic
Format	Print and electronic
Portion	Figure/table
Number of figures/tables	1
Original Wiley figure/table number(s)	scheme 1
Will you be translating?	No
Title of your thesis / dissertation	Thin films of semiconducting polymers and diblock copolymers by surface
Expected completion date	Jul 2016
Expected size (number of pages)	160
Requestor Location	Sang Gil Youm 3942 Gourrier Ave. #220 BATON ROUGE, LA 70808 United States Attn: Sang Gil Youm
Publisher Tax ID	EU826007151
Billing Type	Invoice
Billing address	Sang Gil Youm

Title:	Effects of long-term UV–visible light irradiation in the absence of oxygen on P3HT and P3HT:PCBM blend
Author:	Matthieu Manceau,Sylvain Chambon,Agnès Rivaton,Jean-Luc Gardette,Stephane Guillerez,Noëlla Lemaître
Publication:	Solar Energy Materials and Solar Cells
Publisher:	Elsevier
Date:	October 2010

Order Completed

Thank you for your order.
This Agreement between Sang Gil Youm ("You") and Elsevier ("Elsevier") consists of your license details and the terms and conditions provided by Elsevier and Copyright Clearance Center.

Your confirmation email will contain your order number for future reference.

Get the printable license.

License Number	3887501245702
License date	Jun 14, 2016
Licensed Content Publisher	Elsevier
Licensed Content Publication	Solar Energy Materials and Solar Cells
Licensed Content Title	Effects of long-term UV–visible light irradiation in the absence of oxygen on P3HT and P3HT:PCBM blend
Licensed Content Author	Matthieu Manceau,Sylvain Chambon,Agnès Rivaton,Jean-Luc Gardette,Stephane Guillerez,Noëlla Lemaître
Licensed Content Date	October 2010
Licensed Content Volume	94
Licensed Content Issue	10
Licensed Content Pages	6
Type of Use	reuse in a thesis/dissertation
Portion	full article
Format	print
Are you the author of this Elsevier article?	No
Will you be translating?	No
Title of your thesis/dissertation	Thin films of semiconducting polymers and diblock copolymers by surface-initiated polymerization

Title:	Formation of conjugatedpolymer brushes by surface-initiated catalyst-transfer polycondensation
Author:	S. Kyle Sontag,Nicholas Marshall,Jason Locklin
Publication:	Chemical Communications (Cambridge)
Publisher:	Royal Society of Chemistry
Date:	May 15, 2009

Order Completed

Thank you for your order.

This Agreement between Sang Gil Youm ("You") and Royal Society of Chemistry ("Royal Society of Chemistry") consists of your license details and the terms and conditions provided by Royal Society of Chemistry and Copyright Clearance Center.

Your confirmation email will contain your order number for future reference.

Get the printable license.

License Number	3887511269731
License date	Jun 14, 2016
Licensed Content Publisher	Royal Society of Chemistry
Licensed Content Publication	Chemical Communications (Cambridge)
Licensed Content Title	Formation of conjugatedpolymer brushes by surface-initiated catalyst-transfer polycondensation
Licensed Content Author	S. Kyle Sontag,Nicholas Marshall,Jason Locklin
Licensed Content Date	May 15, 2009
Licensed Content Issue	23
Type of Use	Thesis/Dissertation
Requestor type	academic/educational
Portion	excerpt (<= 400 words)
Number of excerpts	1
Distribution quantity	1
Format	print and electronic
Will you be translating?	no
Order reference number	

Title of the thesis/dissertation	Thin films of semiconducting polymers and diblock copolymers by surface-initiated polymerization

Title:	"Hairy" Poly(3-hexylthiophene) Particles Prepared via Surface-Initiated Kumada Catalyst-Transfer Polycondensation
Author:	Volodymyr Senkovskyy, Roman Tkachov, Tetyana Beryozkina, et al
Publication:	Journal of the American Chemical Society
Publisher:	American Chemical Society
Date:	Nov 1, 2009

PERMISSION/LICENSE IS GRANTED FOR YOUR ORDER AT NO CHARGE

This type of permission/license, instead of the standard Terms & Conditions, is sent to you because no fee is being charged for your order. Please note the following:

- Permission is granted for your request in both print and electronic formats, and translations.
- If figures and/or tables were requested, they may be adapted or used in part.
- Please print this page for your records and send a copy of it to your publisher/graduate school.
- Appropriate credit for the requested material should be given as follows: "Reprinted (adapted) with permission from (COMPLETE REFERENCE CITATION). Copyright (YEAR) American Chemical Society." Insert appropriate information in place of the capitalized words.
- One-time permission is granted only for the use specified in your request. No additional uses are granted (such as derivative works or other editions). For any other uses, please submit a new request.

APPENDIX B: NUCLEAR MAGNETIC RESONACE (NMR) SPECTRA

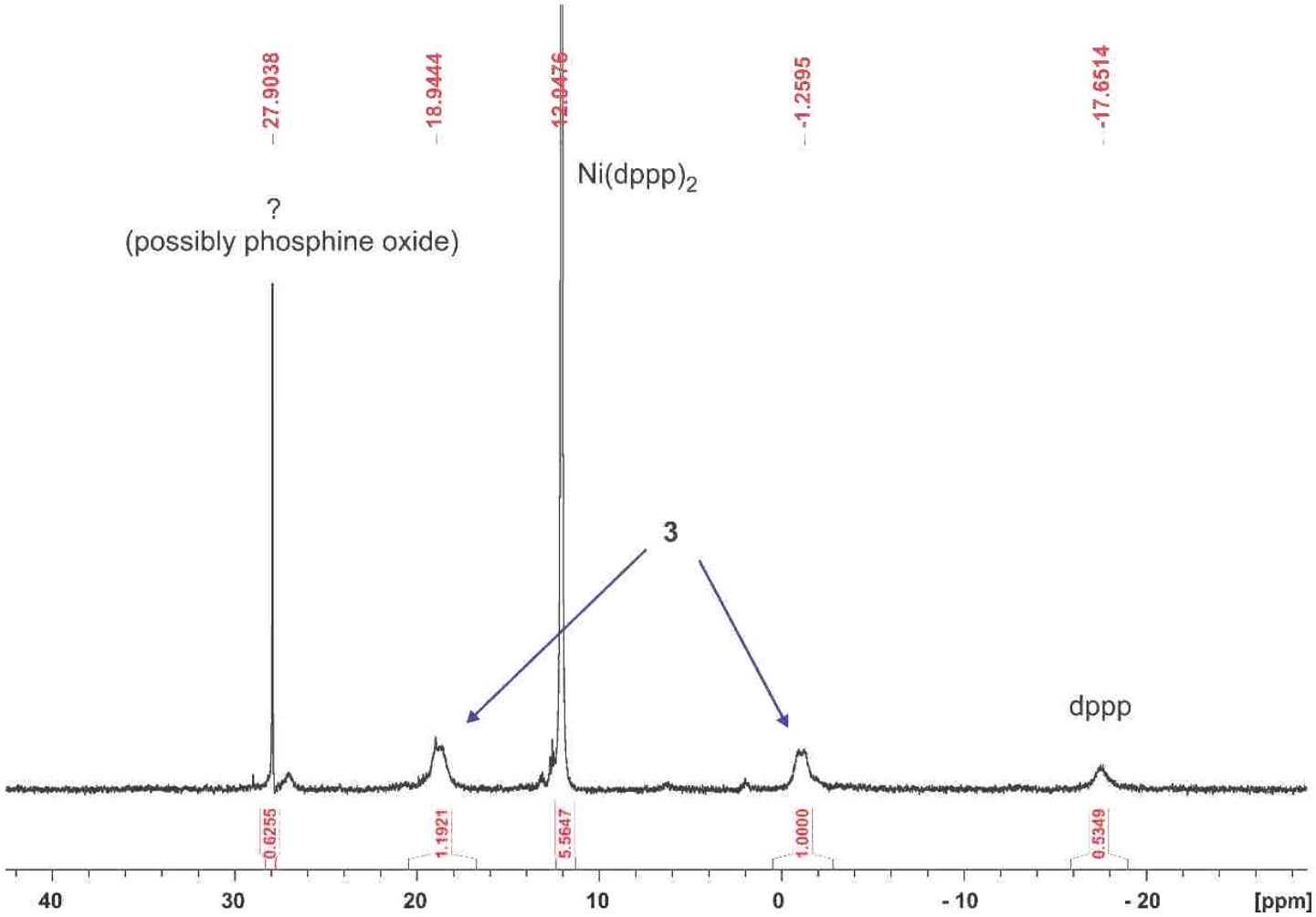

Figure Appendix B.1. ^{31}P NMR spectrum of the reaction between compound **2** and 2 equivalents of $Ni(dppp)_2$ to form Ni(II) catalytic initiator **3**. The reaction was carried out for 24 h in toluene at 45 ℃, followed by removing toluene by evaporating *in vacuo* and redissolving the residue in THF to acquire the NMR spectrum.

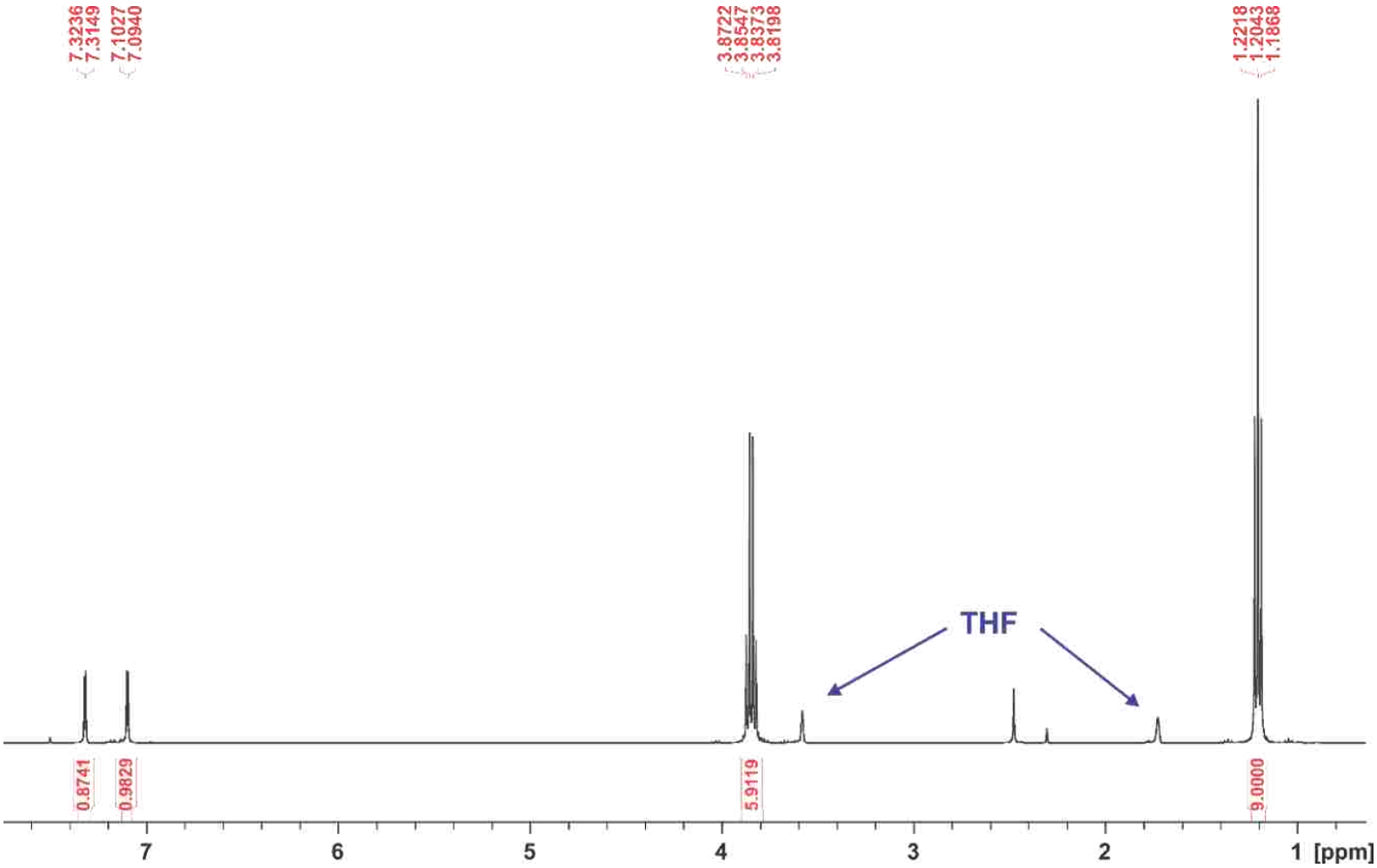

Figure Appendix B.2. ^{1}H NMR spectrum (400 MHz, THF-D_8) of 2-triethoxysilyl-5-iodothiophene **2**.

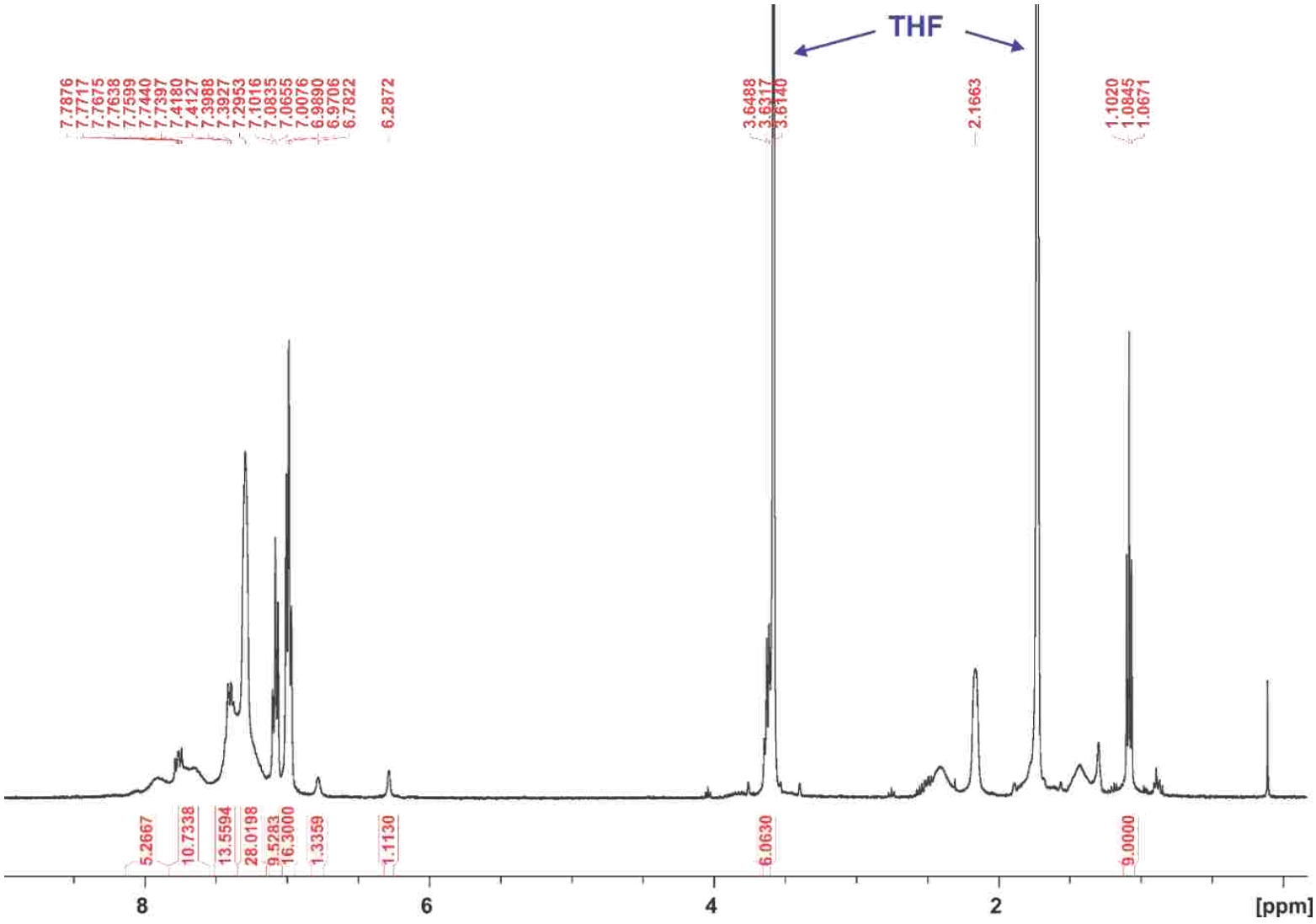

Figure Appendix B.3. ^{1}H NMR spectrum (400 MHz, THF-D_8) of the catalytic initiator **3** prepared as described on page 134. Due to the preparation procedure, in addition to **3**, the sample contains ~1 eq. of Ni(dppp)$_2$, and ~1 eq. of dppp.

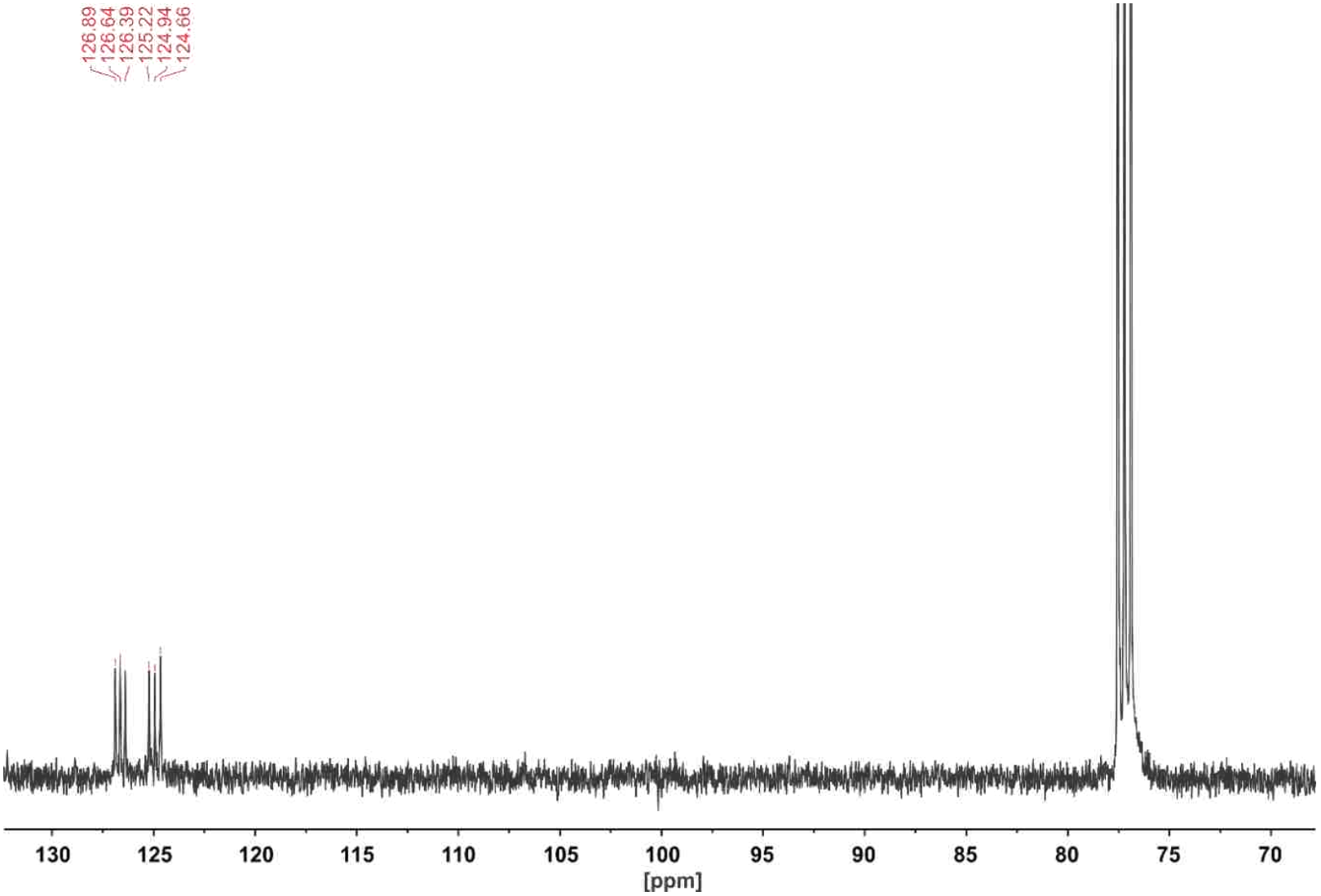

Figure Appendix B.4. ^{13}C NMR spectrum (100 MHz, $CDCl_3$) of thiophene-D_4.

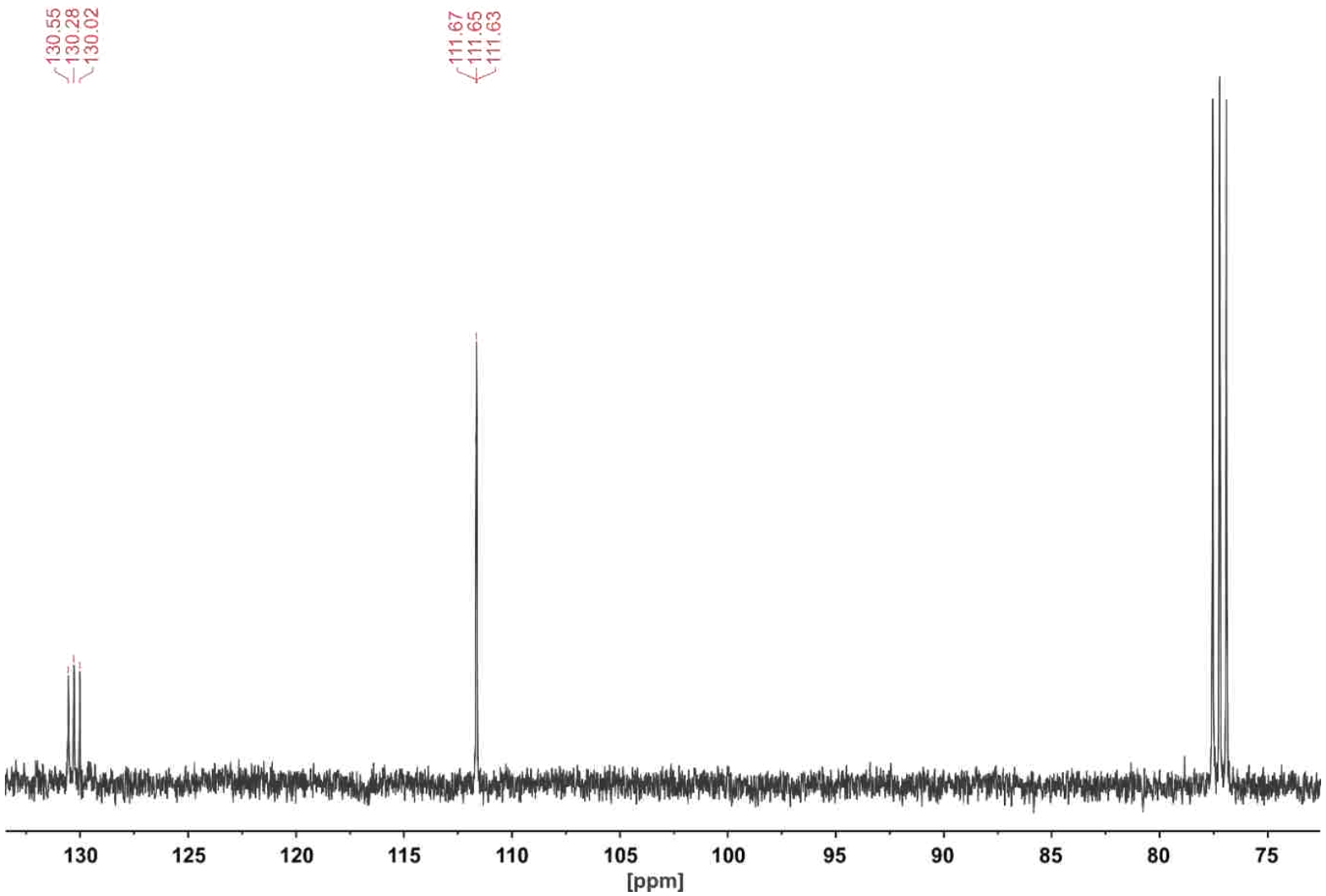

Figure Appendix B.5. ^{13}C NMR spectrum (100 MHz, $CDCl_3$) of 2,5-dibromothiophene-D_2.

VITA

Sang Gil Youm was born in 1980 in Seoul, Korea. After he received a Bachelor of Science in Chemistry from Hanyang University, Seoul, Korea, in February 2002, he began his research at the lab of Professor Deawon Sohn in the Department of Chemistry in Hanyang University. In February 2004, he graduated with a Master of Science in Chemistry, while simultaneously publishing several peer-reviewed articles. He then worked at Dongbu Hitek as an analytical researcher from February 2004 to June 2008. He moved to The Research Institute for Natural Science at Hanyang University as a senior scientist until June 2010. During this period, he published numerous peer-reviewed articles ranging from surface science to inorganic chemistry. Then, he enrolled as a graduate student in the Department of Chemistry at Louisiana State University, Baton Rouge, Louisiana in August 2010. Currently, he conducts research under the supervision of Professor Evgueni E. Nesterov at LSU, which design if surface-initiated polymerization to prepare conjugated polymer thin films and developing analytical methods to elucidate structure-property relationship of conjugated polymer thin films. Sang Gil Youm is a candidate for the Doctor of Philosophy in Polymer Chemistry, which will be awarded in August 2016 with a dissertation entiltled, “Thin Films of Semiconducting Polymers and Diblock Copolymers by Surface-initiated Polymerization.”